AFML-TR-67-254

A STUDY OF NOTCHES IN BRITTLE MATERIALS BY RELATING STRESS INTENSIFICATION AND VOLUME

H. STUART STARRETT
C. D. PEARS

SOUTHERN RESEARCH INSTITUTE

TECHNICAL REPORT No. AFML-TR-67-254

MAY 1968

AIR FORCE MATERIALS LABORATORY
AIR FORCE SYSTEMS COMMAND
WRIGHT-PATTERSON AIR FORCE BASE, OHIO

DISCLAIMER NOTICE

THIS DOCUMENT IS BEST QUALITY PRACTICABLE. THE COPY FURNISHED TO DTIC CONTAINED A SIGNIFICANT NUMBER OF PAGES WHICH DO NOT REPRODUCE LEGIBLY.

NOTICES

When Government drawings, specifications, or other data are used for any purpose other than in connection with a definitely related Government procurement operation, the United States Government thereby incurs no responsibility nor any obligation whatsoever; and the fact that the Government may have formulated, furnished, or in any way supplied the said drawings, specifications, or other data, is not to be regarded by implication or otherwise as in any manner licensing the holder or any other person or corporation, or conveying any rights or permission to manufacture, use, or sell any patented invention that may in any way be related thereto.

This document is subject to special export controls and each transmittal to foreign governments or foreign nationals may be made only with prior approval of the Metals and Ceramics Division (MAM), Air Force Materials Laboratory, Wright-Patterson Air Force Base, Ohio 45433.

Protection of Technical Know-How relating to materials manufacturing processes.

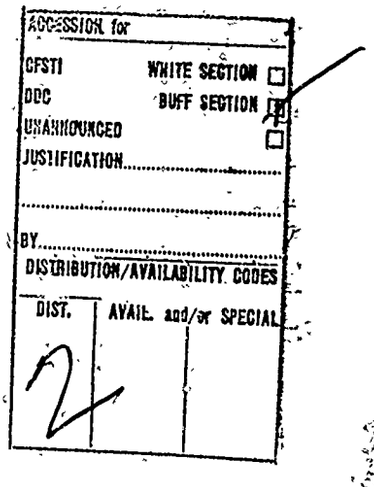

Copies of this report should not be returned to the Research and Technology Division unless return is required by security considerations, contractual obligations, or notice on a specific document.

500 - August 1968 - CO455 - 45-956

AFML-TR-67-254

A STUDY OF NOTCHES IN BRITTLE MATERIALS BY RELATING STRESS INTENSIFICATION AND VOLUME

H. STUART STARRETT

C. D. PEARS

FOREWORD

This report was prepared by Southern Research Institute under USAF Contract No. AF 33(615)-1690. This contract was initiated under Project No. 7350, "Refractory Inorganic Nonmetallic Materials," Task No. 735003, "Theory and Mechanical Phenomena." The work was administered under the direction of the Air Force Materials Laboratory, Air Force Systems Command, Wright-Patterson Air Force Base, Ohio, with Mr. G. R. Atkins acting as project engineer.

This report covers work conducted from January 1966 to 31 December 1966. Manuscript released by the authors May 1967 for publication.

This program was under the direction of H. Stuart Starrett, Project Leader, and the general management of C. D. Pears, Head, Mechanical Engineering Division.

This technical report has been reviewed and is approved.

W. J. TRAPP
Chief, Strength and Dynamics Branch
Metals and Ceramics Division
Air Force Materials Laboratory

ABSTRACT

The effects of notches on the tensile strength of brittle materials were determined experimentally, and the Weibull volume theory was used in conjunction with Neuber stress distributions to examine the results. The experimental portion was performed on a gas-bearing tensile facility. The primary material used was hot pressed alumina made by Avco. The effects of notches on graphite were also investigated to a lesser degree.

The results showed that notches affected the nominal strength of alumina considerably and that for severe notches the effect was greater for larger specimens. The failure stresses predicted by the Neuber analysis were in fair agreement with the strengths predicted by the Weibull volume analysis when the volume was defined as that encapsulating the material subjected to 50 percent of the peak stress. It is postulated that irreversible damage occurs at above 50 percent of ultimate for these types of materials. This event may permit local stress relief. At the roots of the notches, theoretical strengths of over 80,000 psi were obtained. Nominal tensile and flexural strengths on regular specimens were of the order of 42,000 psi and 36,000 psi, respectively, for the minimum volumes tested. Evidence was obtained that the fracture source may exist internally on this material at surface finishes finer than 25 rms.

Notches also reduced considerably the strength of graphite at 70°F and 4000°F, but not at 5000°F, where the effect of the stress concentration was negated by the "ductile like" behavior of the material.

TABLE OF CONTENTS

TABLE OF CONTENTS (continued)

ILLUSTRATIONS

ILLUSTRATIONS (continued)

ILLUSTRATIONS (continued)

TABLES

INTRODUCTION

This is the final summary report under Contract No. AF33(615)-1690 Modification No. 5A5(67-623) to extend the research on the experimental clarification of Weibull's volume effect theory on brittle materials and include notch effects. The alumina specimens for this program were prepared from the end sections of specimens used under an earlier program reported in AFML-TR-66-228. This alumina was a hot pressed material prepared by Avco. ATJ graphite was used to study the notch effects on a semibrittle material and provide a guide to the study on alumina.

The gas-bearing was used for all tensile evaluations. The flexural apparatus used in this work was designed to eliminate all major problems in flexural measurements such as friction at the load points and misalignments. Twenty-seven roller bearings were used in the design. As a result of this care, it seems that better agreement between tensile and flexural results was obtained.

The program essentially was divided into two phases. Phase I was the continuation of a study using ATJ graphite to determine the effects of notches on graphites and to provide information on the number of specimens required to forecast accurately an average ultimate strength, standard deviation, and coefficient of variation. Investigations were also made into the effect of specimen lot size on the Weibull parameters. The results of the Phase I study showed that notches did effect appreciably the strength of the graphite at 70°F and 4000°F, but that at 5000°F (where the material is more plastic) the effect of the notch was reduced considerably. The results of the study to determine the number of specimens needed to characterize statistically the tensile strength of graphite showed that 30 specimens could be used with good accuracy and that more than 30 did not increase appreciably this accuracy. As few as 5 specimens would be sufficient for many applications.

Phase II of this program was the study of notch effects on alumina. To carry out the intents and purposes of this part of the program, alumina specimens of two different sizes were used. There were 48 small and 53 large ones. Notches with two different surface finishes were machined into these specimens to provide stress concentration factors of 3, 5, and 8 for each size. To aid in reducing the data, 10 uniform tensile specimens with two different surface finishes and 20 flexural specimens with two different surface finishes were evaluated. The surface finishes of the polished specimens were about 8 rms, and the as ground specimens had a finish of about 25 rms.

Results of the Phase II investigations showed that notches did affect the strength of the alumina specimens. Reasonable agreements were obtained between the Neuber stresses in the notched specimens and the Weibull strengths found for the uniform tensile specimens as reported in AFML-TR-66-228. That is, stresses as high as 80,000 psi were imposed on volumes where the Weibull analysis predicted strengths of about 110,000 psi.

For the notches, it was necessary to define a volume subjected to a given stress or stress range in order to interrelate the Neuber stress and Weibull strength analyses. For a first comparison, the volume was selected from geometric considerations as the material outlined by extensions of the sides of the notches. With this assumption, the agreement between the Neuber stress and the Weibull strength was poor. However, the agreement became much better when the volume was defined as that material subjected to half of the Neuber peak stress. Since other work here had indicated that aluminas and beryllias had a "damage stress" at about 50 percent of the ultimate strength, this method of defining the volume seemed consistent. A tensile specimen of this alumina was then cycled at increasing stress levels and broke when the cyclic stress reached 55 percent of normal ultimate. Perhaps this is a fortuitous agreement, but it provided confidence in the method of selecting volume. As further confirmation, this treatment of volume for the flexural specimen provided consistency with the curve obtained for strength versus volume for the tensile specimens. A brief study of surface finish was made on the notches and regular specimens. Improving the finish from 25 rms to 5 rms had little influence on the strength of either suggesting that the fracture may be initiating internally for the finer finishes as has been hoped for this program. Earlier work had shown that surface finishes rougher than 30 rms did reduce the strength appreciably.

Normally, standard deviations should be plotted on curves relating variables. In this report, this procedure was not followed because most figures contain either the data points or comparison of so many averages that the symbols for standard deviation confused the appearance. The important standard deviations are in the text or tables.

APPARATUS

Tensile Apparatus

All of the tensile runs were performed in a gas-bearing tensile facility. A typical facility is shown in Figure 1. The facility consisted primarily of the

load frame, gas-bearings, load train, mechanical drive system, and instruments for the measurement of load-time to failure. A 5500°F graphite resistance furnace was used to provide heating for the high temperature evaluations.

Load Frame - The load frame was similar to most standard tensile frames with some modifications to accommodate the gas-bearings. Four steel columns supported the top and bottom base plates. These base plates contained sleeves and journals to align the upper and lower crossheads. A centrally located journal in each base plate accepted a partially threaded column of a precision mechanical screw jack which was secured to the base plate and imparted motion to the crossheads. The crossheads supported the gas-bearings and the load train.

Gas-Bearings - Spherical gas-bearings were employed for the tensile evaluations. Each bearing had a diameter of about 9 inches. This size bearing is sufficient to provide a load capacity of 15,000 pounds when an effective pressure of approximately 1200 psig is maintained within the annulus supplying the bearing nozzles. Gas is supplied by means of a manifold of eight commercial nitrogen cylinders controlled by a high capacity regulator.

This gas was metered by a conventional orifice run that incorporated flange taps and a differential pressure gage. In order to control flow, a hand-operated valve to each bearing was provided downstream of the meter run. Bleed valves also were provided to release the pressure on the gas lines and to float the bearing with a maximum control sensitivity. Flexible hoses were used as the link from the piping to the gas-bearings. These hoses imposed no external force on the specimen since they were not attached to the floating part (ball).

Flowmeters, pressure gages, electrical indicators to warn of bearing contact, and other instruments were provided as necessary and were chosen for their ability to provide accurate data while not encumbering the facility.

Load Train - The load train, see Figure 2, consisted of pull rods, load cell, and specimen grips. A standard 1000 pounds SR-4 Baldwin, type U-1 load cell, stated by the manufacturer to be accurate within $\pm \frac{1}{4}$ percent of capacity, was used for testing the graphite and small alumina specimens. This load cell, as received from the manufacturer, caused misalignments within the load train and bending stresses within the specimen. These misalignments were caused by an off-center weight in the load cell and by the failure of the threaded holes in each end to align on a common centerline. The off-center weight was balanced by a counter-weight and the misalignment of the centerlines of the holes was corrected by machining special adapters for the holes.

The load cell for the large alumina specimens was made by placing strain gages on the steel pull rod from the upper gas-bearing. These strain gages were calibrated in a standard Tinius-Olsen facility using also a standard Baldwin SR-4 5000 pounds load cell as a check up to 5000 pounds.

Two types of grips were used on this program. For the graphite and uniform tensile specimens, a collet-type grip was used; see Figure 3. As the compression nut was advanced, the three-piece compression ring performed two functions. It moved into the groove in the test specimen providing the gripping force required and uniaxial alignment while also forcing together the ground end faces of the test specimen and extension rod to provide parallel axial alignment. Consideration of this grip design and observation of the performance confirmed that alignment was a function only of the precision to which the parts were machined.

Because of the necessary size of the notched alumina specimens, special grips were used. These grips were sleeve-type precision grips. Those ends of the grips which accepted the pull rods from the gas-bearings were machined to within 0.0005 inches of the diameters of the individual pull rods, and the connections between the pull rods and the grips were made with $\frac{1}{4}$ inch steel pins. The other ends of the grips accepted sleeves that had been epoxyed onto the shanks of the specimen. These sleeves were machined to concentricity within 0.0005 inches and the inside diameter was machined 0.001 inches over the size of the specimen to allow for a thin epoxy film. The connections between each sleeve and the grip were made with $\frac{1}{4}$ inch steel pins.

Mechanical Drive System - Separate mechanical drive systems were provided for the upper and lower crossheads. The mechanical drive system for the upper crosshead consisted of a simple reversible electric motor coupled to the mechanical screw jack. The electric motor can be seen on the top base plate of the load frame; see Figure 1. Push-button control switches (jog or non-holding) were mounted on the load frame. This system had a rather fast rate of travel and was normally used in positioning the load train for installation of the specimen.

The mechanical drive system for the lower crosshead consisted of a precision mechanical screw jack, chain driven by a gear reducer. The gear reducer was driven by an Allispede unit (300-3000 rpm). With a 1025/1 gear reducer and different sprocket ratios, this system was capable of providing crosshead rates of from 0.006 in./min to 0.70 in./min. Different crosshead rates within this range were obtained by varying the speed setting on the Allispede Unit. By substituting another gear reducer, a different range of crosshead rates could be obtained.

The mechanical drive system for the lower crosshead had a relatively short travel and was used normally for applying the load or for making small changes in positioning the load train. The control switches for this system were mounted on the panel board and were the push-button (holding) type.

Both mechanical drive systems had limit switches to prevent overtravel of the crossheads. The upper crosshead also had positive stops to prevent the crosshead from falling should the limit switches fail to operate.

Instrumentation - Instrumentation consisted of the load cell, a constant d. c. voltage power supply, and a Moseley "Autograf" X-Y time recorder.

The load cell received a constant d. c. voltage input from the power supply and transmitted a millivolt signal directly proportional to the load to the recorder, thus providing a continuous plot of stress-time to failure.

Prior to beginning the initial run of this program, the small load cell was calibrated to dead weights. The load measuring system was calibrated in place periodically thereafter, again by hanging dead weights from the load cell.

5500° F Furnace - Figure 4 is a drawing of a 5500° F furnace employed for the high temperature graphite evaluations. The furnace consists of a resistively heated graphite element insulated from a water-cooled shell by thermatomic carbon. The furnace and specimen are purged with helium to provide an inert atmosphere. Ports with visual openings are provided on opposite sides of the furnace as a means of allowing strain analyzers to view gage flags on the specimens. Specimen temperatures are determined by optical pyrometer readings taken through another small sight port containing a sapphire window. A calibration curve was established for the loss through the sapphire window, and since the furnace cavity acts essentially as a blackbody, true temperature readings are obtained. Power is supplied to the heating element by means of 25 KVA variable transformer.

Flexural Apparatus - The flexural runs were conducted in a room temperature flexural apparatus designed to accommodate any specimen distortions and friction of the loading parts. This apparatus utilizes four-point loading and the load spans are 4 inches by 2 inches. Figure 5 is a schematic of the apparatus. In all there are 27 sets of bearings in the apparatus to eliminate friction, provide alignment within 1 mil, and allow for specimen warpage. In typical alumina

specimens the normal MOR value as calculated could be 5 to 10 percent high for friction, 5 to 10 percent low for alignment and 5 to 10 percent low for warpage. Wedging would not be a problem for breaks in the gage length since this was a four point apparatus.

Loading of the flexural fixture was accomplished in a Tinius-Olsen Universal Testing Machine. On several specimens, midpoint deflection was monitored with a dial gage. Loading was done incrementally and dial gage readings were taken at each load level.

Nominal specimen dimensions were $\frac{3}{4}$ inch by $\frac{1}{4}$ inch.

SPECIMEN MATERIAL AND PREPARATION

The two materials used for this program were ATJ graphite and high purity alumina. Both of these same materials were used in the earlier study under Contract No. AF33(615)-1690, and at that time an extensive study was made of the materials. The graphite specimens for this program were taken from the remaining billet of the two original 13 inch diameter by 14 inch long billets, and the alumina specimens were prepared from the end sections of some of the original alumina tensile specimens.

ATJ Graphite

The ATJ graphite specimens were machined from a billet 13 inch in diameter by 14 inch long prepared by National Carbon Company. The billets of this size were selected for the original program since they felt that it would be the most reproducible and the best quality that could be obtained.

The density of each specimen was checked to determine the consistency of the material. This was accomplished by cutting constant diameter rods of fixed lengths (specimen blanks) and measuring the density of these rods. The density values are given in Tables 1 and 2 along with other data that will be discussed later. As can be seen the density values were fairly consistent ranging from 1.680 gm/cc to 1.745 gm/cc. The density values of the specimens reported in AFML-TR-66-228 ranged from 1.74 gm/cc to 1.78 gm/cc. The differences in the ranges of density values were attributed to the differences in the billets and the differences in the cutting plans.

The graphite specimens were machined from the billets in such a way so that a maximum number of specimens could be obtained per unit of material while insuring the best consistency from specimen to specimen. The cutting

plans for the graphite specimens from the billet are shown in Figures 6 and 7. A specimen number was devised to identify each specimen as to its location within the billet. Consider the number A-i-7

A - slab designation (Figure 6)
i - location with respect to a circle of radius equal to one-fourth of the billet diameter and the outside diameter; i - inside D/4 radius, c - centered on D/4 radius, m - middle; e - nearest outside edge (Figure 7)
7 - location with respect to reference axis (Figure 7).

The study carried out with the graphite specimens was a continuation of the graphite work in AFML-TR-66-228 and paralleled the work done on alumina in both AFML-TR-66-228 and this report.

A total of 119 graphite tensile specimens were employed for this phase of the program. Of these 119 specimens 84 had a uniform gage section, Figure 8, 28 had a notch machined into the gage section, Figure 9, and 7 specimens had a square cross-section in the gage. The square specimen's gage section was 0.250 inch square by 1.00 inch long. From the 84 uniform gage tensile specimens, 55 yielded room temperature data, 13 for high temperature (4000°F and 5000°F), 6 were broken in handling, and 14 failed outside the gage section. The data from these 14 specimens were not used in the analysis.

The 14 specimens that failed out of the gage section represent about 17 percent of the total number of uniform tensile specimens that were evaluated. These were more specimens than normally fail in this area. It was noted that several of the specimens fractured in what appeared to be isolated porous regions of the material; however, there was not apparent explanation, such as a visible internal flaw, for the majority of the radius breaks.

Of the 28 notched specimens, 9 were evaluated at room temperature, 14 at elevated temperatures (4000°F and 5000°F) and 5 were broken inadvertently in handling. Of the 7 square specimens, 5 failed in the gage and 2 failed in the radii. All of the square specimens were evaluated at room temperature.

Alumina

The alumina specimens were machined from the end sections of specimens used in a prior program. The data for the original specimens were reported in AFML-TR-66-228. Typical specimens whose end sections were used are shown in Figures 10 and 11.

The original alumina body was hot pressed by Avco corporation from Linde "A" grade powder. A total of 24 tiles (12" x 12" x 1⅛") were prepared by a hot pressing technique using graphite dies at a temperature of 1525°C and a pressure of 2000 psi.

The original alumina tensile specimens machined from these tiles exhibited a wide spread in strength values. This spread motivated a close study of the material which has been reported in AFML-TR-66-228 and will not be repeated here. Figure 12 is a plot of tensile strength versus tile number for the original specimens. The specimens for this program were taken from the end sections of specimens from tiles 770, 774, 790, 800, 808, and 826. The tiles were selected so that the effect of material variability would be negated as much as possible.

A total of six configurations (types) of alumina specimens were evaluated under this program. The specimens can be generally classified under two types, small and large, and there were three variations of each type. In order to prevent confusion, the specimen types were labeled S3, S5, S8, L3, L5, and L8 where S signified small and L large, and the number following the S or L was the stress concentration factor for the notch in the specimen. Figures 13 and 14 show pictorially the differences between the large and small specimens and the differences between specimens of the same size but different notch configurations.

The specimens, which were machined at Southern Research, had the configurations shown in Figures 15 and 16. All specimens were machined with diamond grinding wheels. Special diamond wheels as small as 0.004 inch thick were used to machine the small notches. A 20:1 optical comparator was used to examine each notch after it was machined, and these examinations showed that the notch very closely resembled the desired configuration. Only very slight wallowing was detected and could be seen only at the top of the notch.

One half of the specimens were polished in the notch section. Polishing was accomplished using a cotton string charged with nine micron diamond dust. The specimens were turned in a lathe while the string was held taut in the notch. Preliminary tests showed that about 10 minutes of polishing time was required to obtain a good polished surface. There was no way to measure the actual surface finish because of the small area involved. Estimates were made by comparing optically the finishes to known finishes on the same material. The polished specimens had a surface finish of about 10 rms and the as ground finish was from 20-25 rms.

A total of 101 notched alumina specimens were used in this program. These were distributed as follows:

Type S3 -	As Ground	9 Specimens
	Polished	7 Specimens

Type S5 -	As Ground	8 Specimens
	Polished	8 Specimens
Type S8 -	As Ground	8 Specimens
	Polished	8 Specimens
Type L3 -	As Ground	9 Specimens
	Polished	9 Specimens
Type L5 -	As Ground	8 Specimens
	Polished	8 Specimens
Type L8 -	As Ground	11 Specimens
	Polished	8 Specimens

This distribution provided common stress concentrations between two different sizes of specimen and two different surface finishes.

Because of the necessary sizes of the specimens, see Figures 15 and 16, special provisions for gripping them had to be made. Precision collets were machined which were epoxyed to the ends of the specimens. The collets were then gripped using a pin connection. Figure 17 is a schematic showing the gripping arrangement. The internal diameter of the collet was machined to within 0.001 inch of the specimen and the outside diameter was machined concentric within the inside diameter to within 0.0005 inch. The collets and specimens were assembled in a set of ground V-blocks.

In addition to the notched specimens, 10 specimens of the type shown in Figure 18 and 20 flexural specimens were machined. The tensile specimens were used to examine the effects of surface finish (in the range of good finishes at better than 30 rms) and the flexural specimens were employed to provide a different stress gradient. It was not possible to be as selective in the choice of material for these specimens because of the size requirements.

Selection of Notch Configurations - Notches were machined in both graphite and alumina specimens. Factors affecting the selection of the notch size and shape were:

1. Available specimen sizes
2. Material to be machined and equipment available to perform the machining
3. Amenability of configuration to analysis

The alumina specimens were fabricated from the end sections of specimens used under a prior program. The nominal dimensions of the sections were 1 inch diameter by 3 inches long for the large specimens and $\frac{1}{8}$ inch diameter by $1\frac{1}{2}$ inch long for the small specimens. Although there was additional material on the end sections, it was undesirable to use this material since it had been, in effect, proof tested.

Notches which gave three stress concentration factors were machined in both the large and small specimens. The depth of the notch was to be no greater than one-tenth the diameter of the gage section of the specimen. The diameter of the small specimens was selected to be 0.250 inch so that the depth of the notch could not exceed 0.025 inch.

By machining a notch 0.024 inch deep by 0.004 inch wide with a 0.002 inch radius, a stress concentration of 8 could be obtained. A diamond wheel would grind these notch dimensions. Preliminary tests with the grinding wheel indicated the notch could be ground successfully in the alumina specimens.

To obtain a range of stress concentration factors, notch radii were calculated for stress concentration factors of 3 and 5, always maintaining the same notch depth of 0.024 inch on the small specimens.

The gage diameter of the large specimens was set at 0.625 inch and the notch depth at 0.063 inch. Notch radii were employed that gave stress concentration factors of 3, 5, and 8 as before.

These notches had sharp outer corners which are not compatible with Neuber's assumptions for his theoretical stress distribution; however, observing Figure 19 it can be seen that the curves giving the stress concentration factors for notches with smooth and sharp center corners are fairly close together so that the analysis was not affected adversely.

THEORETICAL CONSIDERATIONS

It is impossible to state an exact value for the ultimate strength of a material since some scatter will result from repetition of experimental measurement, regardless of how closely the procedure is duplicated. In some cases the data scatter is considerable. Weibull (1, 2) recognized this fact and reasoned that it should be possible to use the elementary theories of probability and statistics to determine the probability that a given stress conditions would produce fracture.

According to Weibull's theory, a random distribution of flaws exists in each material and the probability that a given stress environment will cause fracture depends on the volume of the body, the state of stress, and certain constants associated with the material.

For a uniform tensile specimen where the stress condition and volume under stress are well defined, Weibull's theory can be expressed rather simply once a material function is assumed. Weibull assumed a material function of the form

$$n(\sigma) = \left(\frac{\sigma - \sigma_u}{\sigma_o}\right)^m$$

where m, σ_u, and σ_o are constants. The strength volume relationship for uniform tensile specimens then becomes

$$\left(\frac{\sigma_1 - \sigma_u}{\sigma_2 - \sigma_u}\right) = \left(\frac{V_2}{V_1}\right)^{\frac{1}{m}}$$

A program carried out by this laboratory to determine experimentally whether or not Weibull's theory would be applicable to a brittle material such as hot-pressed alumina showed that there was definitely a volume effect, but that for the particular material the values of m σ_u, and σ_o were not constant. These findings were reported in AFML-TR-66-228.

When the stress field is not uniform, as in the case of a notch tensile specimen or a flexural specimen then it is not clear what volume should be used when determining the probability of fracture for a given stress condition. Also, since the stress is not uniform, it is not readily apparent what value of stress should be used if an equation like the one above is to be used.

The stress distributions developed by Neuber were used in conjunction with the Weibull theory to gain some insight into the relationships between stress, stress gradients and volume for brittle materials. This will be discussed further.

Synopsis of Weibull's Theory

The distribution function for the probability of fracture, derived by Weibull, based on the "weakest link" theory of fracture is

$$S = 1 - e^{-B} \qquad (1)$$

where S is the probability of fracture and B is defined as the risk of fracture. B is a function of the stress and for a uniform stress is proportional to the volume. For an arbitrary distribution of stress in an isotropic body, the risk of fracture is given by

$$B = \int_V n(\sigma)\, dv \tag{2}$$

where $\int_V$ denotes a volume integral and $n(\sigma)$ is the function which expresses the dependence of the risk of fracture on the stress, σ. The function $n(\sigma)$ is independent of position and the direction of the stress.

If the material is an anisotropic one, $n(\sigma)$ will be a function of the stress, the coordinates, and possibly of the direction of the stress. Weibull indicates that in many cases an apparent departure from isotropy may be due simply to a difference in the material properties on the surface and the interior of the material as a result of the method of manufacture of the material. In this case B could be represented by

$$B = \int_V n_1(\sigma)\, dv + \int_A n_2(\sigma)\, dA \tag{3}$$

where $n_1(\sigma)$ is the material function for the interior of the body, $n_2(\sigma)$ is the material function for the surface, and $\int_A$ an area integral. The form for $n(\sigma)$ most frequently used is

$$n(\sigma) = \left(\frac{\sigma - \sigma_u}{\sigma_o}\right)^m \tag{4}$$

According to Weibull (3) the only merit of this formula for $n(\sigma)$ is to be found in the fact that it is the simplest mathematical expression of the appropriate form which satisfies certain necessary conditions. Also experience has shown that, in many cases, it fits the observations better than any other known functions.

Now B becomes, for a uniform stress distribution,

$$B = \int_V \left(\frac{\sigma - \sigma_u}{\sigma_o}\right)^m dv \tag{5}$$

where

σ = actual fracture stress of specimen
σ_u = a stress below which fracture cannot occur
σ_o = a normalizing factor

m = constant representative of the flaw density of the material

Substitution of Equation 5 into Equation 1 yields:

$$S = 1 - \exp\left[-\int_V \left(\frac{\sigma - \sigma_u}{\sigma_o}\right)^m dv\right] \qquad (6)$$

Let B_1 be the risk of fracture under given set of circumstances for Specimen 1 and B_2 be the corresponding values for Specimen 2. Now by requiring that the two specimens have the same probability of fracture for a given loading condition, the equation

$$\int_{V_1} \left(\frac{\sigma_1 - \sigma_u}{\sigma_o}\right)^m dV = \int_{V_2} \left(\frac{\sigma_2 - \sigma_u}{\sigma_o}\right)^m dV \qquad (7)$$

results. For two uniform tensile specimens where σ_1 and σ_2 are the average tensile strengths the equation reduces to

$$\left(\frac{\sigma_1 - \sigma_u}{\sigma_2 - \sigma_u}\right) = \left(\frac{V_2}{V_1}\right)^{\frac{1}{m}} \qquad (8)$$

For non-uniform stress fields Equation 7 must be used unless some "characteristic" stress and volume, which relate to say the uniform tensile specimen, can be determined.

Synopsis of Neuber Relationships (4)

The relationships to be discussed here are for a notched tensile specimen loaded uniaxially. In order to keep the mathematical analysis relatively simple only the two-dimensional case has been considered.

Because the problem has been considered as a two-dimensional one, the model is a thin bar with a shallow notch on each side, Figure 20. In order to more easily define the geometric restrictions created by the notch, it is convenient to employ a coordinate system different from the usual x-y coordinate system. The one used by Neuber is defined by the equations:

$$x = u + \frac{u}{u^2 + v^2}$$

$$y = v - \frac{v}{u^2 + v^2} \qquad (9)$$

For large values of u or v the coordinate lines u = constant and v = constant approach the x-y coordinate lines; that is to say, the u-v coordinates practically coincide with the x-y coordinates except in the vicinity of the notch, see Figure 21. The value of u which is to be definitive for the edge of the notch will be designated u_o. The depth of the notch, t, which results from the difference in x at the base of the notch $(u, v) = (u_o, o)$ and at a great distance away from the notch $(u, v) = (u_o, \infty)$.

$$t = x\Big|_{\substack{u = u_o \\ v = 0}} - x\Big|_{\substack{u = u_o \\ v = \infty}} = \frac{1}{u_o} \tag{10}$$

The curvature is given by the expression

$$\frac{1}{\rho} = \frac{\partial \phi}{\partial s} \tag{11}$$

where ϕ is the angle of the curve tangent to a fixed direction, ρ is the radius of curvature, and ds is an element of arc length on the curve. For the coordinate system under consideration, it can be shown that at the root of the notch

$$\frac{1}{\rho} = \frac{2 u_o}{(1-u_o^2)^2} \tag{12}$$

The notch curvature, defined to be t/ρ, is given by

$$\frac{t}{\rho} = \frac{2}{(1-u_o^2)^2} \tag{13}$$

To determine the stress distribution, Neuber used his three-function theory. The general procedures for his method are outlined in the Appendix and will not be repeated here. In terms of the u-v coordinates the stress function used by Neuber was

$$F(u, v) = \frac{\sigma_n}{2}(u - u_o)^2 \left[1 - \frac{1}{(2u_o^2 - 1)(u^2 + v^2)}\right] \tag{14}$$

where σ_n is the nominal stress across an unnotched portion of the specimen. The normal stress σ_u and σ_v then may be written in terms of the derivatives of F(u, v).

$$\sigma_u = \frac{1}{h}\frac{\partial}{\partial v}\left(\frac{1}{h}\frac{\partial F}{\partial v}\right) + \frac{1}{h^3}\frac{\partial h}{\partial u}\frac{\partial F}{\partial u}$$

$$\sigma_v = \frac{1}{h}\frac{\partial}{\partial u}\left(\frac{1}{h}\frac{\partial F}{\partial u}\right) + \frac{1}{h^3}\frac{\partial h}{\partial v}\frac{\partial F}{\partial v} \tag{15}$$

where σ_u and σ_v are the stresses normal to the lines u = constant, and v = constant respectively, and h is the factor of distortion (see Appendix) for the particular coordinate system.

$$h = 1 + \frac{2v^2 - 2u^2 + 1}{(u^2 + v^2)^2} \tag{16}$$

The stress at the root of the notch is given by the equation

$$\sigma_v \Big|_{\substack{u = u_o \\ v = 0}} = \sigma_n \frac{u_o^2 (2u_o^2 + 1)}{(2u_o^2 - 1)(u_o^2 - 1)} \tag{17}$$

Now from Equation 13 we can write

$$u_o^2 = 1 + \sqrt{\frac{1}{\frac{t}{2\rho}}}$$

so that the stress concentration factor $\frac{\sigma_v}{\sigma_n}$ can be written

$$K_t = \frac{\sigma_v}{\sigma_n} = 3\sqrt{\frac{t}{2\rho}} - 1 + \frac{4}{2 + \sqrt{\frac{t}{2\rho}}}$$

The dashed curve in Figure 19 shows the stress concentration factor, K_t versus notch curvature, $\frac{t}{\rho}$, plotted from the above equation. Included on the graph is the same plot for notches with sharp outer corners obtained by Neuber using an approximate technique.

DATA AND RESULTS

Graphite

The results for the ATJ graphite are given in Tables 1, 2, and 3 and Figures 22 through 29.

For the uniform tensile specimens evaluated at room temperature, the densities varied from 1.685 gm/cm³ to 1.760 gm/cm³ and the tensile strengths ranged from 3190 psi to 4640 psi. Strength versus density is plotted in Figure 22 for these specimens. The method of least squares was used to determine the

straight line that best described the data points. This line is shown plotted in Figure 22. Note that this line has a positive slope indicating that the tensile strength increased with increasing density; however, a statistical analysis revealed that the correlation between strength and density was not significant. In other words, there was no definite relationship between strength and density.

The average strength of the uniform tensile specimens at room temperature was 3950 psi. This value compared favorably with the values of 4250 psi, 3940 psi, 4070 psi, and 4160 psi for specimens having the same volume whose data were reported in AFML-TR-66-228.

Using these room temperature data, a study of the number of specimens needed for an accurate determination of the material characteristics was carried out. The method of the study was to select random subsets of the tensile strengths of size N. That is, there were "N" number of coupons in each subset. The strength values from each of these subsets were used to calculate the average tensile strength, the standard deviation, the coefficient of variations, and the Weibull material parameters. The values of N used were 10, 15, 20, 30, and 40, and five subsets of each size were selected.

The results are presented in Table 3 and Figures 23 and 24. Figure 23 shows that the average tensile strength when calculated with as few as 10 values fell within 5 percent of the average strength calculated when all 55 values were used. Also there was no advantage in providing 40 tensile strength values over 30 values when the main concern was average strength. From Figure 24 it is seen that the standard deviation was calculated to within about 11 percent with 30 values, and that the use of 40 values did not increase the accuracy by an appreciable amount.

From these data it appears that a sample size of 30 could be used to statistically characterize the strength properties of this graphite with good accuracy and that more values than 30 would not increase the accuracy to any appreciable degree. As few as 5 samples would be sufficient for many applications. With 15 samples the tensile strengths were within 2.5 percent of the mean and the standard deviations were within 19 percent. Another way of considering the data is to say that for 10 data points, differences in average strengths of $\pm$ 4% or more would be necessary for significance. This agrees with the range observed in AFML-TR-66-228 mentioned earlier.

Table 3 reveals that the range of values obtained for the Weibull parameters was still considerable with as many as 40 strength values, hence it is impossible to determine from these data how many values would be required to predict these numbers with any confidence. That this is true supports the idea that these

Weibull parameters m, σ_u and σ_o are not truly material parameters or properties. The equations

$$\bar{\sigma} = \sigma_u + \sigma_o V^{-\frac{1}{m}} \Gamma\left(1 + \frac{1}{m}\right)$$

$$a = \sigma_o V^{-\frac{1}{m}} \sqrt{\Gamma\left(1 + \frac{2}{m}\right) - \Gamma^2\left(1 + \frac{1}{m}\right)}$$

show that the average strength and standard deviation can be expressed as functions of the m, σ_u, and σ_o when the Weibull theory is assumed. These are the only variables in the equations once the specimen configuration is determined. The data have shown that the mean (average) strength $\bar{\sigma}$ is reasonably constant when as few as 10 values are used for its computation; however, the values of m, σ_u, and σ_o are quite inconsistent for this many values, or even 40 values.

For all of these parameters, the numbers of specimens required for reasonably accurate values were in fair agreement with the observations for the alumina specimens reported in AFML-TR-66-228.

As seen in Table 3, the values for the Weibull parameters calculated from the 55 strength values were m = 4.43, σ_u = 2400 psi and σ_o = 120 psi. Figure 25 is the plot of Log Log $\left[\frac{N+1}{N+1-n}\right]$ versus Log $(\sigma - \sigma_u)$ for these values. The values m = 4.43, σ_u = 2400 psi and σ_o = 120 psi were used in Equation 8 to obtain a strength - volume curve. The curve is shown plotted in Figure 26 along with the data points reported in AFML-TR-66-228. This curve represents a constant risk of rupture or probability of fracture. The straight line shown in Figure 26 more nearly agrees with the data, but the relation describing this straight line cannot be related to the function $n(\sigma)$ suggested by Weibull to express the dependence of the risk of fracture on the stress σ.

Consider now the notched tensile graphite specimens. As already pointed out, the notch configuration used on these specimens gave a theoretical stress concentration factor of 7.3 at the notch root for a notch with smooth corners and a stress concentration factor of 8 for a notch with sharp corners. The nature of the graphite material made it difficult to obtain a true radius of the desired dimensions at the root of the notch. There was a tendency for

the grinding wheel to wallow when cutting the notch. Figure 27 is a schematic comparing the desired and the actual notch shape that was obtained. Because the notch was not as sharp as required for a stress concentration factor of 8, the stress distribution for a stress concentration factor of 7.3 was used.

Using an unnotched portion of the gage as a reference, the average nominal strength for the specimens evaluated at room temperature was 1740 psi (σ_n = 1740 psi). If we consider the reduced section as a base, the average nominal strength was 2690 psi (σ_r = 2690 psi). Neuber uses σ_n in his stress analyses; however, it is more appealing from a material standpoint to employ σ_r. At 4000°F the uniform specimens had an average strength of 5140 psi and the notched specimens had a reduced section strength of σ_r = 3360 psi; at 5000°F the uniform specimens had an average strength of 6540 psi and the notched specimens had a reduced section strength of σ_r = 5700 psi. These data are plotted in Figure 28.

The notch decreased the nominal strength (σ_r) of the specimens evaluated at room temperature and 4000°F by 32 percent and 34.5 percent, respectively; whereas, the notch decreased the strength of the specimens evaluated at 5000°F by only 13 percent. Thus the notch was as effective as a "strength reducer" at 4000°F as at room temperature. Considering the stress-strain curves for ATJ graphite in Figure 29, this was not entirely unexpected, since the stress-strain curves for 70°F and 4000°F are very similar with little plastic accommodation. There is slightly more strain for the 4000°F specimen, but there is also higher modulus. On this basis one would have to conclude that the material was just as brittle at 4000°F as at room temperature.

Still considering Figure 29 we see that 4000°F is about the transition point from the brittle to "ductile" range. The curve at 4500°F has a lower modulus with more plastic strain and at 5000°F has still a lower modulus with considerably more "plastic" strain. Hence, based on the above observations, one would expect the notch to be less effective at 5000°F which was the case.

The average strength of the five square tensile specimens was 3600 psi. This point is shown on the strength-volume graph for graphite in Figure 26. Note this specimen was in the range of volumes where strength appears to be unaffected. The individual strength values were 3570 psi, 3570 psi, 3810 psi, 3890 psi and 3150 psi. The average of 3600 psi is about 10 percent below the average of the 55 round specimens. In a separate controlled study, ten specimens with both square and round gages in each were tested providing an even distribution of fractures between the square and round sections. Thus the round section in this experiment was 22% stronger. Since the prior discussion has shown that graphite is affected by stress concentrations, the indication is that the square corners of the specimen provide a type of stress concentration.

To provide further comparison of test methods, strength values for some floated sleeves and for some flexural specimens are shown on Figure 26. A

description of the apparatus for the floated sleeves and the data are given in the Appendix. The ten flexural runs were made on the roller-flexural apparatus described previously. The values for the sleeves (3490 psi) were lower than for the round specimens (3960 psi for equivalent volume) and in close agreement with the square tensile ones (3600 psi); however, comparative sleeve data confirmed the volume effect even for them. The values for the flexural specimens were higher (4550 psi) in spite of the sharp corners, probably because of stress-blunting, difference in compressive and tensile elastic modulus or nonelastic behavior, and shift in the force center (see Appendix C). Of course, the sharp corners in a flexural specimen would not distort the strain lines as for a rod or ring. The stress gradient in a flexural specimen is so steep that meaningful analyses remain for proof.

Alumina

The results of the evaluations on the alumina specimens are presented in Tables 4 through 7 and Figures 30 through 38.

Surface Finish Effects - Figure 30 is a plot of the nominal tensile strength (σ_n) versus stress concentration factor for all of the notched alumina specimens. Viewing this figure along with Table 4 we see that surface finish had a minor roll in the outcome of the results for the notched specimens.

Ten specimens without notches were explored to see if a difference of 25 and 5 rms should influence the strength (recall that rougher finishes reduced the strength). On these ten, five were in the as ground condition and five were polished. The as ground specimens had surface finishes in the range from 23 to 27 rms (profilometer in all cases). The polished specimens had surface finishes from 4 to 8 rms. The results of these evaluations are presented in Table 5. The polished specimens with 4 to 8 rms had an average strength of 38,000 psi with a high value of 40,500 psi and a low value of 36,000 psi. The as ground specimens with 23 to 27 rms had an average strength of 39,100 psi with extreme values of 41,800 psi and 35,000 psi. Thus the rougher as ground specimens were a little stronger than the polished ones; however, the difference was not significant and one would have to conclude that surface finish did not affect the tensile strength over the range of surface finishes (all good) considered for unnotched specimens. The thought occurs that after a surface finish becomes sufficiently fine, the fracture is initiated internally and, indeed, volume effects are controlling.

In addition to the tensile specimens used for the surface finish evaluations, 20 flexural specimens were evaluated. These 20 specimens were divided into four equal groups of five. The groups were provided by using two different surface finishes, as ground (25 rms) and polished (8 rms), and by providing 10 of the specimens with sharp corners on the tensile side and 10 specimens with rounded corners on the tensile side. Thus the four groups were (1) polished round corners, (2) polished square corners, (3) as ground round corners, and (4) as ground square corners.

The results of these evaluations are given in Table 6. For the specimens with square corners the polished specimens had a slightly higher strength of 36,200

psi than the as ground specimens with 35,000 psi; for the specimens with rounded corners, the polished ones were again slightly stronger at 35,700 psi than the as ground ones at 34,600 psi. As seen, the difference was not significant (3 percent) so that surface finish (within this range-all good finishes) did not affect the flexural results significantly. The condition of the corners, square or rounded, did not affect the data significantly. This may be consistent with the results on surface finish since rough corners would introduce cracks and stress concentrations in much the same way as a poor surface finish would. Further, the flexural strengths of these specimens were rather close to the tensile strengths (gas-bearing) of the parent specimens from which they were removed. Recall that square graphite tensile specimens were 10 percent weaker than round ones. Perhaps the small grain size and good finishes for the alumina minimized the corner effects.

Notch Effects - The effect of notches on brittle materials is considered sometimes as an extension of surface finish effects. Data taken by this laboratory on another alumina have shown considerable dependence between strength and surface finish. These earlier data, shown in Figure 31, are for a much wider range of surface finishes than were considered here. Note the similarity between this figure and Figure 30 which was the plot of strength versus stress concentration factor.

However, for a brittle material, such as alumina, there are other test "conditions" that need to be considered along with surface finish. Some of these conditions are not considered when dealing with ductile materials. One of these in particular is volume. The results reported in AFML-TR-66-228 show that the strength of at least some brittle materials (hot-pressed alumina) does depend on the volume under stress. The consideration of notch effects and volume effects jointly presents a very difficult design problem which will not be solved easily.

There are two major contentions on the effects of notches (stress concentrations) on brittle materials. These are:

1. Brittle materials are highly sensitive to notches because there is no plastic flow, and hence no local stress relief can take place in the areas of severe changes in geometry.
2. Brittle materials are relatively insensitive to notches because they already contain stress raisers which may be an order of magnitude greater than can be artifically induced.

The overall results of this investigation have shown that brittle materials are sensitive to notches, but not as sensitive as predicted by the contention of no plastic flow. That is, the volume effect may control.

Let us consider the general effects of the notches used on the various specimens in this program before proceeding on to a more detailed analysis.

For the purposes of discussion, a volume needs be considered that is characteristic of each specimen type. The volume to be considered here is that reduced section of the specimen created by the presence of the notch. It is the volume of a disc whose diameter is equal to the diameter of the reduced section and whose thickness is equal to the width of the notch, see Figure 32.

Figure 33 is a plot of strength versus volume showing the data from the original tensile specimens reported in AFML-TR-66-228. These data are represented by the circles. There are also three curves shown on the graph. One is the best straight line fit for the original data. The other two are curves showing the strength-volume relationship for uniform tensile specimens of Equation 8. The constants used in this relationship were determined from two different sets of ultimate strengths from specimens having two different volumes. The computation of these constants was reported in AFML-TR-66-228.

On Figure 33 points are plotted for each of the notched specimens where the strength value used was the tensile stress at failure across the reduced section, σ_r, and the volume of the disc outlined by the notch. The points are labeled L3, L5, L8, S3, S5, S8 where the L and S refer to large and small specimens and the numbers refer to the nominal theoretical stress concentration factor so that they may be readily identified. Notice that for each set of specimens, small and large, the effect of the notch was as predicted by Contention 1; the strength (σ_r) decreased as the notch became more severe.

Now consider the points S8 and L8. From these points we see that the effect of the notch with a given stress concentration factor was not the same on two geometrically similar but different sized specimens. The small specimen with a stress concentration of 8 was stronger than the large specimen with the same stress concentration factor. This can also be seen to some extent on the small and large specimens with a stress concentration factor of 5. The reverse effect is seen for the specimens with a stress concentration factor of 3; however, in this and the remaining analyses more emphasis will be placed on the results obtained with the sharp notch specimens than on the results obtained with the other specimens. It is believed that the stress analysis and other assumptions become more accurate and applicable as the notch becomes more severe ; however, the notch given the stress concentration factor of 8 was the sharpest that could be machined in this material.

Now let us use the results of Neuber's stress analysis to obtain the theoretical stress σ_v (maximum) at the root of each notch. This is done by multiplying the nominal stress across an unnotched portion of the gage (σ_n) by the appropriate stress concentration factors. The factors used here are the ones directly from Neubers' analysis and are not corrected for the sharp outer corners of the notch. These points are plotted as triangles in Figure 33. The volume used here is again the volume outlined by the notch. The points show to a greater degree the

different effect of the same stress concentration factor on different size specimens. Note that the curve faired in to approximate the results of the small specimens has the same general slope and shape as the Weibull strength-volume curves in the vicinity of smaller volumes; whereas, the curve faired in for the large specimens has the general slope and shape as the Weibull curves for the larger volumes.

The data and calculations presented thus far do not agree to any great extent with the Weibull extrapolation to small volumes as reported in AFML-TR-66-228. The strength values taken using only the area of the reduced section are well below the predicted tensile strength values. By neglecting the effect of the stress concentrations (σ_n), the volume effect appeared to work in reverse. By using the peak stress [σ_v (maximum)] as the strength value, the points fall above the straight line through the original data, but still generally below the Weibull curves. The volume calculation at this point is more intuitive (or geometric) than theoretical, but is the type of calculation that is easily made and is not as bad as it might first be supposed. Later we will return to a better definition of the volume but first consider the general nature of stress intensification as predicted by Neuber and how the volume might be determined with more theoretical or realistic basis.

Weibull-Neuber Analysis - Figures 34, 35, and 36 are contour maps of the stress distribution in the vicinity of the various notches. Shown on each figure is an outline of the specimen under consideration along with the u-v coordinate system used for the calculation of the stresses. In the vicinity of the notch root, lines are shown which represent a constant value of $\frac{\sigma_v}{\sigma_n}$ where σ_v is the stress perpendicular to a line v = constant and σ_n is the nominal stress in an unnotched portion of the gage. The smallest value of $\frac{\sigma_v}{\sigma_n}$ shown is 1.5. This corresponds to a $\frac{\sigma_v}{\sigma_r}$ value of 1.0, where σ_r is the nominal stress across the specimen at its smallest section. It is felt that σ_r is more meaningful from a material's standpoint than σ_n, but Neuber has used σ_n in the derivation of his equations. Neuber's analysis also gives the values for $\frac{\sigma_u}{\sigma_n}$ where σ_u is the stress perpendicular to lines u = constant. This stress is essentially a radial stress created by the presence of the notch. Figure 37 shows a composite stress distribution where both $\frac{\sigma_v}{\sigma_n}$ and $\frac{\sigma_u}{\sigma_n}$ are given for all of the notch configurations. This distribution is taken along a radius extending from the root of the notch toward the centerline of the specimen. We see here that $\frac{\sigma_u}{\sigma_n}$ never exceeds 1.0. According to Weibull some "stress σ" which takes in account both stresses σ_v and σ_u should be used; however, because of the relative magnitudes of σ_v and σ_u in the vicinity of the notches only σ_v will be used.

Consider now Figure 34, the stress distribution for the small notch. The scales shown on the figure are for the S8 specimens. The L8 specimens are $2\frac{1}{2}$ times larger in all dimensions concerning the gage portion. Table 7

shows the values obtained from the calculations of volumes subjected to different conditions of stress. For example, the volume of material in the S8 specimen which is subjected to a stress $\frac{\sigma_v}{\sigma_n} \geq 2.0$ is 0.0028 inch^3. This volume appears as a washer whose cross-section is outlined by the curve $\frac{\sigma_v}{\sigma_n} = 2.0$ in Figure 33.

The problem is to select that volume and stress meaningful from the point of view of the Weibull theory. To select a fixed condition for determining the volume under stress for each specimen would not be very appropriate. For instance, to select as the reference volume that volume for which $\frac{\sigma_v}{\sigma_n} \geq 4$ would be meaningless for a specimen whose notch gave a stress concentration factor of 3. In the same way to chose a volume for which $\frac{\sigma_v}{\sigma_n} \geq 1.5$ would not be meaningful for a specimen where the notch gave a stress concentration factor of 8. To illustrate this, refer to Table 4. We see here that the average value for σ_n for the as ground S8 specimens was 10,840 psi. Then $\sigma_v = 1.5\ (\sigma_n) = 16,300$ psi, but the so called "zero stress" from one set of data in AFML-TR-66-228 was 21,500 psi. Hence to consider the volume for which $\frac{\sigma_v}{\sigma_n} \geq 1.5$ using this data would not be meaningful.

One method of selecting the volume of material that is subjected to stress range that will cause fracture is to define a "damage stress" below ultimate and above which failure is an inevitability. This damage stress has been observed here recently on different beryllias where the regular ultimate strength from normal tensile experiments was 100 percent (about 19,000 psi), the ultimate strength after 20 to 40 stress cycles to 70 percent of regular ultimate was reduced to 85 percent regular ultimate, the precision elastic limit (first detectable departure from elastic response) was 70 percent of regular ultimate, and initial irreversible creep was detected at 40 to 60 percent of regular ultimate. Thus, below 40 percent of regular ultimate, the material behaved elastically and exhibited no creep failures.

With this background in mind, one of the specimens made from the hot pressed alumina used in this program was cycled 6 times to about 50 percent regular ultimate and had a subsequent ultimate of 55 percent of regular ultimate. Thus this material also appears to have a damage stress.

The damage stress may be related to a kind of supercrazing that is a combination of micro and macrocracking that invades a volume of the material before fracture proceeds and starts at well below the ultimate. This nonelastic

behavior at such a low stress is alarming since it challenges the use of the elastic theory in many applications such as study of beams, fracture energies and crack propagations; however, there is mounting evidence from the point of view of mechanics. For example, in addition to the above cases, gross macrocracks are found in the tail ends of broken tensile specimens, flexural tests suggest blunting of peak stresses as an explanation of deformations and strengths being higher than theoretical, and many broken tensile specimens of some beryllias and some aluminas have rounded ends and long ($\frac{1}{8}$") sections that have pulverized to a powder upon post mortem inspection.

Admittedly, all of this information requires extensive confirmation in extensive programs directed to this end. However, let us use this damage stress (50 percent of ultimate) as a method of selecting the volume in the notched samples that may be used with the Weibull analysis. That is, let us compare the Neuber stresses with the Weibull strengths, selecting the Weibull volumes as those subject to a stress greater than 50 percent of the peak stress. This means that the volume for the notches with a stress concentration factor of 3 would be defined as that volume subjected to a stress greater than 1.5 of σ_n. For a stress concentration factor of 5, the Weibull volume would be that volume subjected to a stress greater than 2.5. For a factor of 8, the volume would that subjected to a stress greater than 4. Since this volume results from a damage stress, perhaps it is a critical volume that is related to the material, the peak stress and the stress gradient.

The results of this approach are shown in Figure 38 where the stress values used are the theoretical peak stress at the root of the notch. Note that the points fall fairly close to the curve predicted by Weibull's strength-volume relation using the constants determined from the small volume, uniform gage tensile specimens (unnotched). The volume of this specimen was 0.031 inch^3 which is comparable with the volumes being used here.

It may be only fortuitious that the selection of these volumes and the use of peak stresses gave values that agree closely with the Weibull curve. The criteria for the selection of the volumes was based on observed phenomena for some ceramic materials; however the decision to use peak stress in place of some other value was somewhat arbitrary. In an actual design problem it would be difficult, if not impossible, for one to be sure he was making the right choices as to the volumes and strengths. Also the calculations involved at this stage of the development are laborious and tedious.

One other approach is to calculate the risk of rupture given by Equation 5, but this would be quite involved for most stress distributions. This approach was attempted but did not yield any useful information.

Consider now the flexural data. Assuming the moduli in tension and compression are equal, the average flexural strength was 35,300 psi. Using the volume as that volume between the center load points and subjected to 50 percent of the peak tensile stress, the data point is shown plotted on Figures 33 and 38. The point is seen to fall in line with both the data from the uniform tensile specimens and from the notched tensile specimens indicating true elastic behavior.

From the above discussion and reviews of all data, it is seen that both volume and stress concentrations affect the strength of brittle materials, and that neither of the major contentions regarding notches and brittle materials was completely correct. The actual case seems to be somewhere between the two extremes. It is also seen that the Weibull and Neuber analyses can be applied to the problem to a certain degree. As more data become available, the extent to which these relations may be used will become more evident. At present, it appears that simpler calculations of the type discussed in the section of general results will provide meaningful information.

Fractology - Each specimen was examined individually after it had been run. As was mentioned earlier, two of the large specimens (L3) fractured outside of the notch. No visible flaws were detected. All other specimens broke in the notch and the fracture planes were flat. Because of the sizes of the notches, it was difficult to determine the exact location of the fracture planes, but their location did vary and did not always occur at the root of the notch.

CONCLUSIONS

Most of the specific conclusions were included in the discussion of Data and Results; however, there were several important conclusions which should be summarized and emphasized.

For graphite it was demonstrated that a total of 30 tensile specimens could be used to statistically characterize the strength properties and more than 30 specimens did not appear to increase the accuracy to any degree. As few as 5 specimens gave good results tha could be used for many applications. Notches in graphite specimens reduced the nominal strength considerably at 70°F and 4000°F; however, at 5000°F the notches had little effect probably because of "plasticity." The peak fracture stress in the notched graphite specimen was on the order of 11,000 psi ($K\sigma_n$) for this small volume. A volume effect for graphite was observed. Finally, general sense was obtained for the strengths obtained by different test methods including a round rod, square rod, sleeve and flexural specimen.

For alumina, several observations seem particularly important:

1. Over a range of 5 to 25 rms, surface finish had little influence on the strength of either notched or unnotched tensile specimens, nor upon the flexural specimens. This is contrary to a dramatic effect of rougher surface finish on strength of other aluminas evaluated here. Thus the fracture may indeed be initiating internally at these finer finishes.

2. The strength of the flexural specimens was not influenced by using sharp or rounded corners at the tensile face. This also is contrary to other experience here and may have resulted from the quite small grain size and the fact that failures were initiating internally.

3. The tensile and flexural strengths were in fair agreement when compared on the basis of equivalent volumes as determined by a "damage stress".

4. The nominal strength of the notched specimens was reduced to about 40 percent of unnotched ones.

5. The volume effect existed for notched specimens in that the smaller ones were generally stronger when comparing similar stress concentration factors.

6. A combination of Neuber and Weibull analyses does apply to notches in that there was general agreement in the peak stress predicted by the Neuber analysis and the strength predicted by the Weibull analysis for a reasonably selected volume.

7. The Weibull volume was reasonably well defined in the notched specimens as that volume of material encased by stresses at over 50 percent of the peak stress $\left[\sigma_V \text{ (maximum)}\right]$.

8. Evidence accumulates that these brittle materials experience a "damage stress" at over 50 percent of ultimate strength.

9. Assuming that the Neuber analysis is correct, this alumina (in small volumes) had a strength of over 80,000 psi. This infers that the material has considerable potential for strength enhancement.

For both the graphite and alumina, extrapolation of the strengths to the values observed for volumes of 0.3 mil fibers provided unusual agreement. The difference in structures between the polycrystalline and fiber bodies is such that the agreement probably is fortuitous.

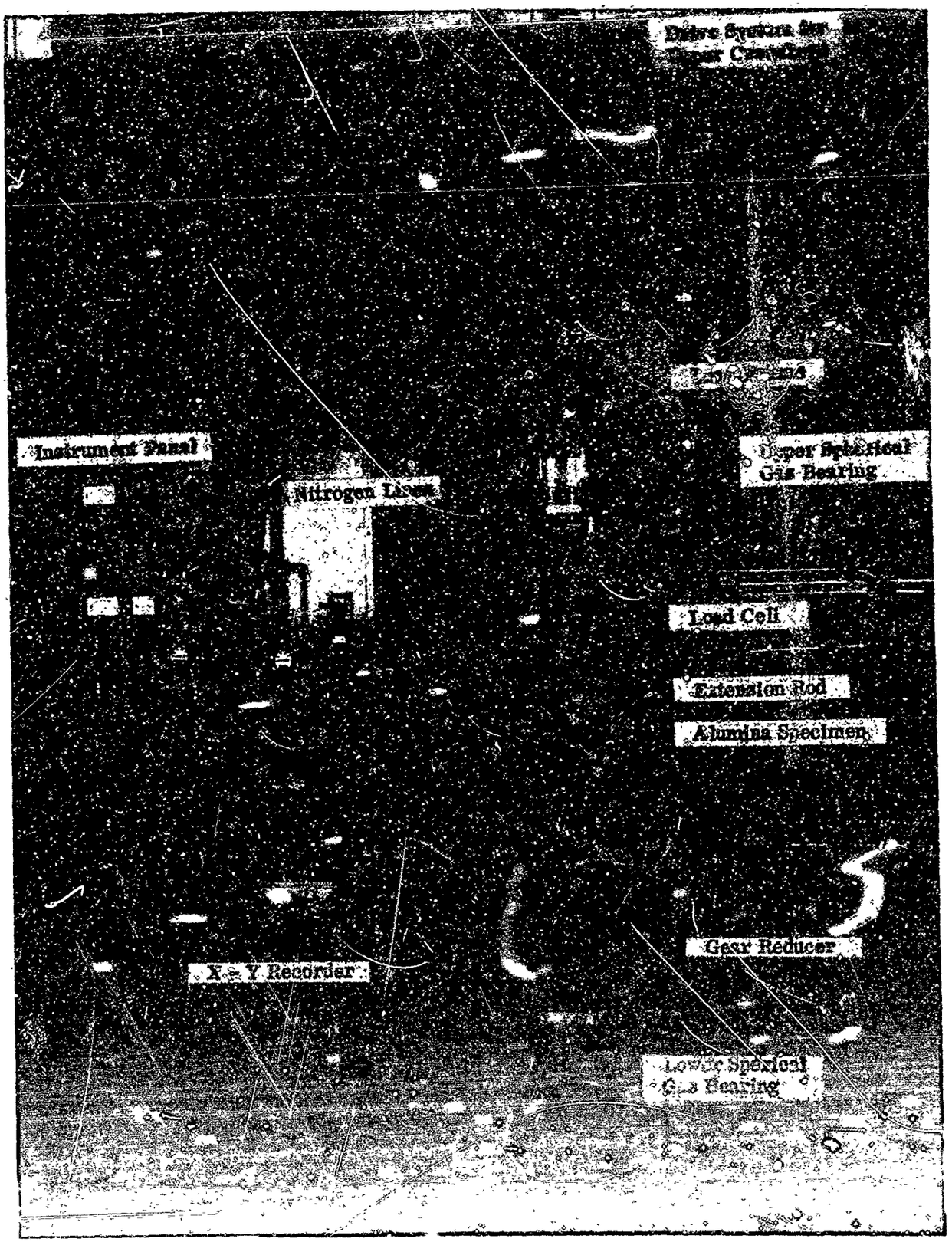

Figure 1. Gas-Bearing Tensile Facility

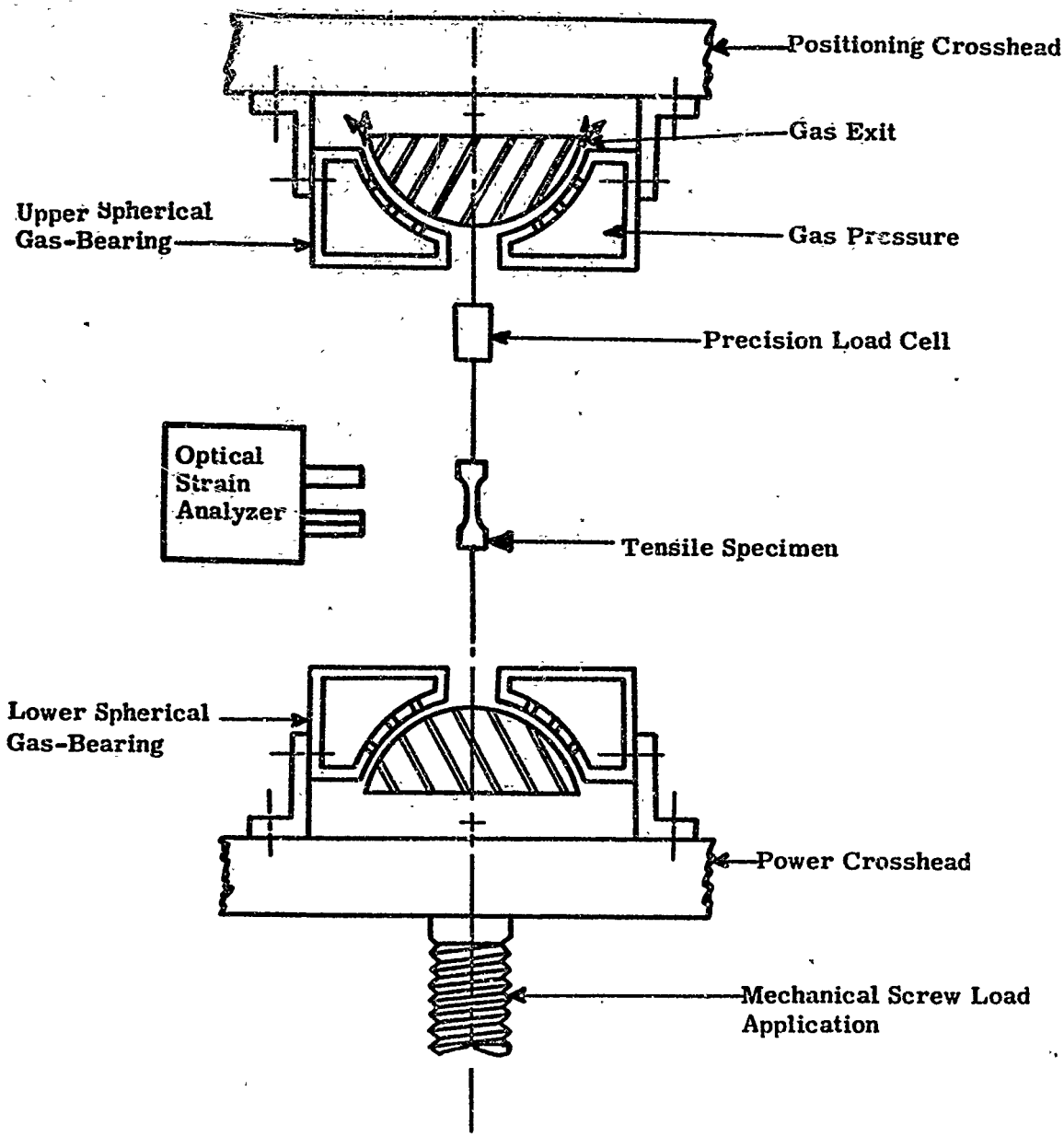

Figure 2. Schematic Arrangement of Gas-Bearing Universals, Specimen, and Load Train

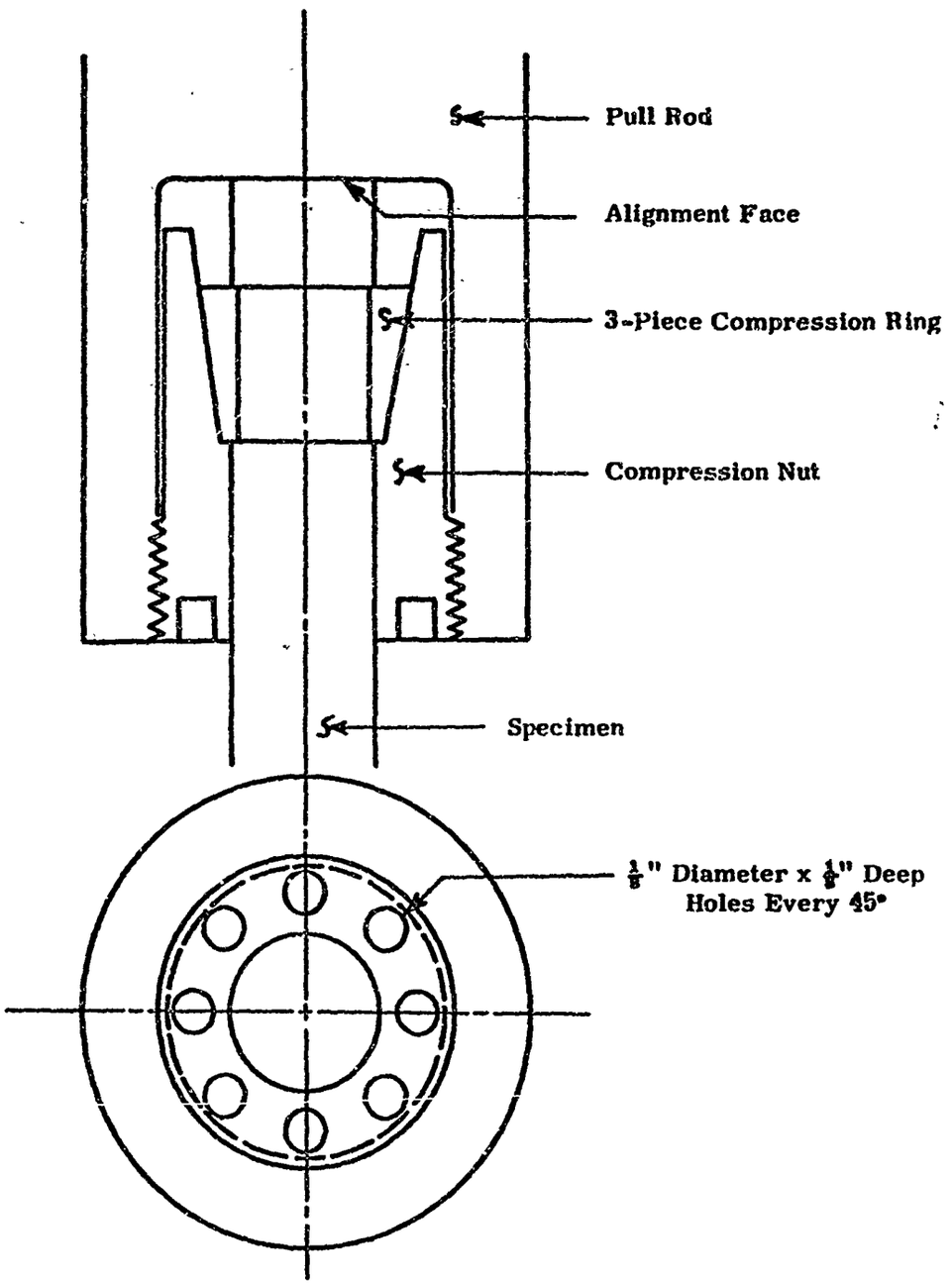

Figure 3. Schematic of Collet-Type Specimen Grip

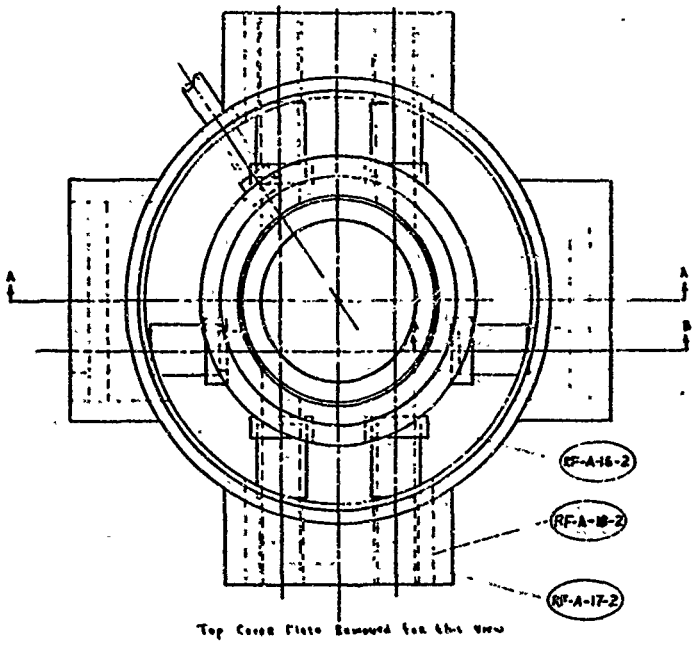

Assy.	Item	Quan.	Description
	A-2	1	Top pyrolytic graphite ring
	A-3	1	Bottom pyrolytic graphite ring
	A-4	1	Pyrolytic graphite temperature sight plate
	A-5A	1	CS graphite protector tube
	A-6	1	CS graphite temperature sight tube
	A-7	1	Bottom Micarta insulating disc
	A-8	1	Top steel base plate
	C-9A	1	Steel shell
	A-10	1	Top Micarta insulating disc
	A-11	1	Top zirconia disc
	A-12	1	Bottom steel base plate
	A-13	1	Bottom zirconia disc
	A-14A	1	CS graphite heater tube
	A-15	2	Steel sight port tube
	A-16-1	2	CS graphite sight port plate
	A-16-2	2	CS graphite sight port plate
	A-17-1	2	Firebrick sight port plate
	A-17-2	2	Firebrick sight port plate
	A-18-1	2	Zirconia sight port disc
	A-18-2	2	Zirconia sight port disc
	A-19	4	CS graphite sight tube
	A-20	2	Fiberfrax insulator
	A-21	1	Top electrode
	A-22	1	Bottom electrode
	A-23	1	Thermatomic carbon

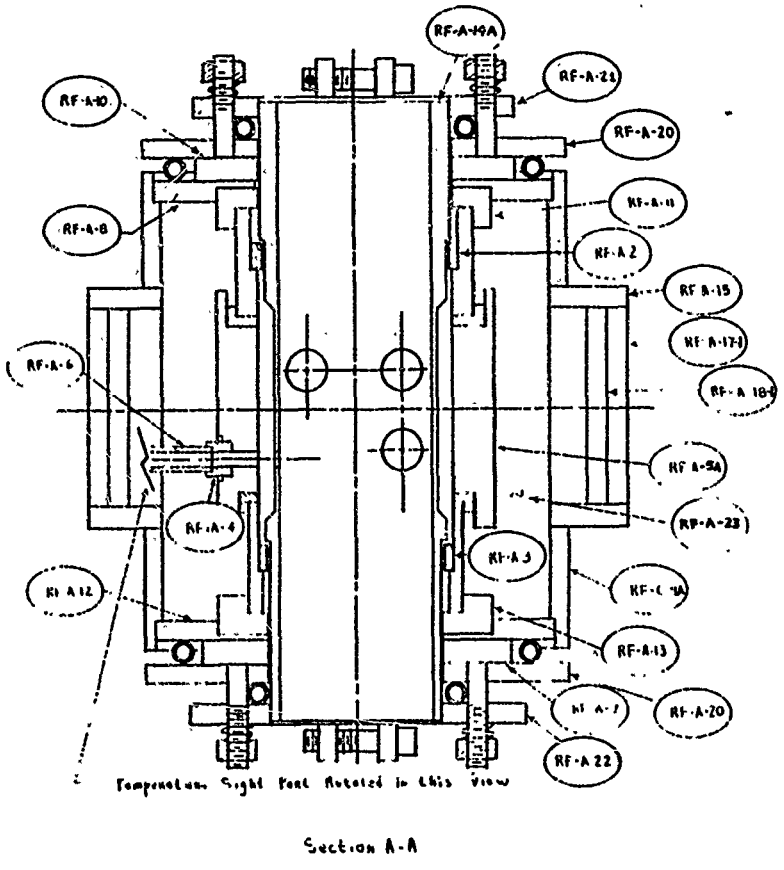

Section A-A

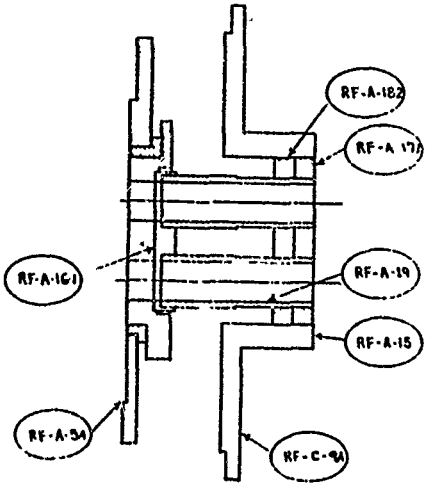

Section B-B

Figure 4. Small 5500°F Graphite Resistance Furnace

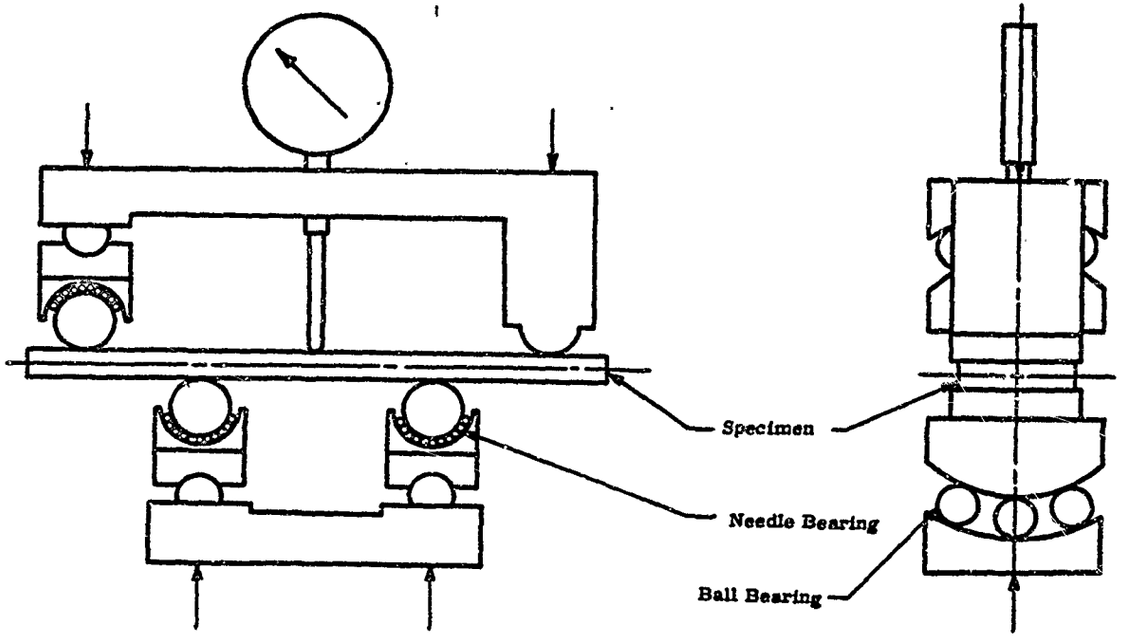

Figure 5. Schematic of Flexure Facility

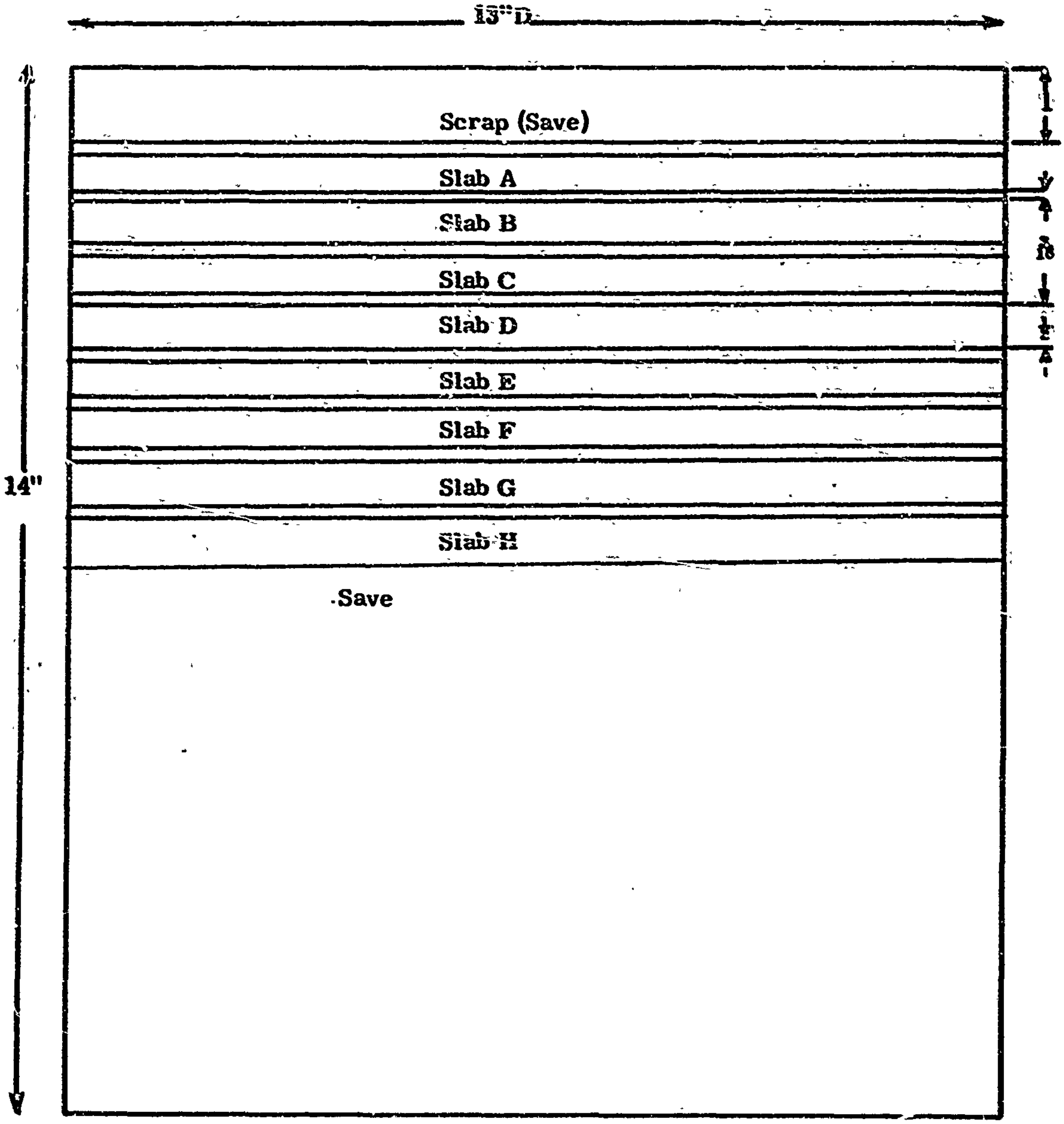

Figure 6. Cutting Plan for Block of ATJ Graphite

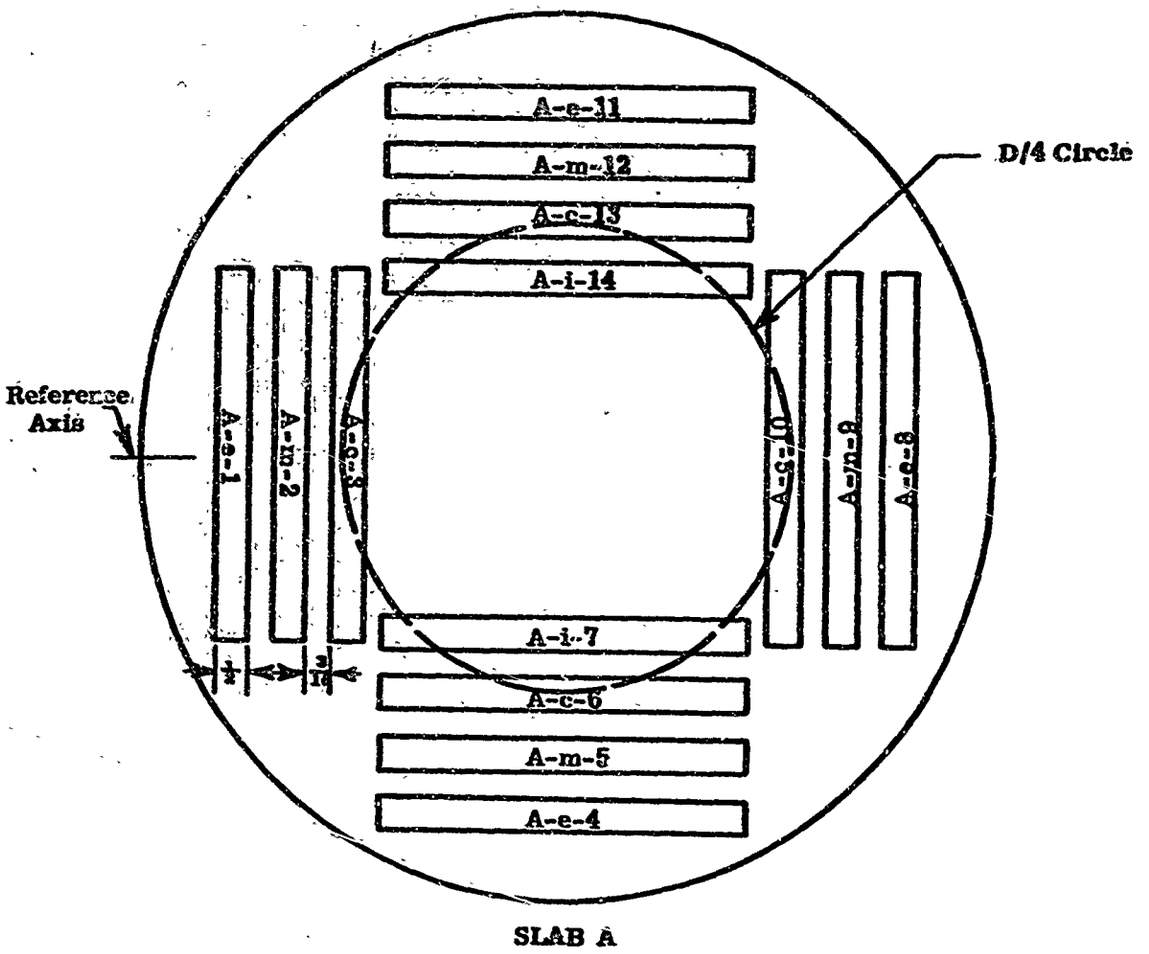

Figure 7. Specimen Location within a Typical Slab

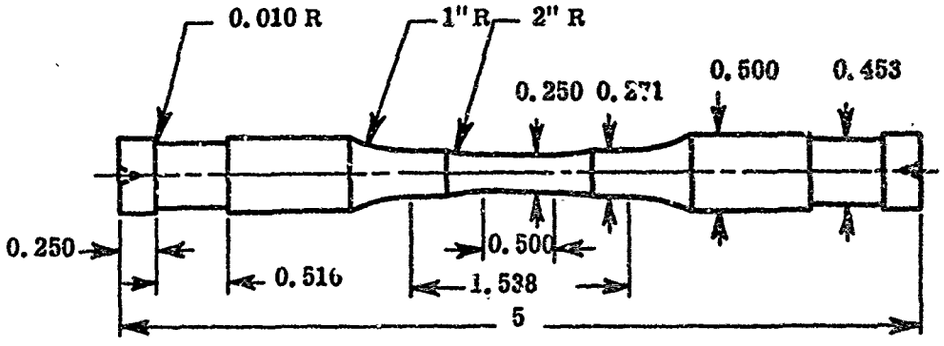

Notes:

1) All diameters must be true and concentric to within 0.0005 in.
2) Both ends must be flat and perpendicular to the ℄ to within 0.0005 in.
3) Do not undercut radii at tangent point.
4) All dimensions are in inches.

Figure 8. Urnotched Graphite Tensile Specimen

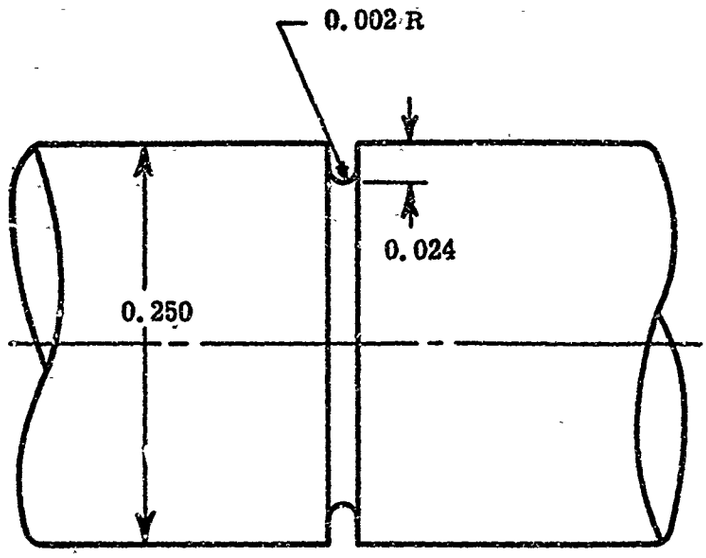

Figure 9. Detail of the Notch Configuration Used on Graphite Tensile Specimens

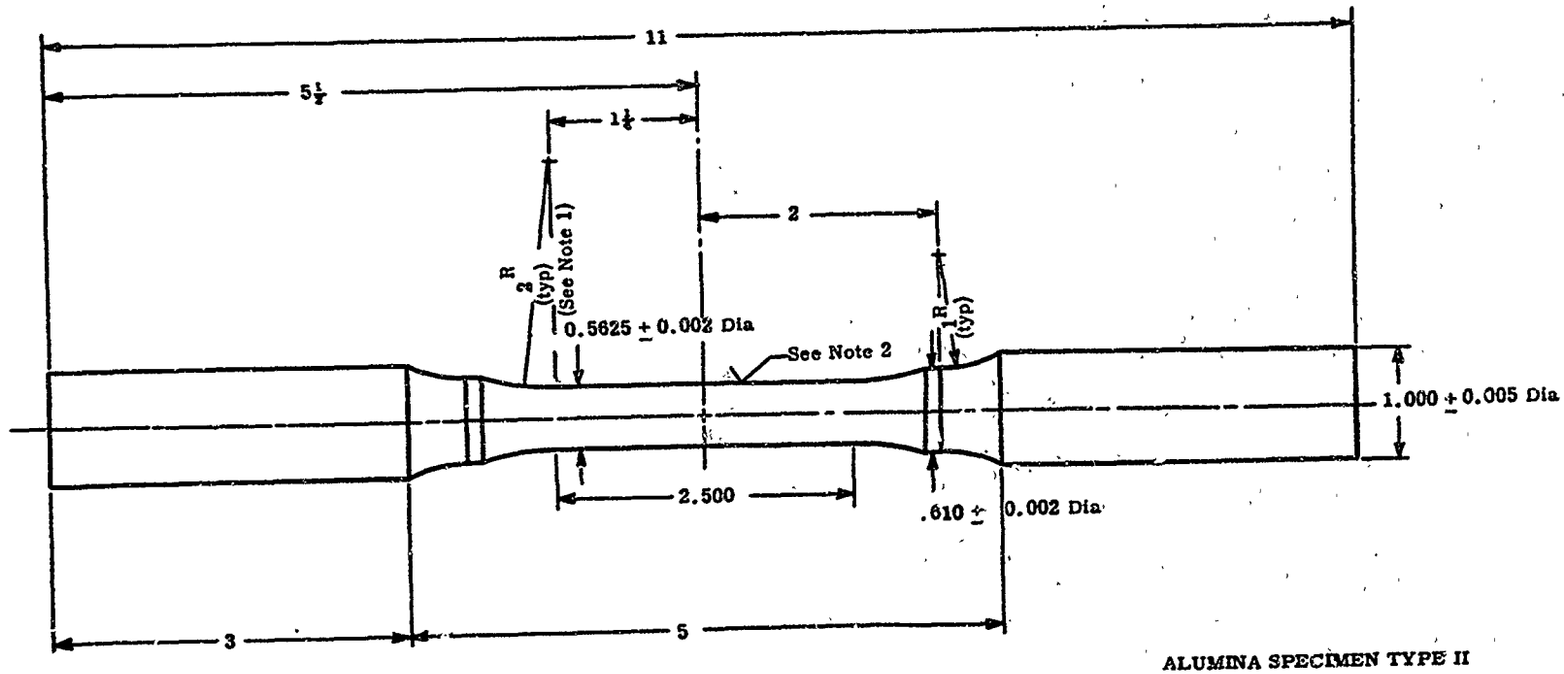

ALUMINA SPECIMEN TYPE II

Note:
1) Do Not Undercut Radii
2) Surface Finish to be Established on 1st Specimen (Approx. 10 RMS) and Held Within 5 RMS or Less on All Others
3) Do Not Handle Gage Portion of Specimen
4) All Diameters True and Concentric to Within 0.0005

Figure 10. Configuration of Typical Alumina Specimen whose End Section Was Used for Large Notched Specimen

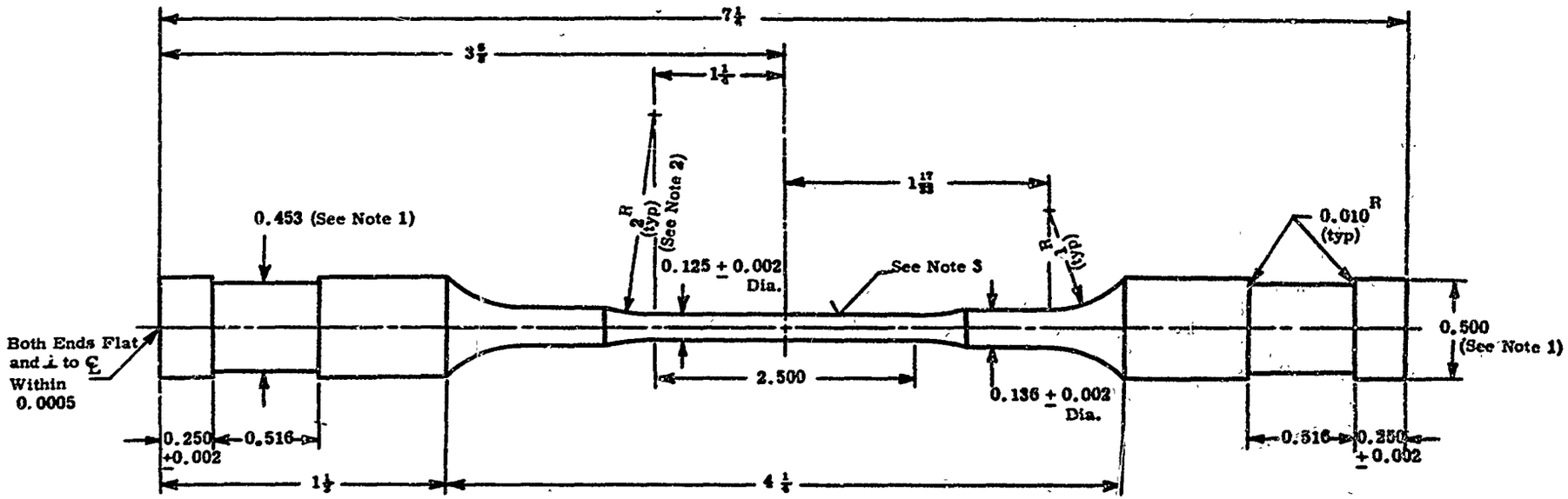

ALUMINA SPECIMEN TYPE IV

Note:
1) Fit to Furnished Compression Ring and And Nut Within 0.0005
2) Do Not Undercut in Radii
3) Surface Finish to be Established on 1st Specimen (Approx. 10 RMS) and Held Within 5 RMS or Less on All Others
4) Do Not Handle Gage Portion of Specimen
5) All Diameters True and Concentric to Within 0.0005

Figure 11. Configuration of Typical Alumina Specimen whose End Section Was Used for Small Notched Specimen

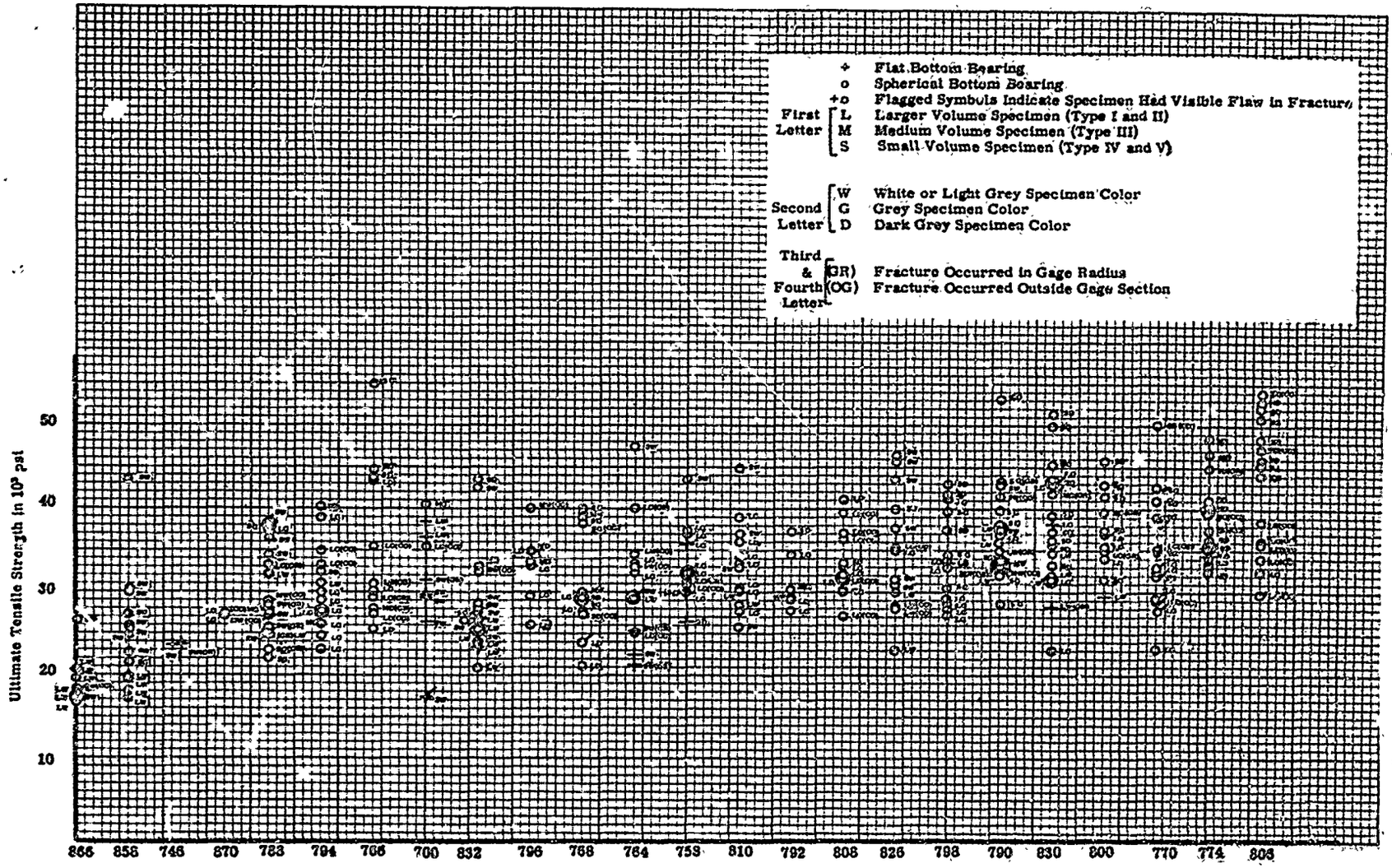

Figure 12. Ultimate Strength Versus Tile Number Indicating Variation of Strength between Tiles for Unnotched Specimens

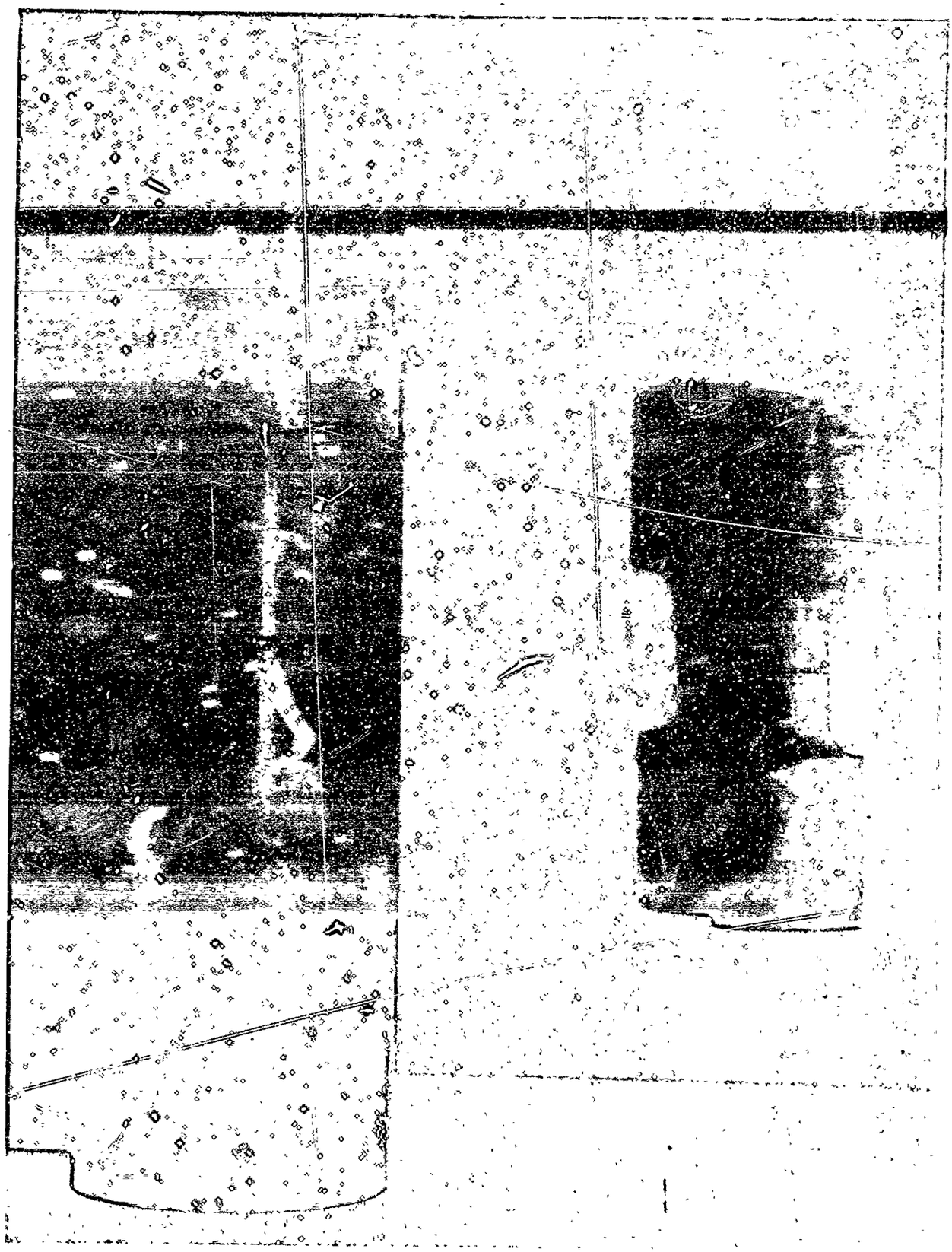

Figure 13. Photograph Showing Relative Sizes of Large and Small Notched Alumina Specimens.

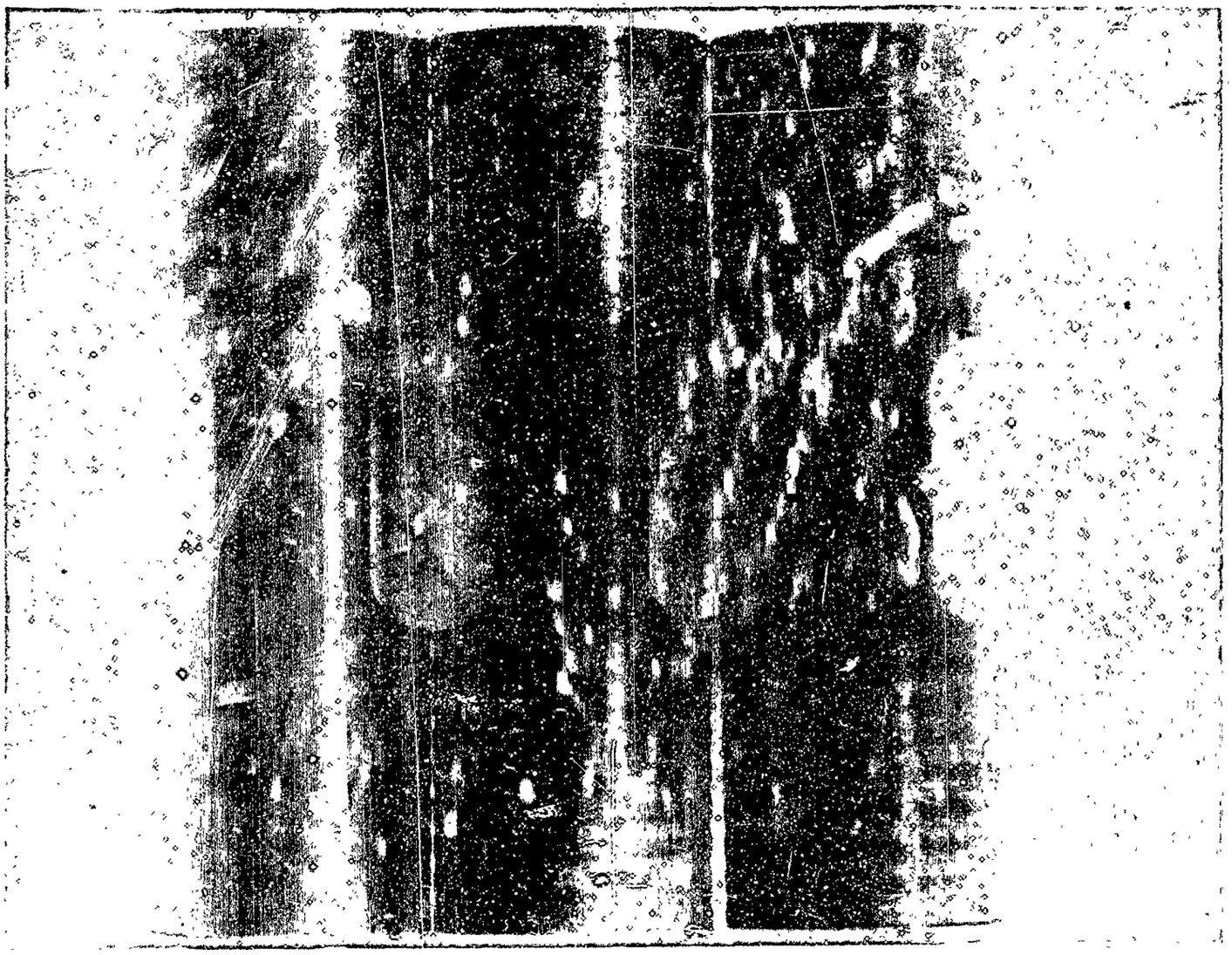

Figure 14. Photograph Showing Relative Notch Sizes for the Three Stress Concentration Factors on Small Notched Alumina Specimens.

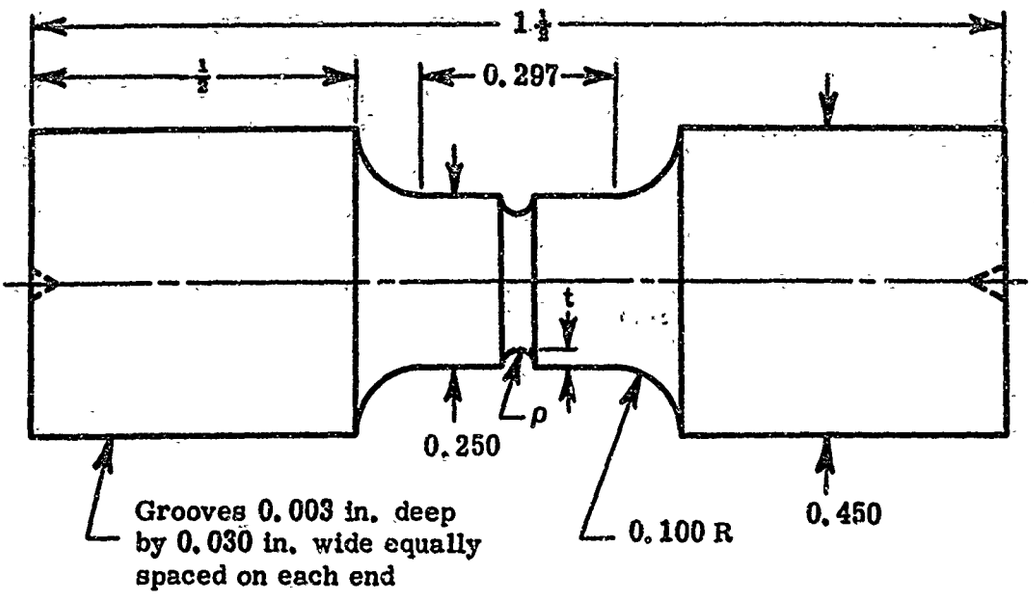

Stress Concentration Factor	t in.	ρ in.
3	0.024	0.024
5	0.024	0.006
8	0.024	0.002

Figure 15. Small Volume Alumina Specimens with Notch

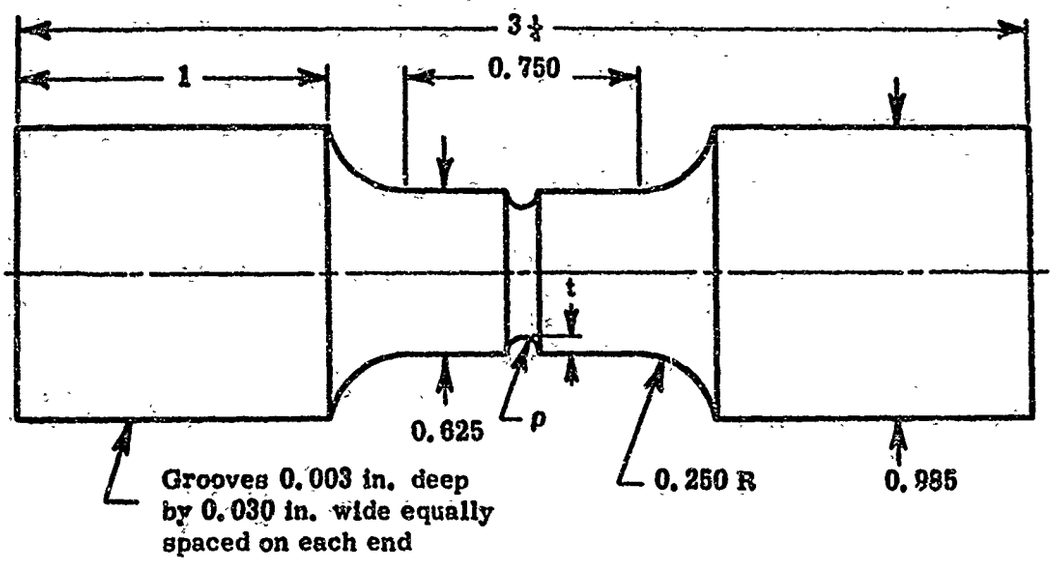

Stress Concentration Factor	t in.	ρ in.
3	0.063	0.063
5	0.063	0.016
8	0.063	0.005

Figure 16. Large Volume Alumina Specimens with Notch

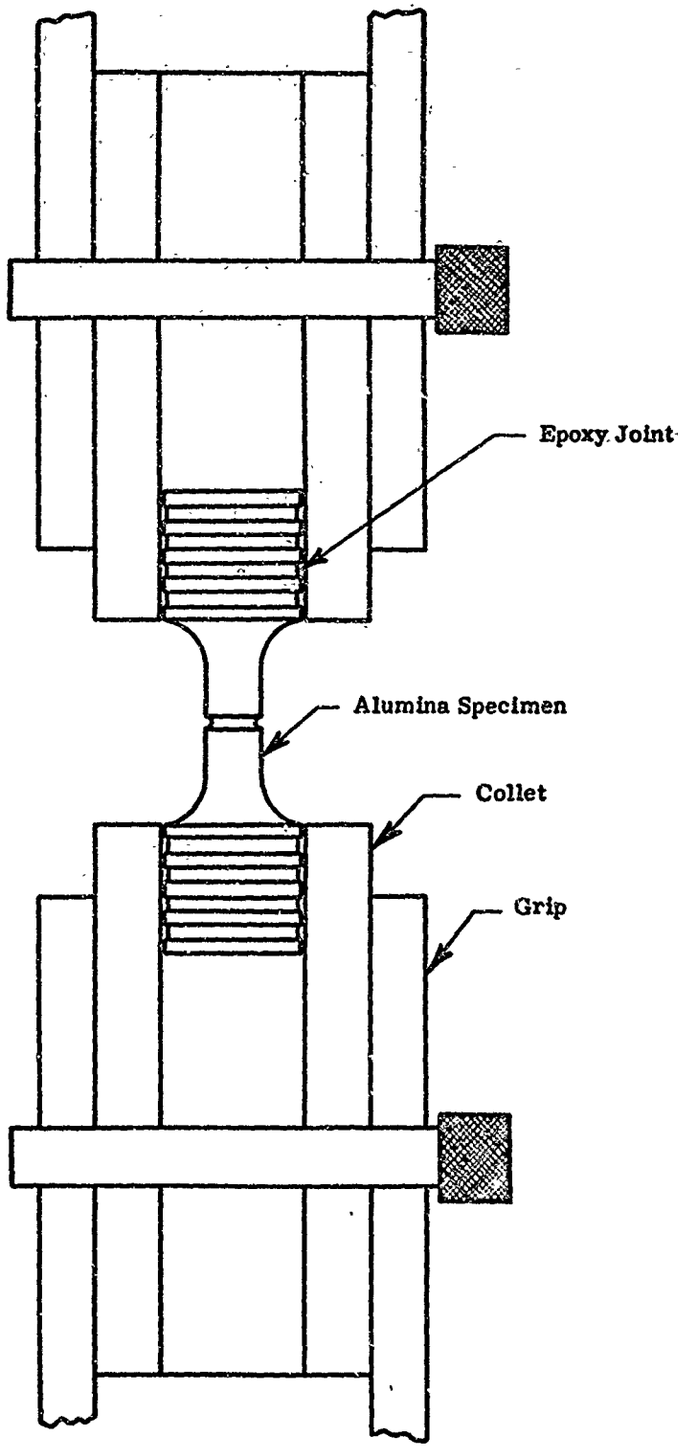

Figure 17. Schematic of Gripping Arrangement for Notched Alumina Specimen

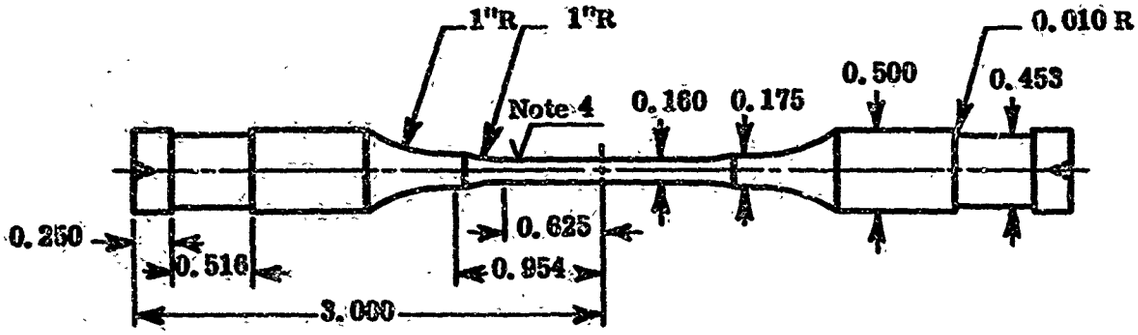

Notes:

1) All diameters must be true and concentric to within 0.0005 in.
2) Both ends to be flat and perpendicular to ℄ to within 0.0005 in.
3) Do not undercut radii at tangent points.
4) Surface finish of gage section to be selected after specimen is machined to final configuration

Figure 18. Unnotched Alumina Tensile Specimen

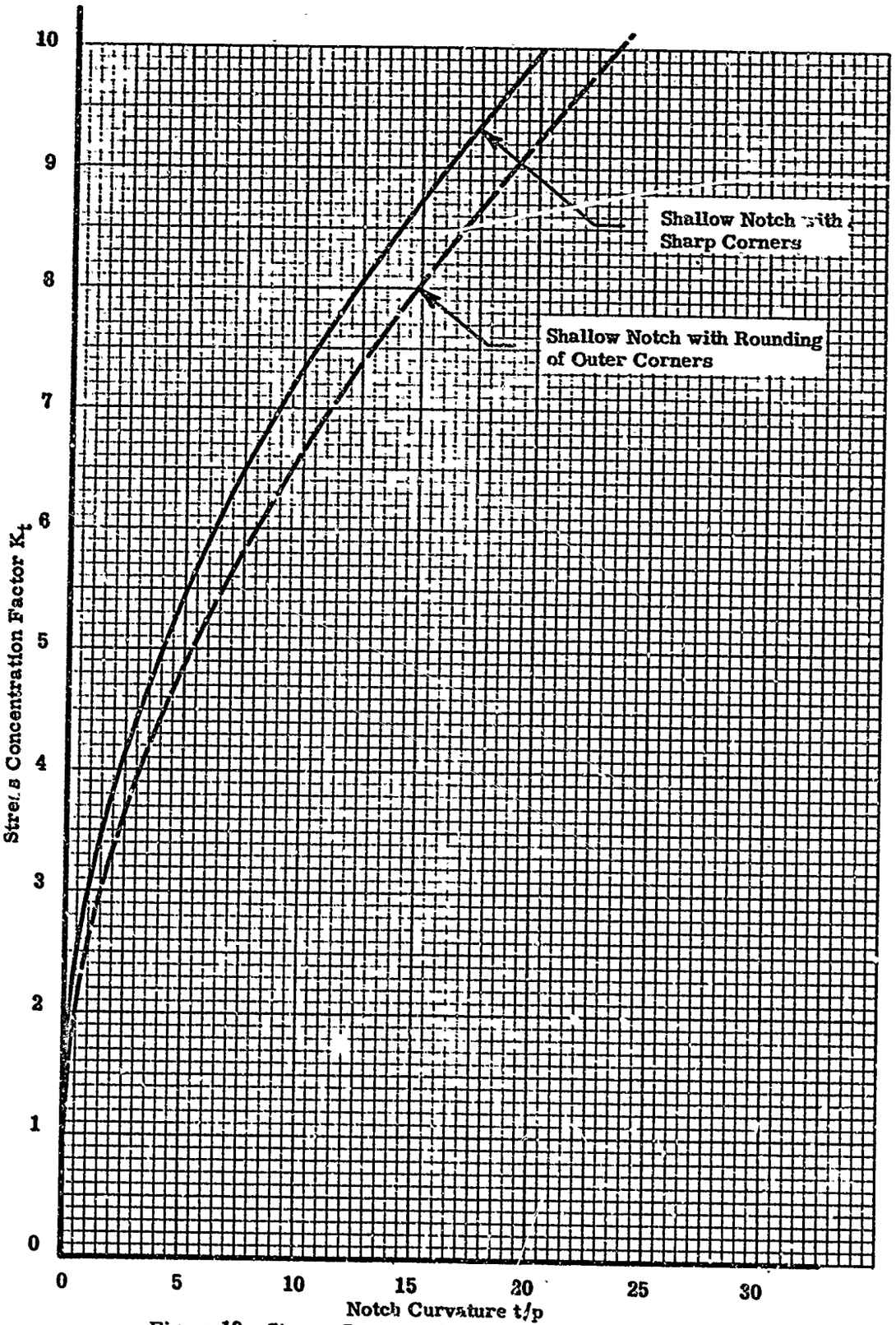

Figure 19. Stress Concentration Factors Versus Notch Curvature for Shallow Circumferential Notches in Pure Tension

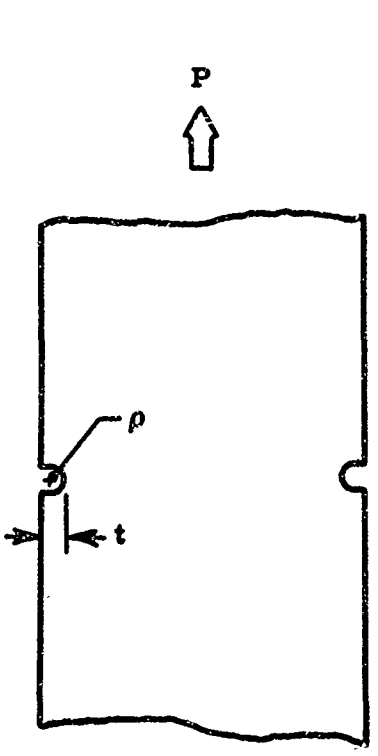

Figure 20. Thin Bar with a Shallow Notch on Each Side

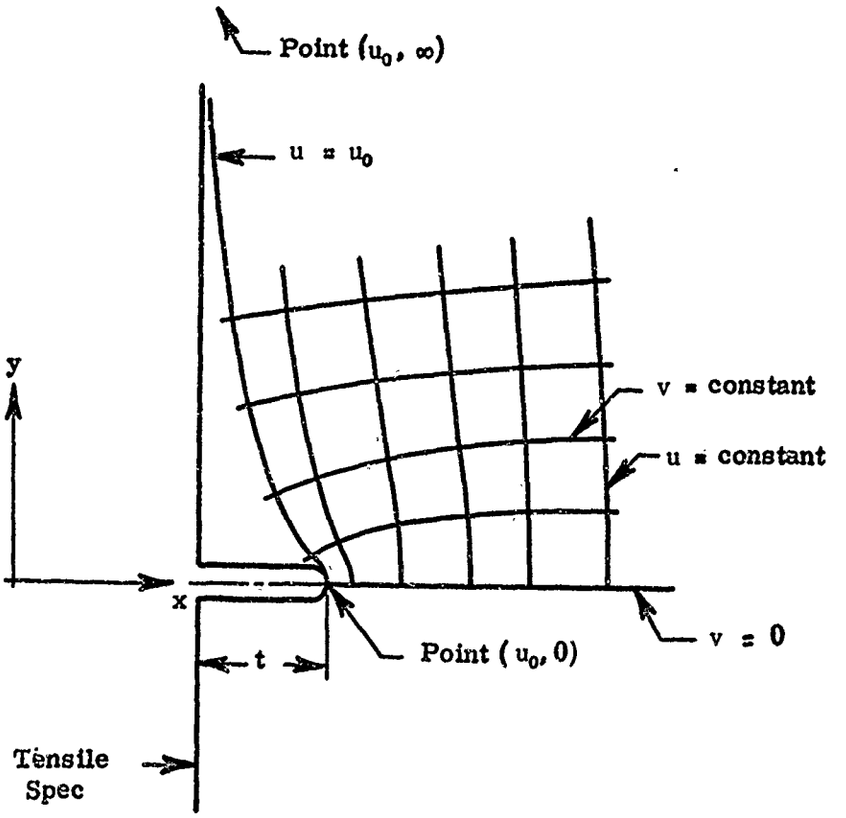

Figure 21. Sketch Showing Relationships between the Notch Geometry and u-v Coordinate System

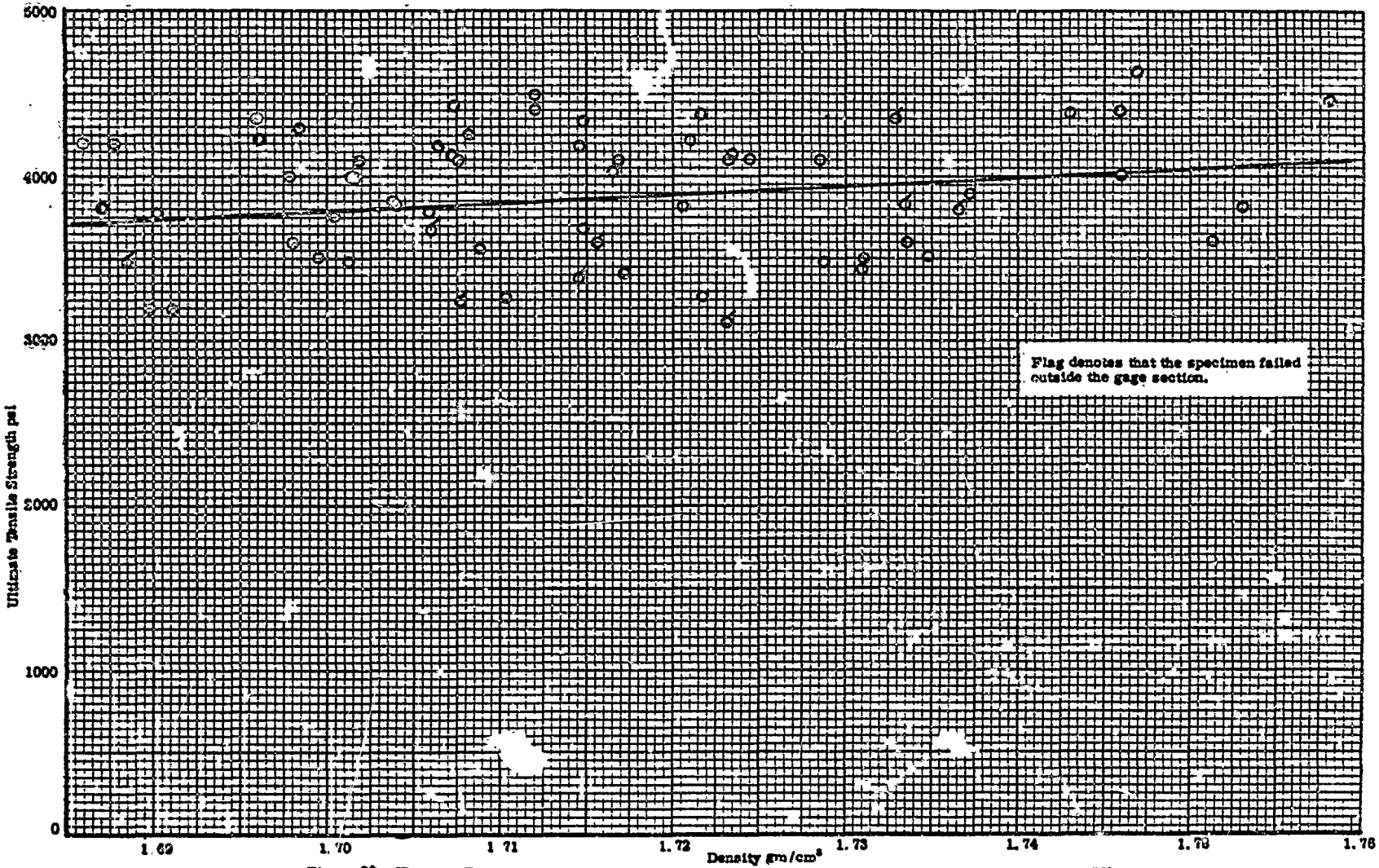

Figure 22. Ultimate Tensile Strength Versus Density for Unnotched [illegible] Grain ATJ Graphite Specimens at 70° F

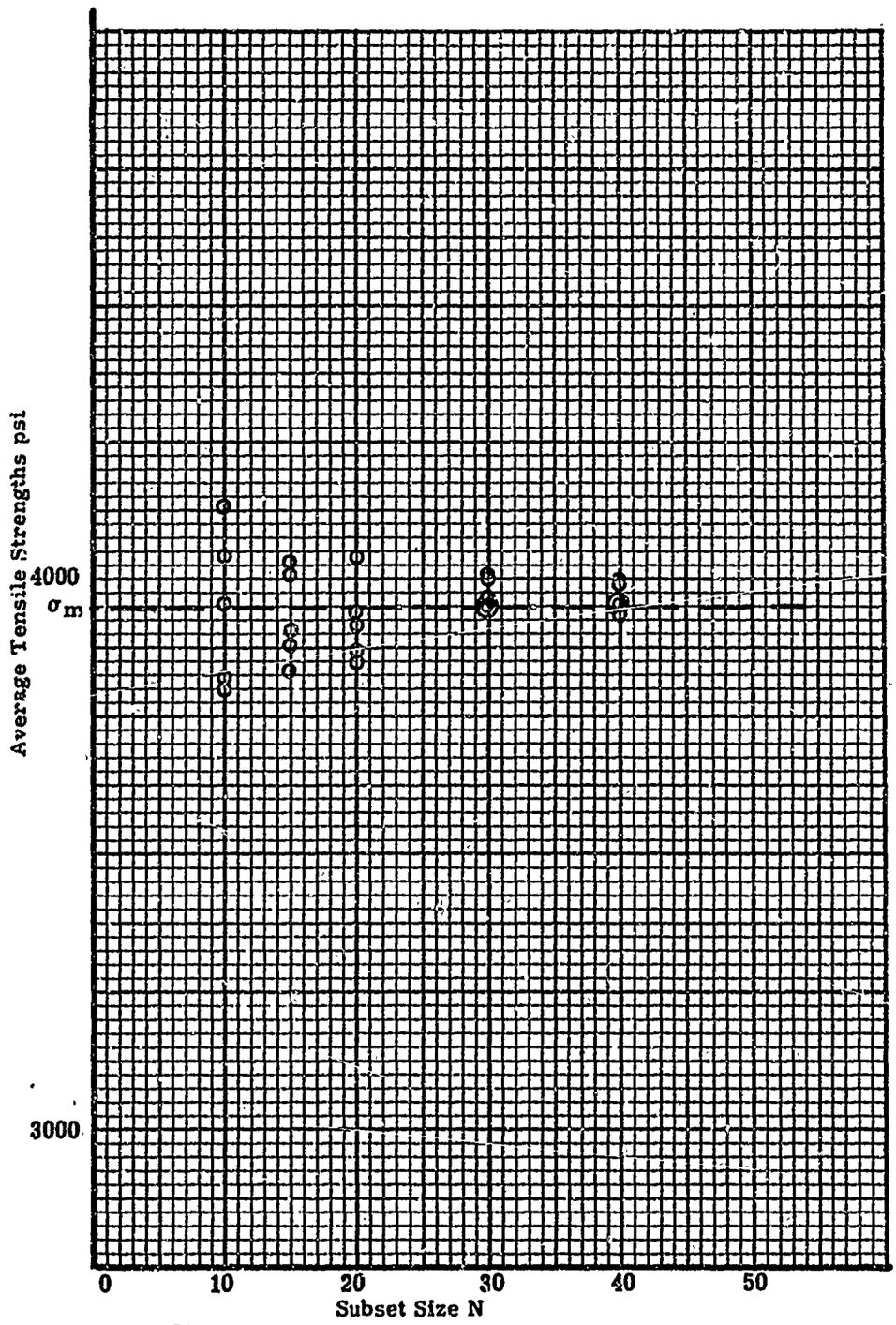

Figure 23. Average Tensile Strength Versus Subset Size for Unnotched With Grain ATJ Graphite

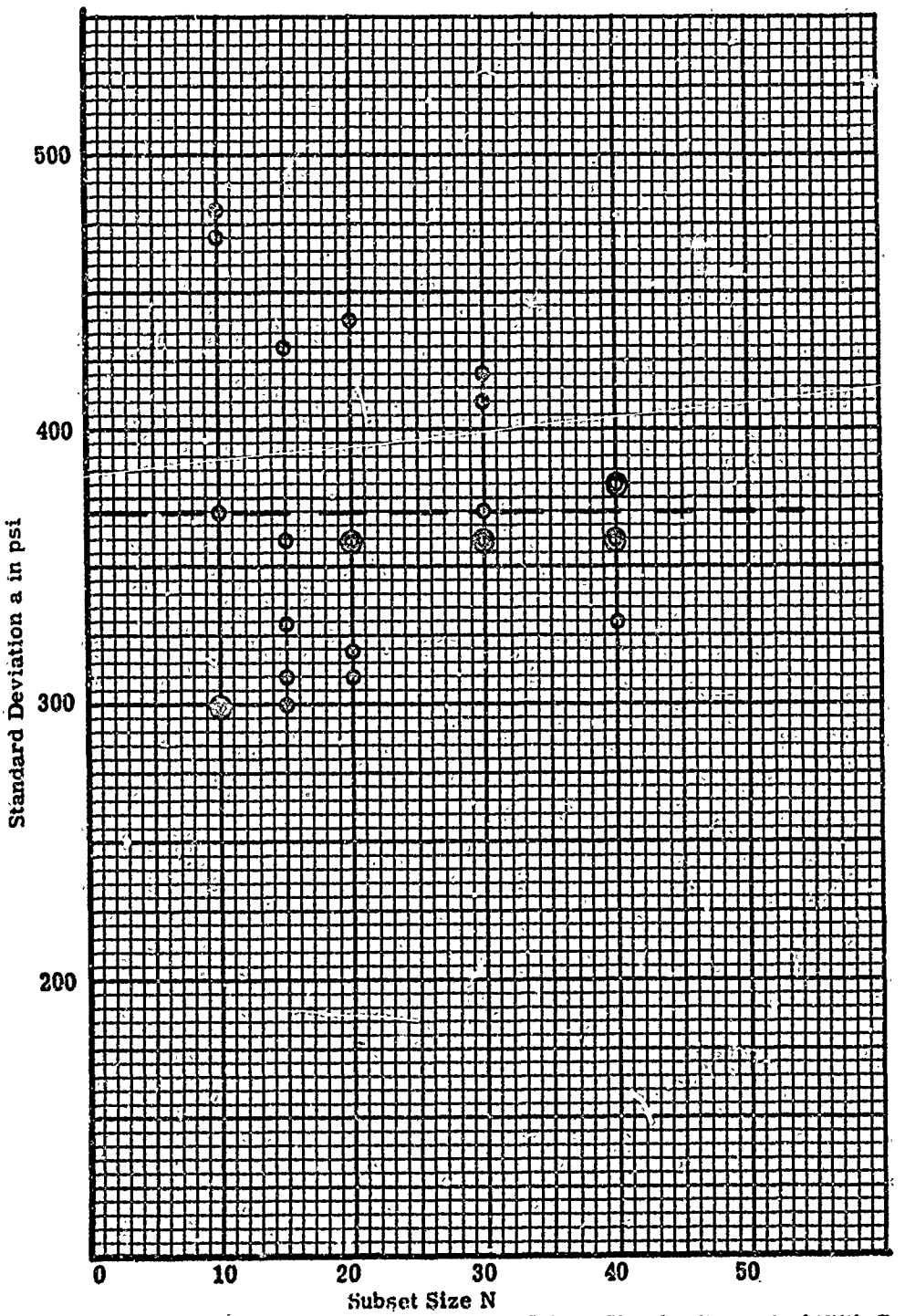

Figure 24. Standard Deviation Versus Subset Size for Unnotched With Grain ATJ Graphite

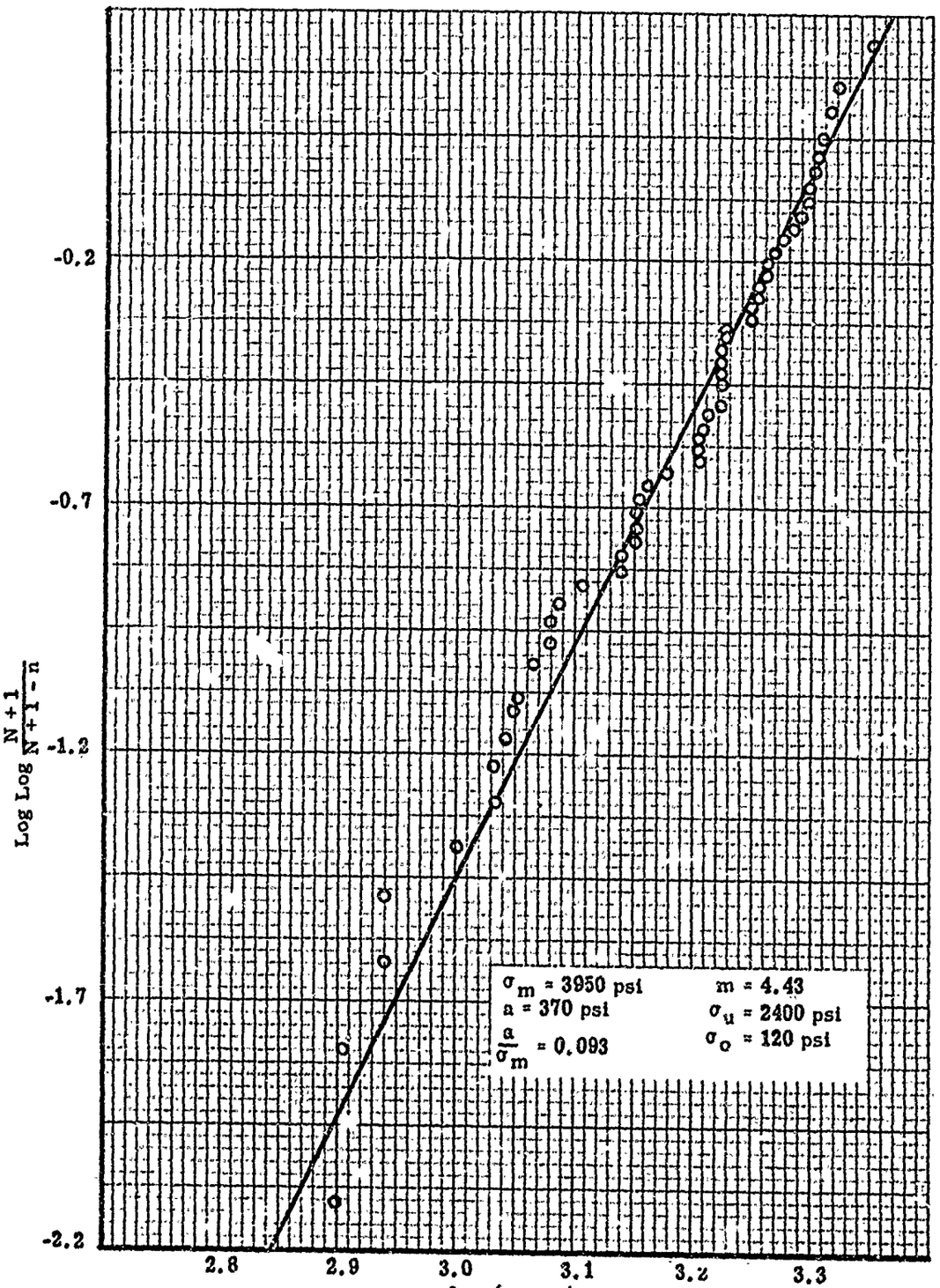

Figure 25. Log Log $\frac{N+1}{N+1-n}$ Versus Log $(\sigma - \sigma_u)$ for Unnotched With Grain ATJ Graphite

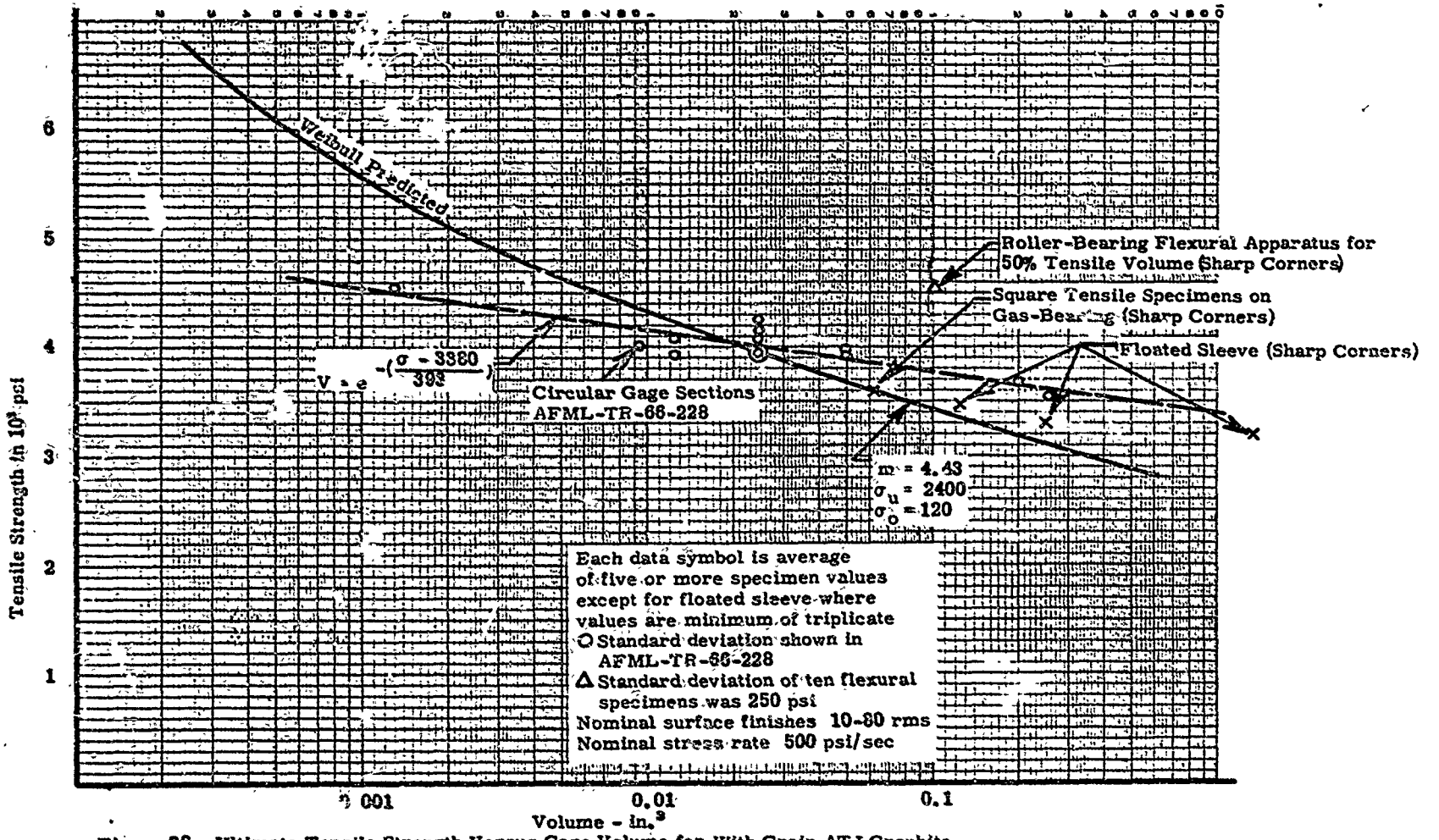

Figure 26. Ultimate Tensile Strength Versus Gage Volume for With Grain ATJ Graphite

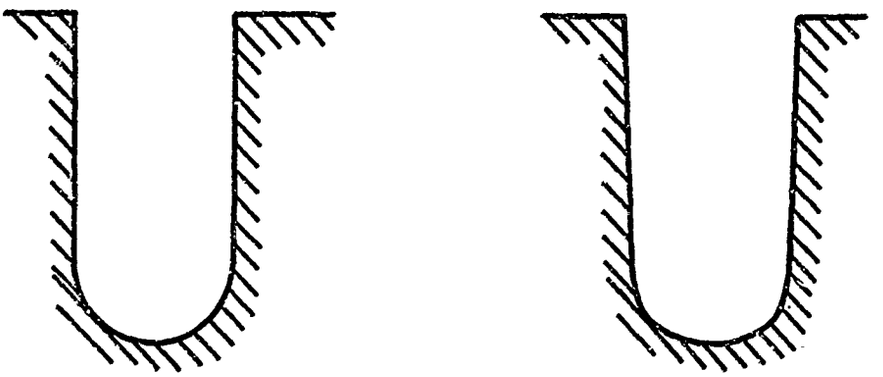

Figure 27. Comparison of Desired and Actual Notch Configuration for Notched Graphite Tensile Specimens

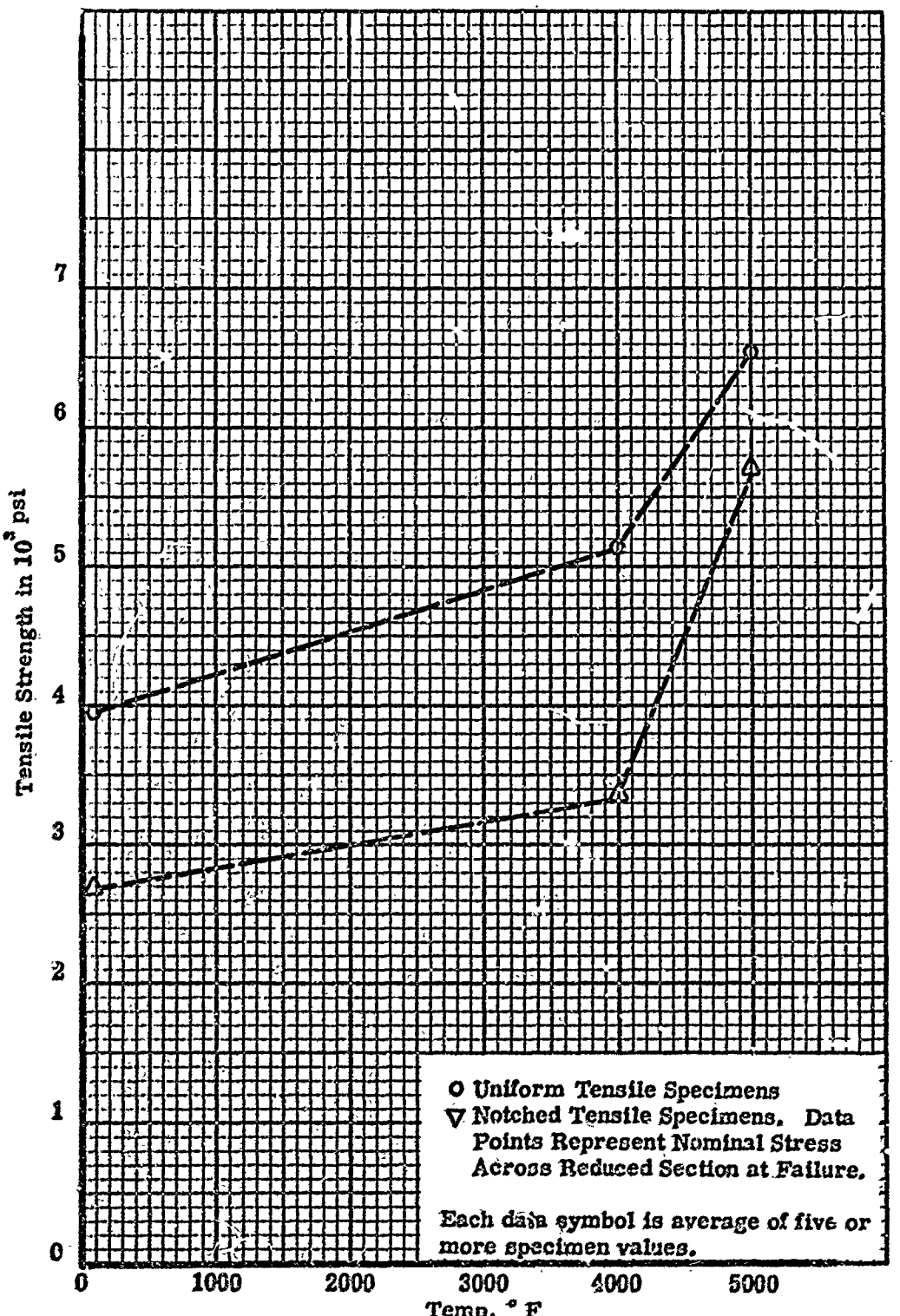

Figure 28. Tensile Strength Versus Temperature for With Grain ATJ Graphite for Notched and Unnotched Specimens

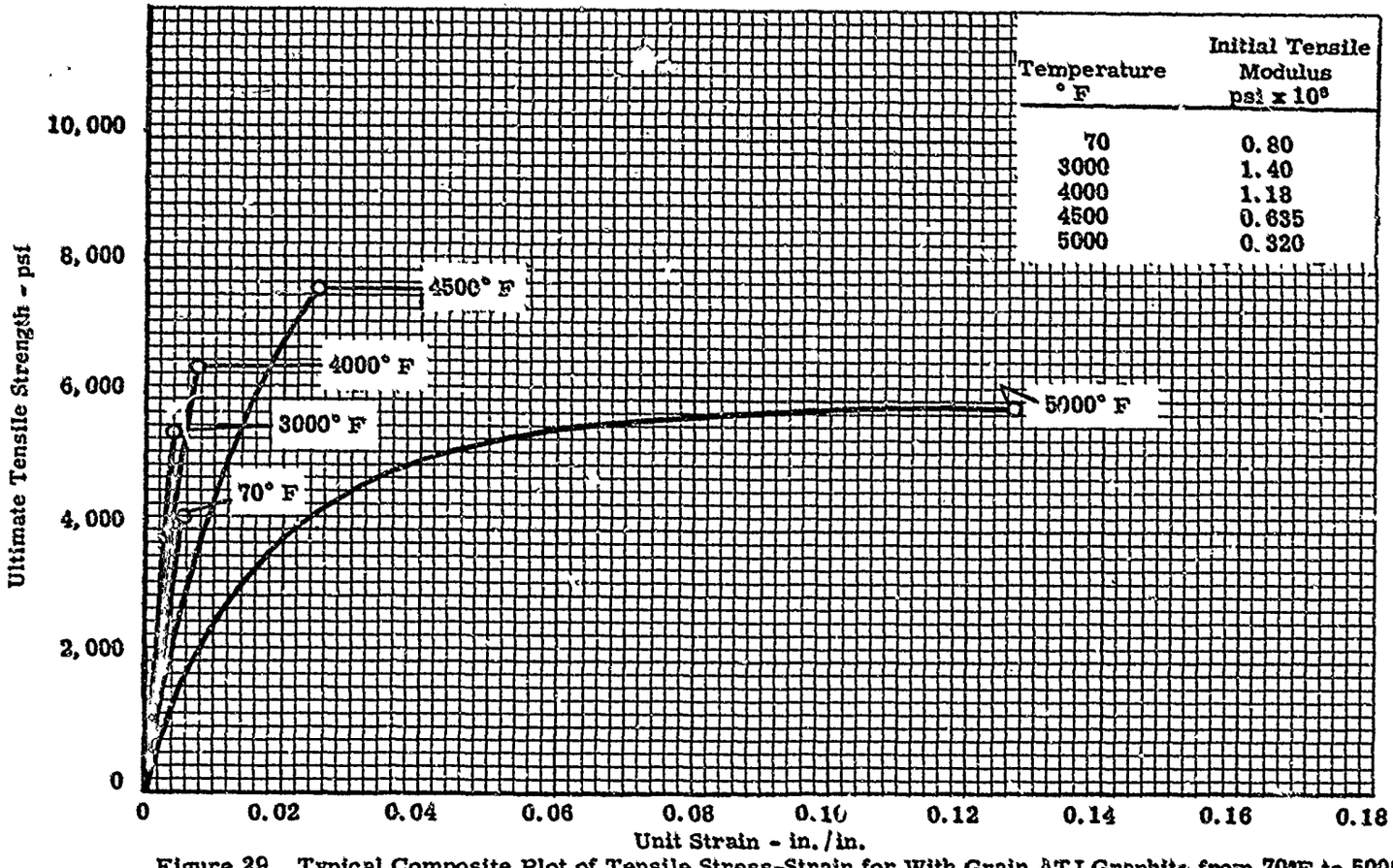

Figure 29. Typical Composite Plot of Tensile Stress-Strain for With Grain ATJ Graphite from 70°F to 5000°F

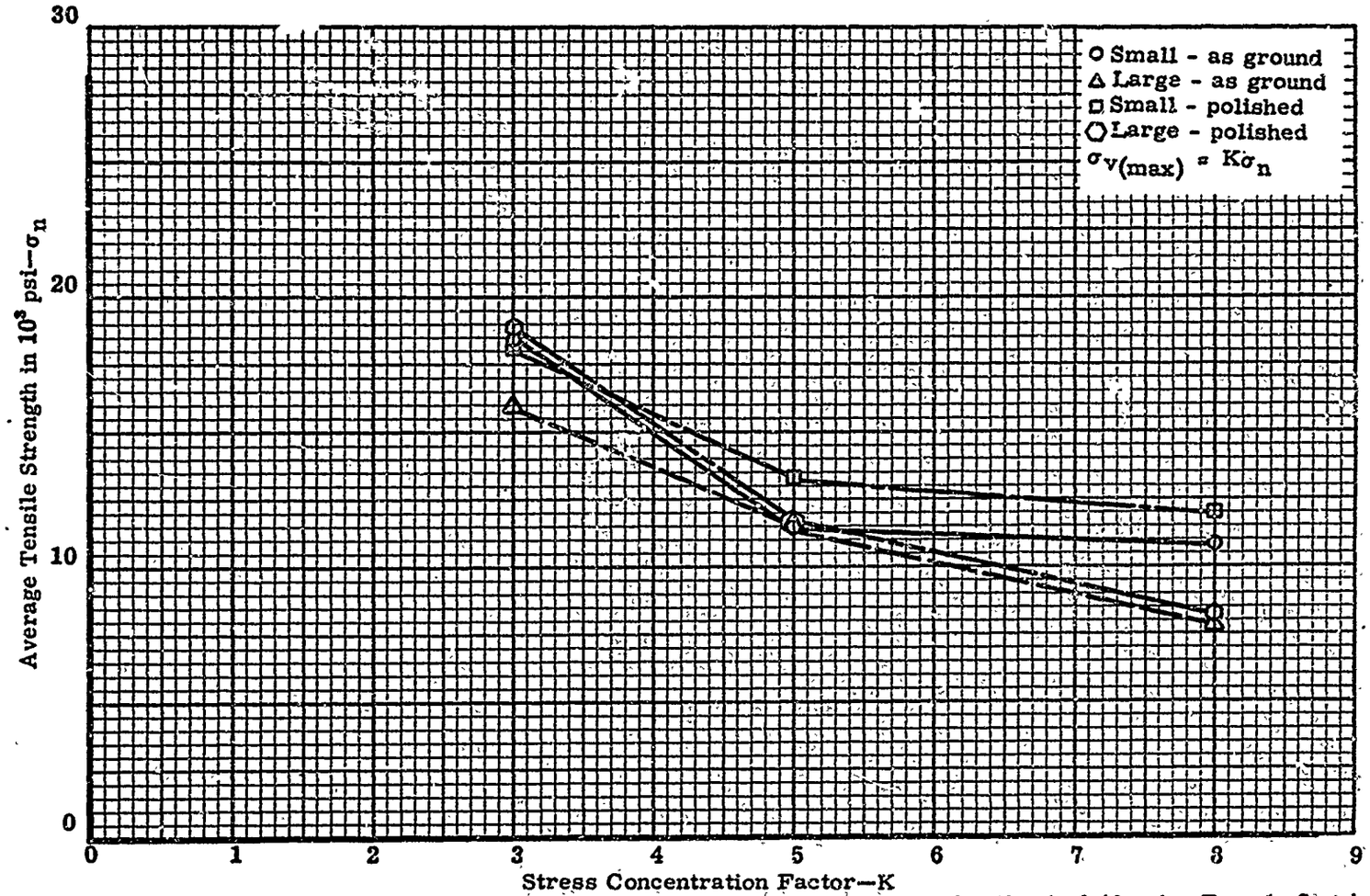

Figure 30. Nominal Tensile Strength Versus Stress Concentration Factor for Notched Alumina Tensile Specimen

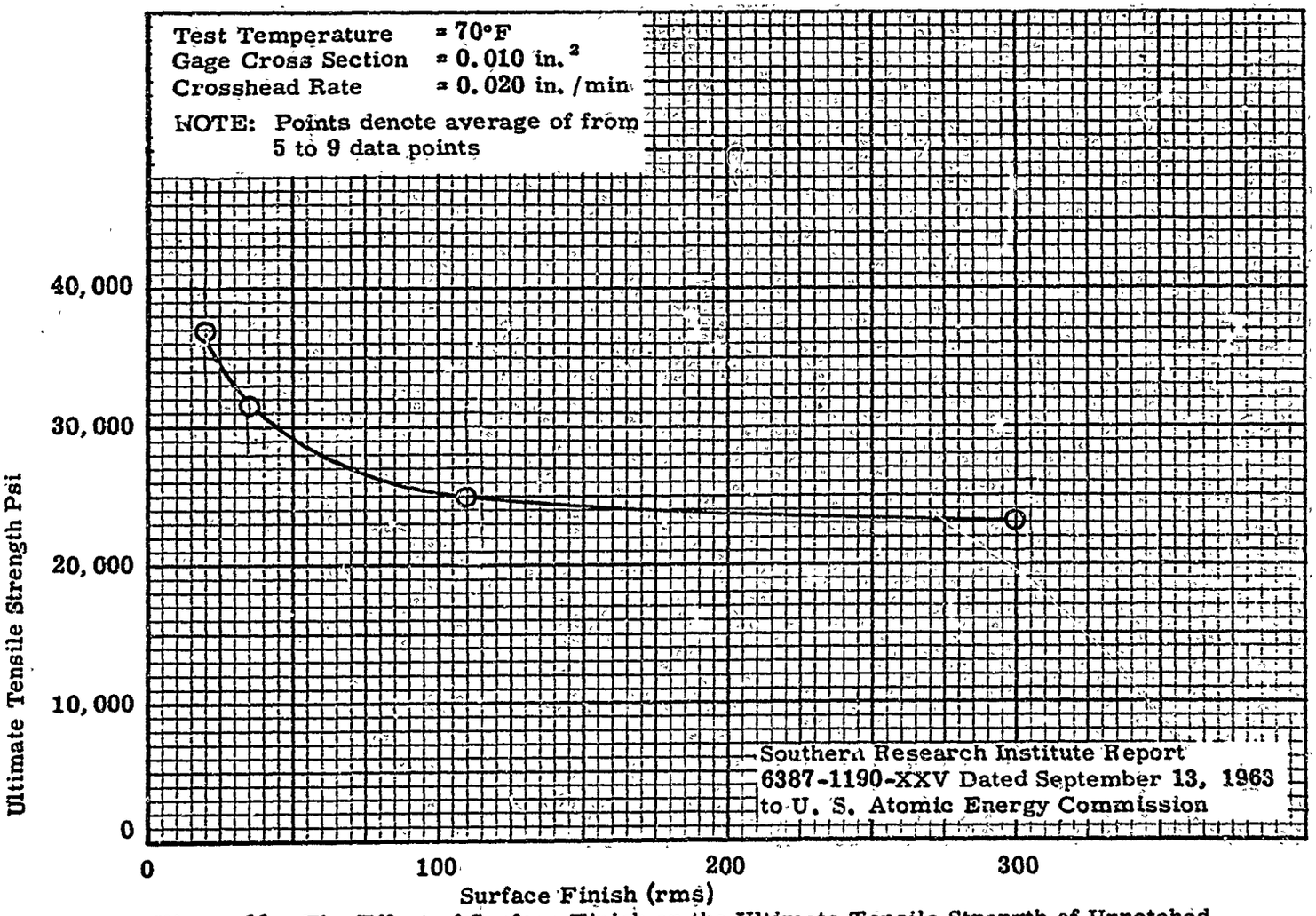

Figure 31. The Effect of Surface Finish on the Ultimate Tensile Strength of Unnotched Alumina at 70°F and One Stress Rate (Pressed and Fired Alumina)

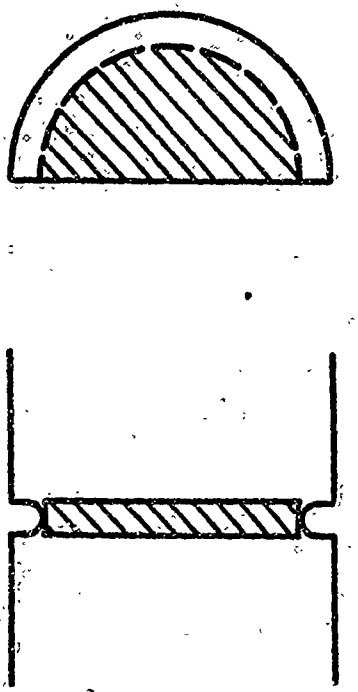

Figure 32. Disc Assumed for Defining Volume in Preliminary Calculation

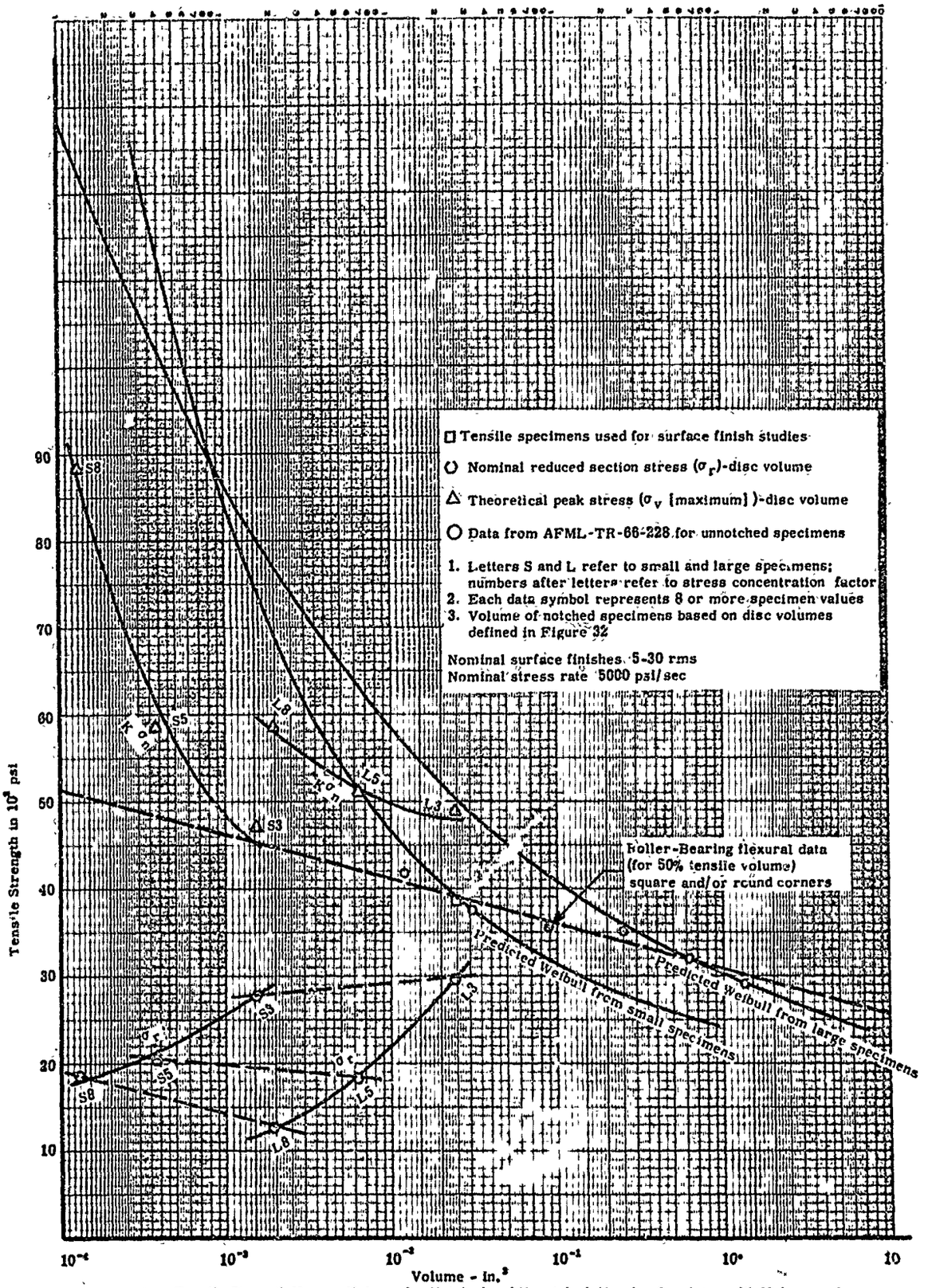

Figure 33. Tensile Strength Versus Volume for Notched and Unnotched Alumina Specimen with Volumes of Notched Specimens Based on "Disc Volumes"

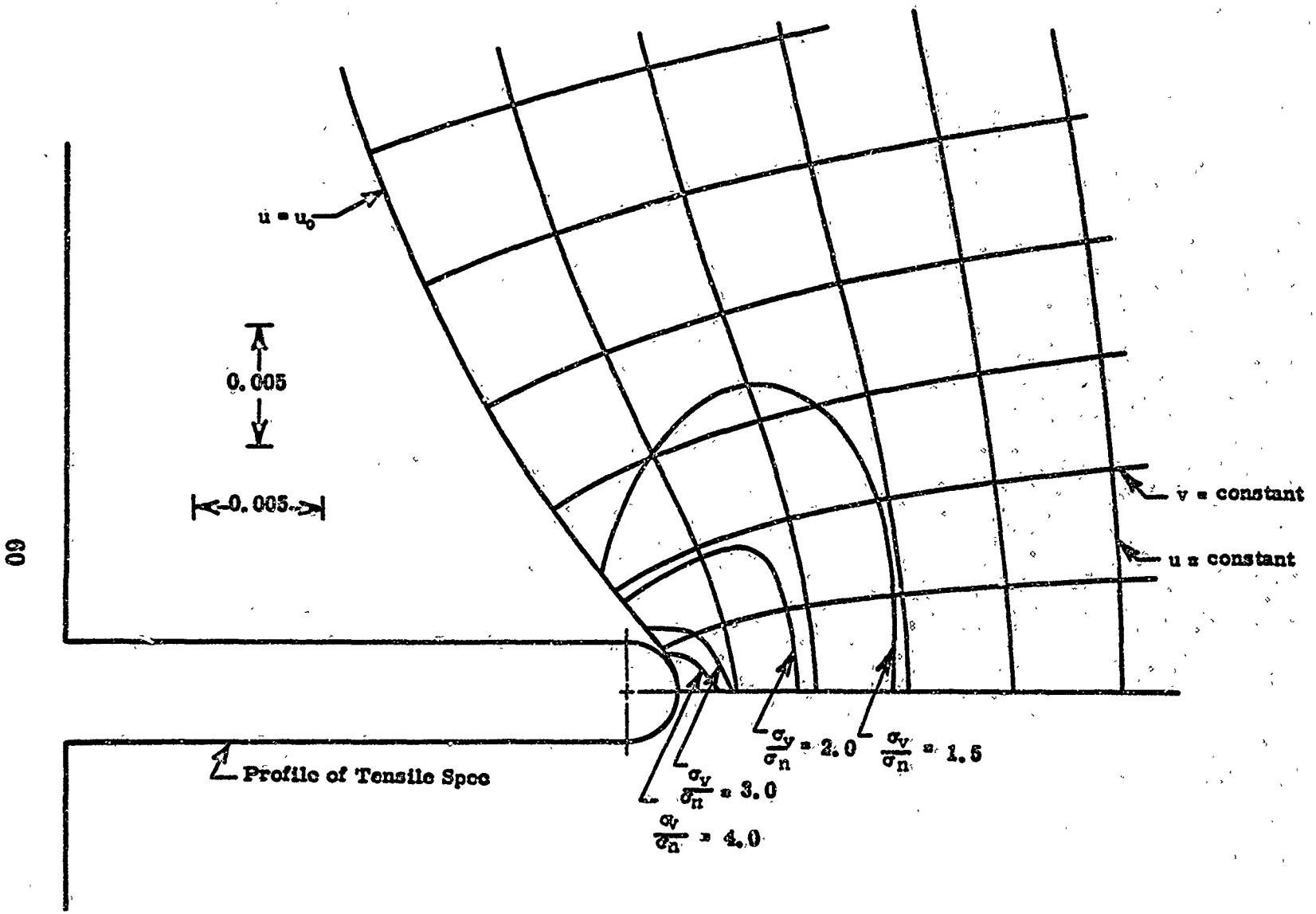

Figure 34. Contour Map of Stress Distribution in the Vicinity of the Notch for a Notch where $K_t = 8$

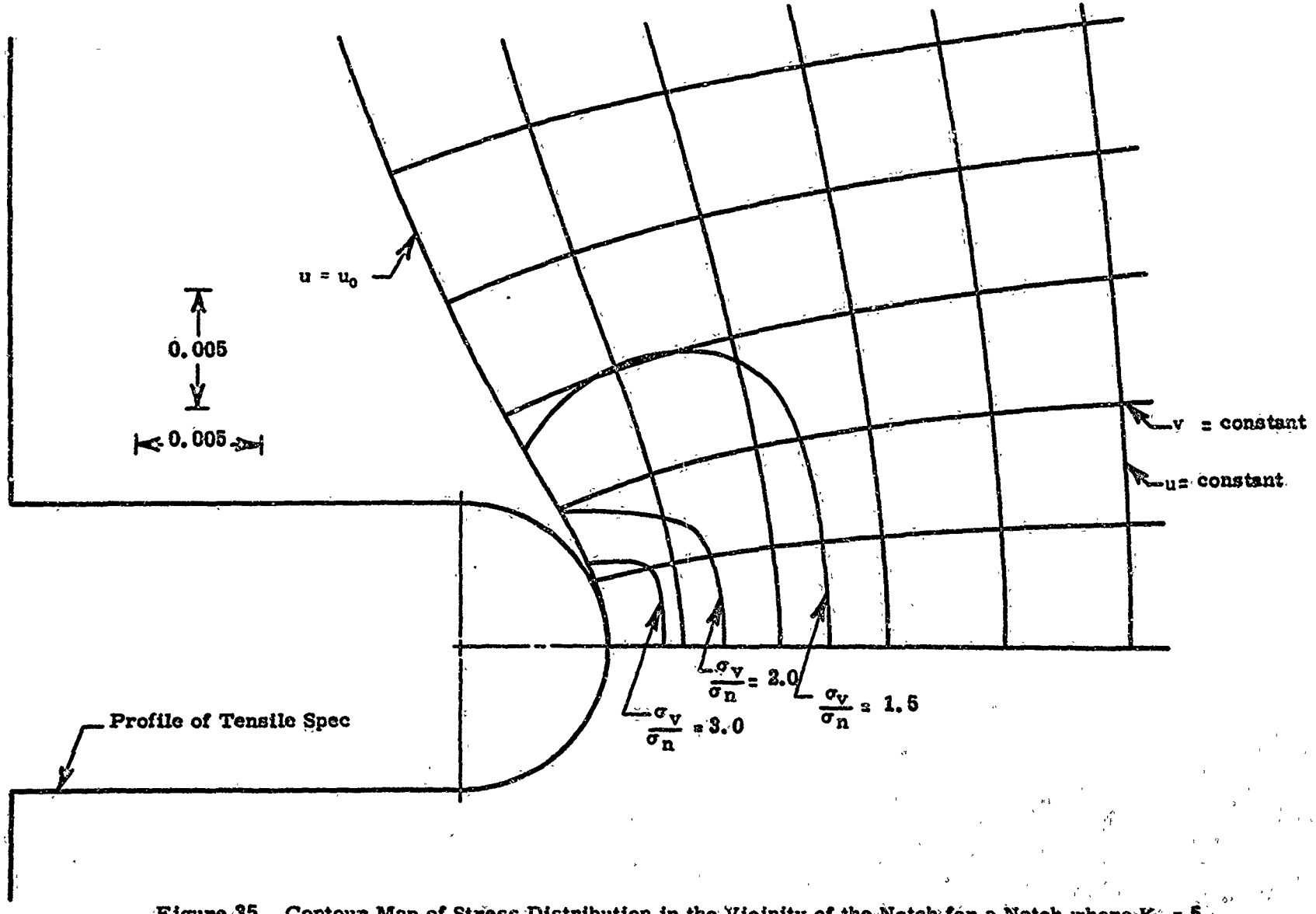

Figure 35. Contour Map of Stress Distribution in the Vicinity of the Notch for a Notch where $K_t = 5$

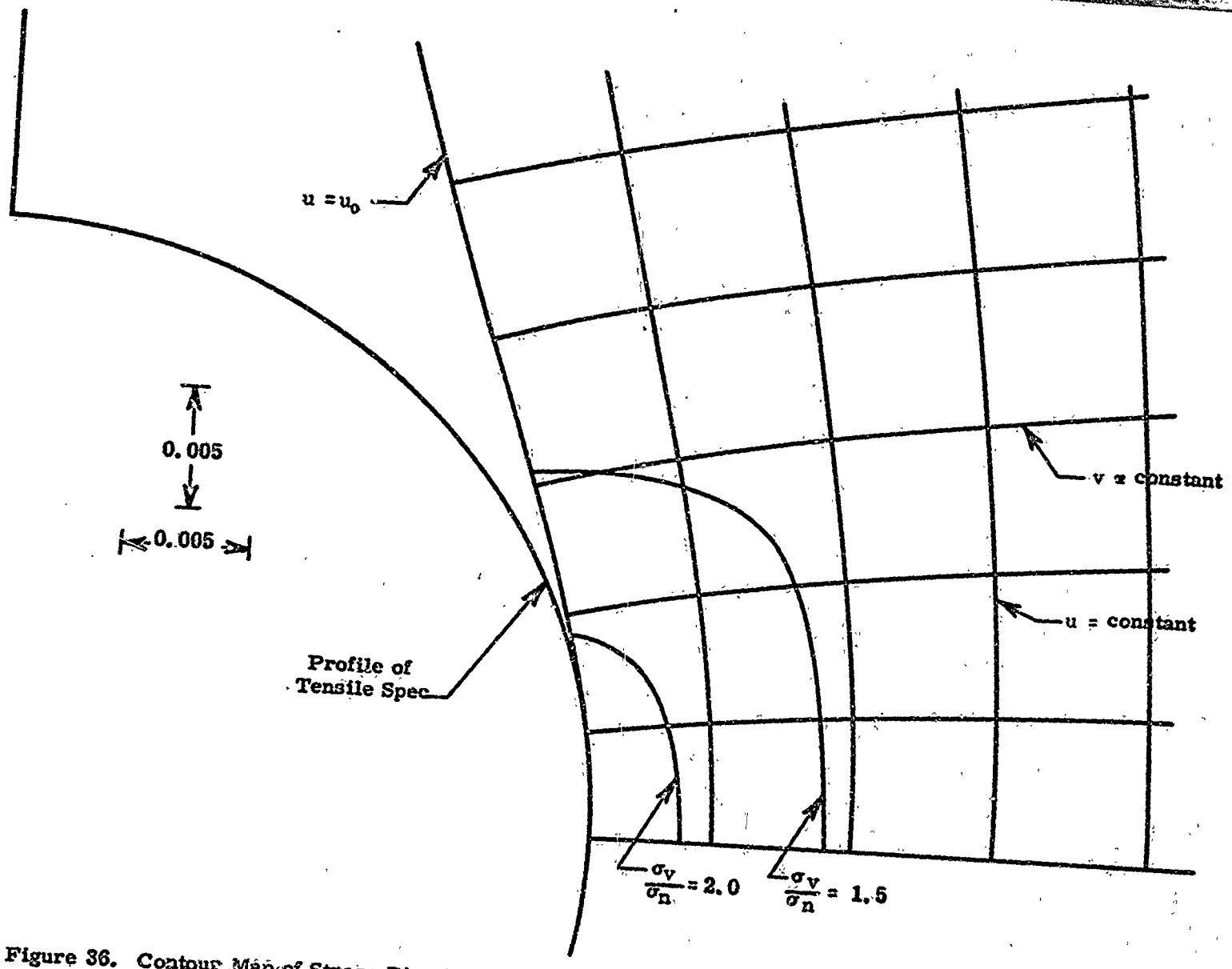

Figure 36. Contour Map of Stress Distribution in the Vicinity of the Notch for a Notch where $K_t = 3$

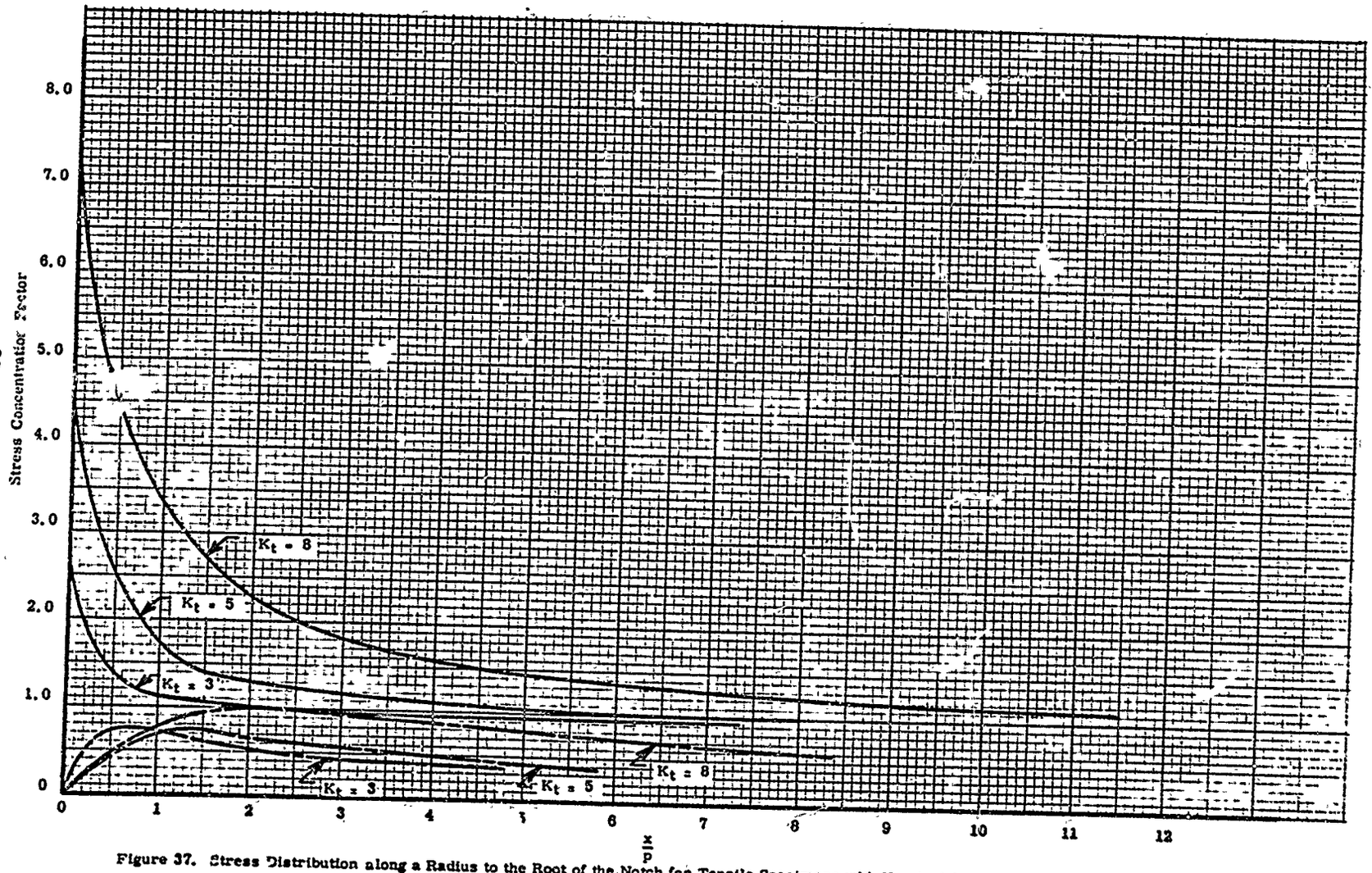

Figure 37. Stress Distribution along a Radius to the Root of the Notch for Tensile Specimens with Nominal Stress Concentrations of 3, 5, and 8

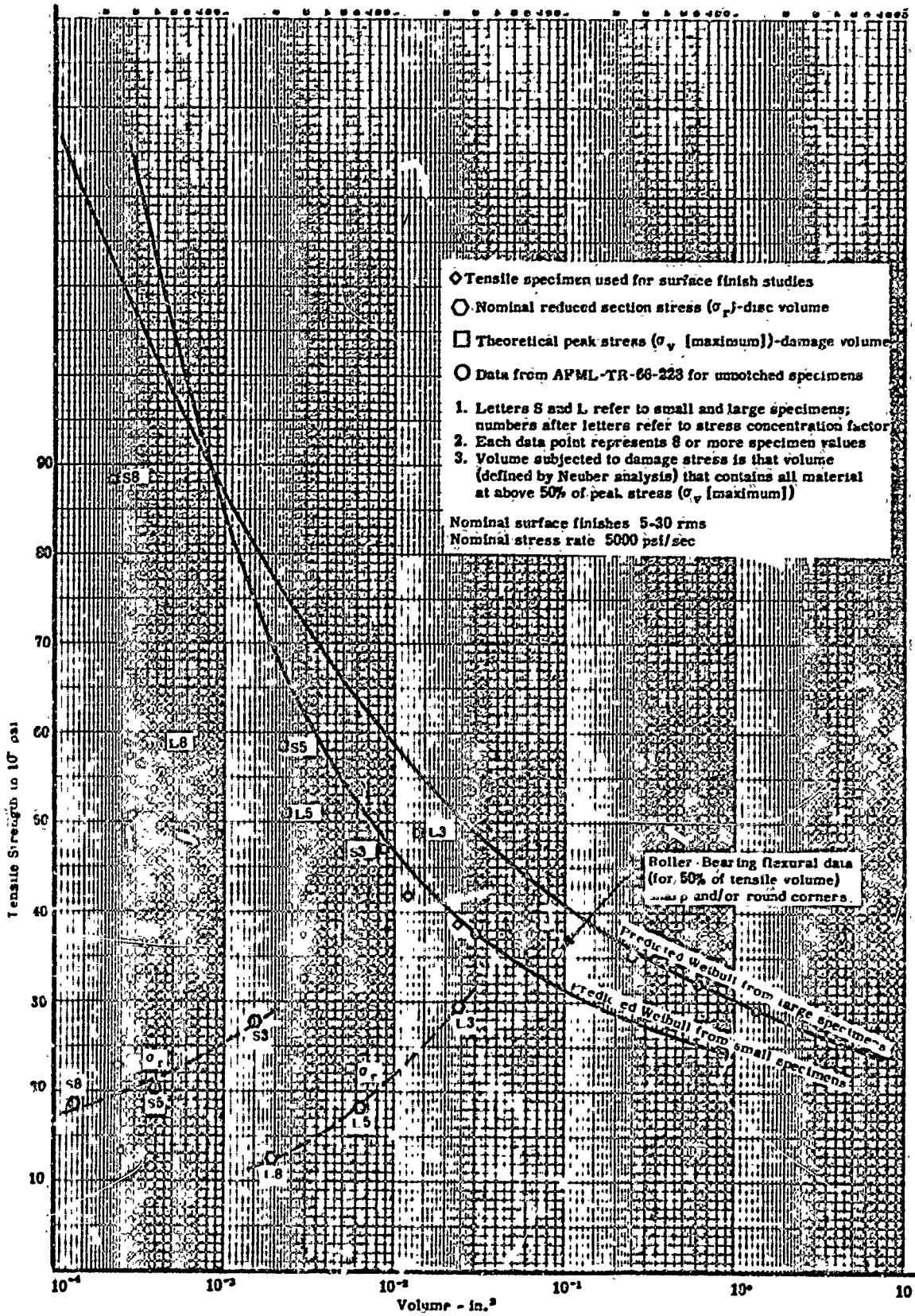

Figure 38. Tensile Strength Versus Volume for Alumina Specimens with Volumes of Notched Specimens Based on "Damage Stress"

TABLE 1

ULTIMATE TENSILE STRENGTH FOR UNNOTCHED ATJ GRAPHITE SPECIMENS

Loading Direction	Temperature °F	Specimen	Bulk Density gm/cc	Stress Rate psi/sec	Ultimate Tensile Strength psi
With Grain	70	A-m-2	1.724	325	4130
	70	A-m-5	1.753	325	3820
	70	A-c-6	1.743	325	4360
	70	A-i-7[1]	1.734	325	3830
	70	A-m-9	1.751	325	3820
	70	A-e-11[2]	1.756	-	-
	70	A-m-12	1.737	325	3900
	70	A-i-14	1.722	325	3270
	70	B-m-2	1.717	325	3420
	70	B-c-3	1.729	325	3480
	70	B-c-4	1.758	325	4470
	70	B-m-5	1.746	325	4400
	70	B-e-8	1.747	325	4640
	70	B-m-9	1.735	325	3530
	70	B-e-11	1.746	325	4020
	70	B-m-12[1]	1.737	325	3800
	70	B-c-13	1.715	325	3680
	70	C-e-1[2]	1.709	-	-
	70	C-m-2	1.704	325	3830
	70	C-c-3	1.704	325	3850
	70	C-e-4[1]	1.731	325	3430
	70	C-m-5	1.725	325	4100
	70	C-i-7[1]	1.715	325	3380
	70	C-e-8	1.734	325	3600
	70	C-m-9	1.729	325	4100
	70	C-c-10	1.721	325	3820
	70	C-e-11[1]	1.733	325	4350
	70	C-m-12[1]	1.723	325	3120
	70	C-c-13	1.717	325	4030
	70	C-i-14	1.709	325	3560
	70	D-m-2	1.698	325	3600
	70	D-m-5[2]	1.718	-	-
	70	D-c-6	1.710	325	3270
	70	D-i-7	1.707	325	4130
	70	D-m-9	1.723	325	4100
	70	D-m-12	1.722	325	4380
	70	D-c-13	1.715	325	4330
	70	E-m-1	1.693	325	4000
	70	E-m-2	1.691	325	3190
	70	E-c-3	1.698	325	4200
	70	E-m-5	1.707	325	4180
	70	E-c-6[1]	1.701	325	3770
	70	E-i-7[1]	1.699	325	3460
	70	E-e-8[1]	1.716	325	3600
	70	E-m-9	1.712	325	4420
	70	E-m-12	1.717	325	4100
	70	E-i-14	1.702	325	4100

TABLE 1 (CONT)

Loading Direction	Temperature °F	Specimen	Bulk Density gm/cc	Stress Rate psi/sec	Ultimate Tensile Strength psi
	70	F-e-1	1.690	325	3200
	70	F-m-2	1.687	325	3620
	70	F-e-4	1.703	325	4100
	70	F-m-5	1.701	325	3480
	70	F-c-6[2]	1.698	-	-
	70	F-i-7	1.699	325	4290
	70	F-e-8[1]	1.706	325	3880
	70	F-m-9	1.712	325	4500
	70	F-e-11	1.721	325	4220
	70	F-m-12	1.715	325	4180
	70	F-i-14	1.702	325	4000
	70	G-m-2	1.690	325	3780
	70	G-c-3	1.698	325	4200
	70	G-e-4	1.700	325	3520
	70	G-c-6	1.696	325	4280
	70	G-i-7[1]	1.696	325	43\0
	70	G-e-8	1.703	325	3240
	70	G-m-9	1.707	325	4440
	70	G-c-10	1.703	325	4260
	70	G-e-11[3]	1.715	-	-
	70	G-m-12	1.731	325	3500
	70	G-c-13	1.703	325	3780
	70	G-i-14	1.702	325	4000
	70	H-e-8[2]	1.7105	-	-
				Average	3950
	4000	H-e-1	1.696	325	4300
	4000	H-m-2	1.699	325	5400
	4000	H-e-4[1]	1.719	325	5250
	4000	H-m-5	1.716	325	5400
	4000	H-c-6	1.713	325	4720
	4000	H-c-10	1.712	325	5900
	4000	H-m-12[1]	1.7018	325	4580
				Average	5140
	5000	H-c-3	1.695	325	6450
	5000	H-i-7[1]	1.703	325	6700
	5000	H-m-9	1.712	325	6700
	5000	H-e-11	1.703	325	6100
	5000	H-c-13	1.702	325	6350
	5000	H-i-14	1.704	325	7100
				Average	6520

[1] Specimen failed outside of the gage section.
[2] Specimen inadvertently broken during handling.
[3] Specimen borken during machining.

TABLE 2

RESULT OF NOTCHED GRAPHITE SPECIMEN TENSILE EVALUATIONS

Loading Direction	Temperature °F	Specimen	Bulk Density gm/cc	σ_n psi	σ_r psi
With Grain	70	A-c-3-n[2]	1.716	-	
	70	A-e-8-n[2]	1.764	-	
	70	B-c-8-n	1.735	1730	
	70	D-e-1-n	1.704	1830	
	70	D-c-3-n	1.693	1780	
	70	D-e-4-n[2]	1.729	-	
	70	D-e-8-n	1.729	1610	
	70	D-c-10-n	1.715	2020	
	70	D-e-11-n[2]	1.732	-	
	70	D-i-14-n	1.709	2170	
	70	E-c-10-n	1.708	1560	
	70	E-e-11-n	1.724	1650	
	70	E-c-13-n[2]	1.708	-	
	70	F-c-13-n	1.706	1760	
			Average	1790	2690
	4000	A-c-10-n	1.737	2330	
	4000	A-c-13-n	1.732	2130	
	4000	B-i-7-n	1.729	2320	
	4000	B-c-10-n	1.733	2180	
	4000	B-i-14-n	1.727	2320	
	4000	C-c-6-n	1.715	2540	
	4000	E-e-4-n	1.717	2130	
	4000	F-c-10-n	1.711	1880	
	4000	G-m-5-n	1.700	2300	
			Average	2240	3360
	5000	A-e-1-n	1.728	4110	
	5000	A-e-4-n	1.773	4130	
	5000	B-e-1-n	1.716	3460	
	5000	F-c-3-n	1.685	3820	
	5000	G-e-1-n	1.687	3480	
			Average	3800	5700

[2] Specimen inadvertently broken during handling.

TABLE 3

AVERAGE TENSILE STRENGTH, STANDARD DEVIATION, COEFFICIENT OF VARIATION, AND WEIBULL MATERIAL CONSTANTS FOR SUBSETS OF SIZE N FOR UNNOTCHED ATJ GRAPHITE

N	σ_m	a	a/σ_m	m	σ_u	σ_o
10	3960	480	0.122	7.30	0	2500
	4040	370	0.092	8.63	500	2400
	3820	470	0.124	1.39	3000	150
	3800	300	0.078	11.76	0	2900
	4130	300	0.071	7.83	1600	1700
15	3830	330	0.085	11.43	0	2900
	4030	310	0.075	5.16	2400	120
	4010	360	0.090	10.62	0	3000
	3910	300	0.077	12.65	0	3000
	3880	430	0.110	1.61	3000	970
20	4040	310	0.076	3.25	3000	270
	3870	360	0.093	2.17	3000	550
	3940	330	0.091	11.18	0	3000
	3850	320	0.084	4.17	2500	160
	3920	440	0.113	3.27	2400	180
30	3970	370	0.093	7.32	1400	1600
	3950	410	0.103	7.58	1000	2200
	4000	420	0.105	9.05	400	2500
	4010	360	0.089	11.93	0	3100
	3950	360	0.092	3.48	2700	210
40	3950	380	0.097	5.64	1900	1100
	4000	330	0.083	13.31	0	3100
	3950	380	0.097	3.26	2700	220
	3930	360	0.092	4.69	2300	120
	3990	360	0.091	5.81	2000	1100
55	3950	370	0.093	4.43	2400	120

TABLE 4

TENSILE DATA FOR THE NOTCHED ALUMINA SPECIMENS

Specimen Size	Condition of Notch Surface	Stress Concentration Factors								
		K = 3			K = 5			K = 8		
		Specimen	σ_n psi	σ_r psi	Specimen	σ_n psi	σ_r psi	Specimen	σ_n psi	σ_r psi
Small	Polished ~8 rms	790-I	13,500	20,600	790-L	13,800	21,200	790-J	16,200	24,700
		800-36	20,200	31,100	774-30A	14,000	21,400	774-32	11,600	17,700
		790-L	23,400	35,800	826-42	15,900	24,400	790-M	13,600	20,800
		826-41	16,100	24,600	826-44	13,100	20,000	800-36	11,500	17,600
		774-32	16,900	25,800	790-M	13,900	21,300	774-30	10,200	15,600
		826-44	17,100	26,200	790-I	12,100	18,500	826-42	10,700	16,400
		774-32	19,700	30,100	774-33	10,100	15,400	826-43	12,600	19,300
					826-43[3]	-	-	774-33	10,200	15,600
	Average		18,130	27,740		13,270	20,310		12,080	18,460
	Standard Deviation		3,230	4,980		1,010	2,800		2,040	3,090
	Coefficient of Variation		0.179	0.179		0.137	0.137		0.168	0.168
Large	Polished ~8 rms	770-2	19,000	29,700	826-49	13,900	21,700	770-5	7,900	12,500
		808-39	17,000	26,600	808-8	11,400	17,900	808-8	7,800	12,200
		770-2	18,800	29,400	808-11	10,500	16,500	808-10	8,400	13,100
		808-10[4,5]	18,500	28,900	770-5	10,100	15,800	826-4	8,700	13,700
		826-47	19,500	30,500	770-4	10,300	16,100	808-39	7,700	12,000
		808-8[5]	19,400	30,300	808-42	10,500	16,500	826-49	7,700	12,000
		826-50	21,000	32,800	826-48	13,500	21,200	800-38	7,050	11,000
		800-37	17,700	27,800	800-37	12,800	20,100	770-3	9,150	12,600
		770-2	18,900	29,600						
	Average		18,540	29,490		11,630	18,220		8,050	12,600
	Standard Deviation		1,350	1,970		1,550	2,420		660	1,060
	Coefficient of Variation		0.087	0.087		0.133	0.133		0.082	0.082
Small	As Ground ~25 rms	826-41	18,600	28,400	774-29	11,700	17,900	800-34	12,200	18,700
		790-L	19,300	29,600	790-J	11,700	17,900	774-32	10,200	15,600
		800-35	18,400	28,100	826-41[6]	-	-	790-K	10,500	16,100
		774-32	18,300	28,000	808-1B	9,650	14,800	790-J	11,500	17,600
		800-35	18,400	28,100	800-32	13,100	20,000	774-30	10,900	16,700
		826-46[6]	-	-	800-31	12,000	18,400	800-31	10,100	15,500
		790-I[6]	-	-	790-K	11,600	17,700	790-J	11,400	17,400
		790-A[7]	-	-	800-34	10,100	15,500	800-32	9,950	15,300
		790-M	17,900	27,200						
	Average		18,350	28,230		11,410	17,460		10,840	16,610
	Standard Deviation		462	781		1,170	1,770		800	1,210
	Coefficient of Variation		0.026	0.026		0.101	0.101		0.074	0.073
Large	As Ground ~25 rms	800-38[3]	16,900	25,000	808-42	12,100	18,900	826-52	7,640	11,900
		774-24	17,700	26,100	790-D	13,100	20,400	800-41	7,560	11,800
		774-22	12,900	19,600	774-25	12,400	19,400	770-3	7,300	11,400
		774-24[3]	-	-	826-53	10,800	16,900	808-2	7,700	12,000
		774-22	17,900	27,400	774-25	9,750	15,300	826-50	7,960	12,500
		808-4	14,100	13,600	808-11	11,400	17,900	808-6	7,760	12,100
		826-48	16,900	25,800	826-53[7]	-	-	808-4	8,430	13,200
		800-42[6]	15,400	24,000	808.9[7]	-	-	808-7	7,700	12,000
		790-F	17,900	27,400				800-43[6]	-	-
								774-28[6]	-	-
								800-41[6]	-	-
	Average		15,910	24,990		11,590	18,130		7,760	12,110
	Standard Deviation		1,780	2,720		1,200	1,840		329	535
	Coefficient of Variation		0.112	0.110		0.103	0.103		0.043	0.044

1. Specimen slipped in grips before failure.
2. Specimen pulled out of grips.
3. Strain gage was attached to specimen.
4. Bearing bottomed during run.
5. Specimen failed outside the notch.
6. Specimen inadvertently broken while being placed in load train.
7. Lost zero on recording equipment.

TABLE 5

ALUMINA TENSILE DATA FROM UNNOTCHED TENSILE SPECIMEN FOR SURFACE FINISH STUDIES

Condition of Specimen	Specimen Number	Surface Finish rms	Tensile Strength psi
Polished ~8 rms	758-1	6-8	36,000
	758-4	8	38,000
	758-9	6-7	36,000
	810-27	4-6	39,300
	830-G	6-8	40,500
		Average	38,000
As Ground ~25 rms	758-5	27	40,300
	758-6	23	41,800
	758T-7	23	35,000
	810-30	25	40,800
	810-28	25	37,700
		Average	39,100

TABLE 6

ALUMINA FLEXURAL DATA FOR UNNOTCHED SPECIMEN

Condition of Specimen	Specimen Number	Location of Break	Tensile Strength (Flexural) psi	E in 10^6 psi
Square Corners; As Ground ~25 rms	792-0	Midspan	31,900	55.5
	774-27	Midspan	35,900	54.0
	766-18	Midspan	39,100	-
	788-8	Load Point	35,800	-
	792-W	Load Point	32,500	-
		Average	35,000[1]	
Square Corners; Polished ~8 rms	794-28	Midspan	35,300	52.3
	788-5	Midspan	37,400	49.8
	794-25	Load Point	43,800	
	790-H	Midspan	34,700	
	768-6	Midspan	30,000	
		Average	36,200[2]	
Round Corners; As Ground ~25 rms	774-26	Midspan	35,000	69.2
	764-12	Midspan	26,100	46.0
	766-8	Midspan	38,500	
	794-24	Load Point	40,000	
	792-T	Midspan	33,200	
		Average	34,560[3]	
Round Corners; Polished ~8 rms	794-31	Midspan	28,600	45.3
	794-24	Midspan	38,000	47.0
	866-8	Midspan	29,200	
	790-H	Midspan	40,000	
	770-14	Midspan	42,800	
		Average	35,700[4]	

[1]Average gas-bearing tensile value was 32,100 psi.

[2]Average gas-bearing tensile value was 32,200 psi.

[3]Average gas-bearing tensile value was 27,500 psi.

[4]Average gas-bearing tensile value was 28,300 psi.

Averages noted in footnotes 1, 2, 3 and 4 were for parent tensile specimens which had larger volumes. Specimens which broke in the radius or where a visible flaw was found were not included in tensile averages.

TABLE 7

VOLUMES OF MATERIAL IN NOTCH REGIONS SUBJECTED TO STRESSES AS SHOWN FOR ALL NOTCH SPECIMEN CONFIGURATION

SMALL SPECIMENS (NOMINAL DIAMETER = 0.250 in.)
VOLUME IN 10^{-2} in.^{3}

Kt \ $\frac{\sigma_v}{\sigma_n} \geq$	1.5	2.0	2.5	3.0	4.0
3	0.86	0.28			
5	1.46	0.34	0.12	0.094	
8	1.35	0.37	-	0.079	0.022

LARGE SPECIMENS (NOMINAL DIAMETER = 0.625 in.)
VOLUME IN 10^{-2} in.^{3}

Kt \ $\frac{\sigma_v}{\sigma_n} \geq$	1.5	2.0	2.5	3.0	4.0
3	1.38	0.44			
5	2.27	0.51	0.23	0.15	
8	2.11	0.59	-	0.12	0.035

REFERENCES

1. W. Weibull, "A Statistical Theory of the Strength of Materials." Ing. Ventenskaps Akard Handl. No. 151. Stockholm (1939).

2. W. Weibull, "The Phenomenon of Rupture in Solids." Ing. Ventenskaps Akard Handl. No. 153. Stockholm (1939).

3. W. Weibull, "A Statistical Distribution Function of Wide Applicability." J. Appl. Mech. 18. pp 223. 1952.

4. Heinz Neuber. "The Theory of Notch Stress." AEC-TR-4547.

5. C. D. Pears and H. S. Starrett. "An Experimental Study of the Weibull Volume Theory." AFML-TR-66-228. June 1966.

APPENDIX A - GENERAL STRESS-STRAIN EQUATION IN CARTESIAN COORDINATES

APPENDIX B - THE FLOATED SLEEVE TENSILE TEST

APPENDIX C - FLEXURAL ANALYSIS

APPENDIX A

GENERAL STRESS-STRAIN EQUATION IN CARTESIAN COORDINATES

The equilibriam conditions are

$$\frac{\partial \sigma_x}{\partial x} + \frac{\partial \gamma_{xy}}{\partial y} + \frac{\partial \gamma_{xz}}{\partial z} = 0$$

$$\frac{\partial \gamma_{xy}}{\partial x} + \frac{\partial \sigma_y}{\partial y} + \frac{\partial \gamma_{yz}}{\partial z} = 0$$

$$\frac{\partial \gamma_{xz}}{\partial x} + \frac{\partial \gamma_{yz}}{\partial y} + \frac{\partial \sigma_z}{\partial z} = 0 \qquad (1)$$

Using Hooke's Law the relations between the stresses and strains are given by the equations

$$\epsilon_x = \left[\frac{1}{E}\ \sigma_x - \frac{1}{m}\ (\sigma_y + \sigma_z)\right]$$

$$\epsilon_y = \left[\frac{1}{E}\ \sigma_y - \frac{1}{m}\ (\sigma_z + \sigma_x)\right]$$

$$\epsilon_z = \left[\frac{1}{E}\ \sigma_z - \frac{1}{m}\ (\sigma_x + \sigma_y)\right]$$

$$\nu_{xy} = \frac{1}{G}\,\tau_{xy},\ \gamma_{yz} = \frac{1}{G}\,\tau_{yz},\ \gamma_{zx} = \frac{1}{G}\,\tau_{zx} \qquad (2)$$

The cubical dilation is defined to be the sum of the principal strains, and it is invariant under coordinate transformations so that

$$e = \epsilon_x + \epsilon_y + \epsilon_z \qquad (3)$$

Using equation (2) this may be written as

$$e = \frac{1}{E}\ (1 - \frac{2}{m})\ (\sigma_x + \sigma_y + \sigma_z) \qquad (4)$$

Consider the equation

$$\epsilon_x = \frac{1}{E}\left[\sigma_x - \frac{1}{m}(\sigma_y + \sigma_z)\right]$$

$$= \frac{1}{E}\left[(1 + \frac{1}{m})\,\sigma_x - \frac{1}{m}(\sigma_x + \sigma_y + \sigma_z)\right]$$

$$= \frac{1}{E}(1 + \frac{1}{m})\,\sigma_x - \frac{1}{m}\,\frac{e}{(1 - \frac{2}{m})}$$

or

$$\sigma_x = \frac{E}{(1 + \frac{1}{m})}(\epsilon_x + \frac{e}{m - 2})$$

Now $G = \frac{E}{2(1 + \frac{1}{m})}$ so that (5)

$$\sigma_x = 2G(\epsilon_x + \frac{e}{m - 2})$$

Also $\sigma_y = 2G(\epsilon_y + \frac{e}{m - 2})$

$$\sigma_z = 2G(\epsilon_z + \frac{e}{m - 2}) \quad (6)$$

Let ξ, η, and ζ be the displacements in the x, y, and z directions, respectively. Then

$$\epsilon_x = \frac{\partial \xi}{\partial x},\ \epsilon_y = \frac{\partial \eta}{\partial y},\ \epsilon_z = \frac{\partial \zeta}{\partial z}$$

$$\nu_{xy} = \frac{\partial \eta}{\partial x} + \frac{\partial \xi}{\partial y},\ \nu_{yz} = \frac{\partial \zeta}{\partial y} + \frac{\partial \eta}{\partial z},\ \nu_{zx} = \frac{\partial \xi}{\partial z} + \frac{\partial \zeta}{\partial x} \quad (7)$$

Using these equations along with equation (2) and (6) and substituting into the first equilibrium equation

$$\frac{\partial \sigma_x}{\partial x} + \frac{\partial \gamma_{xy}}{\partial y} + \frac{\partial \gamma_{xz}}{\partial z} = 0$$

yields

$$\frac{\partial^2 \xi}{\partial x^2} + \frac{\partial^2 \xi}{\partial y^2} + \frac{\partial^2 \xi}{\partial z^2} + \frac{\partial}{\partial x}\left(\frac{\partial \xi}{\partial x} + \frac{\partial \eta}{\partial y} + \frac{\partial \zeta}{\partial z}\right) + \frac{2}{m-2}\frac{\partial e}{\partial x} = 0$$

$$\Delta\xi + \frac{m}{m-2}\frac{\partial e}{\partial x} = 0$$

$$\text{also } \Delta\eta + \frac{m}{m-2}\frac{\partial e}{\partial y} = 0 \qquad (8)$$

$$\Delta\zeta + \frac{m}{m-2}\frac{\partial e}{\partial z} = 0$$

$$\text{where } e = \frac{\partial \xi}{\partial x} + \frac{\partial \eta}{\partial y} + \frac{\partial \zeta}{\partial z}$$

To solve equations (8), let

$$2G\xi = \frac{-\partial F}{\partial x} + 2\alpha\phi_1$$

$$2G = \frac{-\partial F}{\partial y} + 2\alpha\phi_2 \qquad (9)$$

$$2G\zeta = \frac{-\partial F}{\partial z} + 2\alpha\phi_3$$

where
F is a three dimensional stress function
α is a constant
ϕ_1, ϕ_2, and ϕ_3 are harmonic functions of x, y, and z

The relation between the stress function and the harmonic functions can be shown to be

$$(2 - \frac{2}{m})\Delta F = 2\alpha\left(\frac{2\phi_1}{\partial x} + \frac{2\phi_2}{\partial y} + \frac{2\phi_3}{\partial z}\right) \qquad (10)$$

Let

$$F = \phi_0 + x\phi_1 + y\phi_2 + z\phi_3 \qquad (11)$$

where ϕ_0 is a harmonic function

Then

$$F = 2\left(\frac{\partial \phi_1}{\partial x} + \frac{\partial \phi_2}{\partial y} + \frac{\partial \phi_3}{\partial z}\right) \tag{12}$$

so that

$$\alpha = 2\left(1 - \frac{1}{m}\right) \tag{13}$$

The stresses may be written as follows

$$\sigma_x = \frac{\partial F}{\partial y} + \frac{\partial F}{\partial z} + \alpha\left(\frac{\partial \phi_1}{\partial x} - \frac{\partial \phi_2}{\partial y} - \frac{\partial \phi_3}{\partial z}\right) \text{ etc.} \tag{14}$$

$$\gamma_{xy} = \frac{-\partial^2 F}{\partial x \partial y} + \alpha\left(\frac{\partial \phi_1}{\partial y} + \frac{\partial \phi_2}{\partial x}\right) \text{ etc.} \tag{15}$$

It can be shown that one of the four harmonic functions (ϕ_0, ϕ_1, ϕ_2, and ϕ_3) may always be set identically equal to zero. It is immaterial which of the four is used.

TWO-DIMENSIONAL STRESS PROBLEM

$$F = \phi_0 + x\phi_1 + y\phi_2 + z\phi_3$$

Immediately set $\phi_2 = 0$. Now, so that $F = F(x, y)$ only ϕ_3 must be identically zero. Hence

$$F = \phi_0 + x\phi_1$$

where

$$\phi_0 = \phi_0(x, y)$$

$$\phi_1 = \phi_1(x, y) \tag{16}$$

Then

$$2G\xi = \frac{-\partial F}{\partial x} + 2\alpha\phi_1$$

$$2G\eta = \frac{-\partial F}{\partial y}$$

$$\zeta = 0 \tag{17}$$

These equations correspond to a plane strain condition.

For purposes of simplification let

$$\phi_1 = \frac{\partial \phi_1'}{\partial x} \qquad \phi_0 = \alpha\phi_1' + \phi_0' \tag{18}$$

$$F' = \phi_0' + \frac{x\partial\phi_1'}{\partial x} + \alpha\phi_1' = F' + \alpha\phi_1' \tag{19}$$

where

$$F' = \phi_0' + x\frac{\partial\phi_1'}{\partial x} \tag{20}$$

Then

$$2G\xi = -\frac{\partial}{\partial x}(F' - \alpha\phi_1')$$

$$2G\eta = -\frac{\partial}{\partial y}(F' + \alpha\phi_1')$$

$$\zeta = 0 \tag{21}$$

and the stresses become

$$\sigma_x = \frac{\partial^2 F'}{\partial y^2}, \qquad \sigma_y = \frac{\partial^2 F'}{\partial x^2}, \quad \tau_{xy} = -\frac{\partial^2 F'}{\partial x \partial y} \tag{22}$$

$$\tau_{xz} = \tau_{yz} = 0 \tag{23}$$

$$\sigma_z = \frac{\partial^2 F'}{\partial x^2} + \frac{\partial^2 F'}{\partial y^2} - \alpha\frac{\partial^2 \phi_1'}{\partial x^2} \tag{24}$$

Now

$$\Delta F = \Delta F' = 2\frac{\partial^2 \phi'}{\partial t^2} \tag{25}$$

so that

$$\sigma_z = \Delta F' - \frac{\alpha}{2}\Delta F' = \left(1 - \frac{\alpha}{2}\right)\Delta F'$$

$$\sigma_z = \frac{1}{m}\Delta F' = \frac{1}{m}(\sigma_x + \sigma_y) \tag{26}$$

The above relationships for the stresses σ_x, σ_y, and γ_{xy} can be shown to be valid for the plane stress condition also.

Then the initial equations for a two-dimensional sresss problem are

$$F = \phi_0 + x\phi_1$$

where

$$\phi_0 = \phi_0(x, y)$$

$$\phi_1 = \phi_1(x, y) \tag{27}$$

and

$$\Delta\phi_0 = \Delta\phi_1 = 0$$

The boundary conditions for a nonloaded boundary in two dimensions are expressed by the relations

$$\frac{\partial F}{\partial x} = \text{constant}$$

$$\frac{\partial F}{\partial y} = \text{constant} \tag{28}$$

CURVILINEAR COORDINATES

In many problems it is more convenient to deal with a curvilinear coordinate system rather than a rectilinear one. This is especially true when dealing with bodies that have a curved surface. By using a coordinate system whose coordinate lines and planes outline the body under consideration, it is generally easier to describe and satisfy the pattern of the stresses which act on the surface. This discussion will be limited to orthogonal systems, since they are simpler and are the most commonly used.

Consider a set of three independent functions of the Cartesian variables, x, y, z, implicitly defined by the equations

$$x = x(u, v, w)$$

$$y = y(u, v, w)$$

$$z = z(u, v, w) \tag{29}$$

Then the intersections of the surfaces

$$u = \text{constant}$$

$$v = \text{constant}$$

$$w = \text{constant}$$

pair by pair determine the coordinate lines of the curvilinear system, and the intersections of the coordinate lines determine a point (u, v, w). The u-direction is understood to be the direction normal to the surface u-constant and positive in the direction of the increasing values of u. Similarly for the v and w directions.

Deformation

The displacements in the u, v, and w directions will be labeled U, V, and W, respectively. In terms of the x, y, z displacements ξ, η, and ζ, the U, V, and W displacements are given by

$$U = \frac{1}{h_u}\left(\xi\frac{\partial x}{\partial u} + \frac{\partial y}{\partial u} + \zeta\frac{\partial z}{\partial u}\right)$$

$$V = \frac{1}{h_v}\left(\xi\frac{\partial x}{\partial v} + \frac{\partial y}{\partial v} + \zeta\frac{\partial z}{\partial v}\right)$$

$$W = \frac{1}{h_w}\left(\xi\frac{\partial x}{\partial w} + \frac{\partial y}{\partial w} + \zeta\frac{\partial z}{\partial w}\right) \qquad (30)$$

where

$$h_u^2 = \left(\frac{\partial x}{\partial u}\right)^2 + \left(\frac{\partial y}{\partial u}\right)^2 + \left(\frac{\partial z}{\partial u}\right)^2$$

$$h_v^2 = \left(\frac{\partial x}{\partial v}\right)^2 + \left(\frac{\partial y}{\partial v}\right)^2 + \left(\frac{\partial z}{\partial v}\right)^2$$

$$h_w^2 = \left(\frac{\partial x}{\partial w}\right)^2 + \left(\frac{\partial y}{\partial w}\right)^2 + \left(\frac{\partial z}{\partial w}\right)^2 \qquad (31)$$

These h's are sometimes referred to as "factors of distortion." The strains ϵ_u, ϵ_v, and ϵ_w can be shown to be given by the equations

$$\epsilon_u = \frac{1}{h_u}\left(\frac{\partial U}{\partial u} + \frac{V}{h_v}\frac{\partial h_u}{\partial v} + \frac{W}{h_w}\frac{\partial h_u}{\partial w}\right)$$

$$\epsilon_v = \frac{1}{h_v}\left(\frac{U}{h_u}\frac{\partial h_v}{\partial u} + \frac{\partial V}{\partial v} + \frac{W}{h_w}\frac{\partial h_v}{\partial w}\right)$$

$$\epsilon_w = \frac{1}{h_w}\left(\frac{U}{h_u}\frac{\partial h_w}{\partial u} + \frac{V}{h_v}\frac{\partial h_w}{\partial v} + \frac{\partial W}{\partial w}\right) \qquad (32)$$

and the shearing strains are given by

$$\gamma_{uv} = \frac{h_u}{h_v}\frac{\partial}{\partial v}\left(\frac{U}{h_u}\right) + \frac{h_v}{h_u}\frac{\partial}{\partial u}\left(\frac{V}{h_v}\right)$$

$$\gamma_{vw} = \frac{h_v}{h_w}\frac{\partial}{\partial w}\left(\frac{V}{h_v}\right) + \frac{h_w}{h_v}\frac{\partial}{\partial v}\left(\frac{W}{h_w}\right)$$

$$\gamma_{wu} = \frac{h_w}{h_u}\frac{\partial}{\partial u}\left(\frac{W}{h_w}\right) + \frac{h_u}{h_w}\frac{\partial}{\partial w}\left(\frac{U}{h_u}\right) \qquad (33)$$

Since the cubical dilation is invariant under co-ordinate transformation, it is given simply as

$$e = \epsilon_u + \epsilon_v + \epsilon_w \tag{34}$$

Stresses

By Hooke's Law the stresses are given by

$$\sigma_u = 2G\left(\epsilon_u + \frac{e}{m-2}\right)$$

$$\sigma_v = 2G\left(\epsilon_v + \frac{e}{m-2}\right)$$

$$\sigma_w = 2G\left(\epsilon_w + \frac{e}{m-2}\right) \tag{35}$$

$$\tau_{uv} = G\gamma_{uv}\,,\ \tau_{vw} = G\gamma_{vw}\,,\ \tau_{wu} = G\gamma_{wu}$$

Consider now the calculation of the stresses in terms of the stress function F and the harmonic functions ϕ_1, ϕ_2, and ϕ_3. Using equation (30) and (9) we can write

$$2GU = \frac{1}{h_u}\left[-\frac{\partial F}{\partial u} + 2\alpha\left(\phi_1\frac{\partial x}{\partial u} + \phi_2\frac{\partial y}{\partial u} + \phi_3\frac{\partial z}{\partial u}\right)\right]$$

$$2GV = \frac{1}{h_v}\left[-\frac{\partial F}{\partial v} + 2\alpha\left(\phi_1\frac{\partial x}{\partial v} + \phi_2\frac{\partial y}{\partial v} + \phi_3\frac{\partial z}{\partial v}\right)\right]$$

$$2GW = \frac{1}{h_w}\left[-\frac{\partial F}{\partial w} + 2\alpha\left(\phi_1\frac{\partial x}{\partial w} + \phi_2\frac{\partial y}{\partial w} + \phi_3\frac{\partial z}{\partial w}\right)\right] \tag{36}$$

Now from the first equations of each of the sets of equations (32) and (35)

$$\sigma_u = \frac{1}{h_u}\left\{\frac{\partial}{\partial u}\left(\frac{1}{h_u}\left[-\frac{\partial F}{\partial u} + 2\alpha\left(\phi_1\frac{\partial x}{\partial u} + \phi_2\frac{\partial y}{\partial u} + \phi_3\frac{\partial z}{\partial u}\right)\right]\right)\right.$$
$$+\frac{1}{h_u^2}\left[\frac{-\partial F}{\partial v} + 2\alpha\left(\phi_1\frac{\partial x}{\partial v} + \phi_2\frac{\partial y}{\partial v} + \phi_3\frac{\partial z}{\partial v}\right)\right]\frac{\partial hu}{\partial v} + \frac{1}{h_w^2}\left[-\frac{\partial F}{\partial w}\right.$$
$$\left.\left.+ 2\alpha\left(\phi_1\frac{\partial x}{\partial w} + \phi_2\frac{\partial y}{\partial w} + \phi_3\frac{\partial z}{\partial w}\right)\right]\frac{\partial hu}{\partial hw}\right\} + \frac{2Ge}{m-2}$$

This may be written as

$$\sigma_u = -\frac{1}{h_u}\frac{\partial}{\partial u}\left(\frac{1}{h_u}\frac{\partial F}{\partial u}\right) - \frac{1}{h_u h_v^2}\frac{\partial F}{\partial v}\frac{\partial h_u}{\partial v} - \frac{1}{h_u h_w^2}\frac{\partial F}{\partial w}\frac{\partial h_u}{\partial w}$$
$$+\frac{2\alpha}{h_u^2}\left(\frac{\partial \phi_1}{\partial u}\frac{\partial x}{\partial u} + \frac{\partial \phi_2}{\partial u}\frac{\partial y}{\partial u} + \frac{\partial \phi_3}{\partial u}\frac{\partial z}{\partial u}\right)$$
$$+2\alpha\phi_1\left\{\frac{1}{h_u}\frac{\partial}{\partial u}\left(\frac{1}{h_u}\frac{\partial x}{\partial u}\right) + \frac{1}{h_u h_v^2}\frac{\partial h_u}{\partial v}\frac{\partial x}{\partial v} + \frac{1}{h_u h_w^2}\frac{\partial h_u}{\partial w}\frac{\partial x}{\partial w}\right\}$$
$$+2\alpha\phi_2\left\{\frac{1}{h_u}\frac{\partial}{\partial u}\left(\frac{1}{h_u}\frac{\partial y}{\partial u}\right) + \frac{1}{h_u h_v^2}\frac{\partial h_u}{\partial v}\frac{\partial y}{\partial v} + \frac{1}{h_u h_w^2}\frac{\partial h_u}{\partial w}\frac{\partial y}{\partial w}\right\}$$
$$+2\alpha\phi_3\left\{\frac{1}{h_u}\frac{\partial}{\partial u}\left(\frac{1}{h_u}\frac{\partial z}{\partial u}\right) + \frac{1}{h_u h_v^2}\frac{\partial h_u}{\partial v}\frac{\partial z}{\partial v} + \frac{1}{h_u h_w^2}\frac{\partial h_u}{\partial w}\frac{\partial z}{\partial w}\right\}$$
$$+\frac{2Ge}{m-2}$$

$$\sigma_u = -\frac{\partial^2 F}{\partial \eta_u^2} + \frac{2\partial}{h_u^2}\left(\frac{\partial \phi_1}{\partial u}\frac{\partial x}{\partial u} + \frac{\partial \phi_2}{\partial u}\frac{\partial y}{\partial u} + \frac{\partial \phi_3}{\partial u}\frac{\partial z}{\partial u}\right)$$
$$+2\alpha\left(\phi_1\frac{\partial^2 x}{\partial \eta_u^2} + \phi_2\frac{\partial^2 y}{\partial \eta_u^2} + \phi_3\frac{\partial^2 z}{\partial \eta_u^2}\right) + \frac{2Ge}{m-2}$$

Now $2Ge = \left(1-\frac{2}{m}\right)\Delta F$ and $\frac{1}{m} = 1 - \frac{\alpha}{2}$ so that

$$\frac{2Ge}{m-2} = \left(1 - \frac{\alpha}{2}\right)\Delta F \qquad (37)$$

and

$$\sigma_u = -\frac{\partial^2 F}{\partial \eta_u^2} + \frac{2\alpha}{h_u^2}\left(\frac{\partial \phi_1}{\partial u}\frac{\partial x}{\partial u} + \frac{\partial \phi_2}{\partial u}\frac{\partial y}{\partial u} + \frac{\partial \phi_3}{\partial u}\frac{\partial z}{\partial u}\right)$$
$$+2\alpha\left(\phi_1\frac{\partial^2 x}{\partial \eta_u^2} + \phi_2\frac{\partial^2 y}{\partial \eta_u^2} + \phi_3\frac{\partial^2 z}{\partial \eta_u^2}\right) + \left(1 - \frac{\alpha}{2}\right)\Delta F \qquad (38)$$

where

$$\frac{\partial}{\partial \eta_u^2} = \frac{1}{h_u}\frac{\partial}{\partial u}\left(\frac{1}{h_u}\frac{\partial}{\partial u}\right) + \frac{1}{h_u h_v^2}\frac{\partial h_u}{\partial v}\frac{\partial}{\partial v} + \frac{1}{h_u h_w^2}\frac{\partial h_u}{\partial w}\frac{\partial}{\partial w} \qquad (39)$$

Consider the special case where

ϕ_1 = constant = C $\phi_2 = 0$
$\phi_0 = -xC$ $\phi_3 = 0$

Then $F = \phi_0 + x\phi_1 + y\phi_2 + z\phi_3 = 0$

$$2G\xi = -\frac{\partial F}{\partial x} + 2\alpha\phi_1 = 2\alpha C$$

$$\xi = \frac{\alpha}{G} C$$

$$\eta = 0$$
$$\zeta = 0$$

All points of the body are displaced in the same direction for the same distance. There are no stresses or deformations; hence from the above the coefficient of ϕ_1 must be zero, that is

$$\frac{\partial^2 x}{\partial \eta_u^2} = 0$$

In a similar manner it can be shown that $\frac{\partial^2 y}{\partial \eta_u^2}$ and $\frac{\partial^2 z}{\partial \eta_u^2}$ must also be zero. Hence

$$\sigma_u = -\frac{\partial F}{\partial \eta_u^2} + \frac{2\alpha}{h_u^2}\left(\frac{\partial \phi_1}{\partial u}\frac{\partial x}{\partial u} + \frac{\partial \phi_2}{\partial u}\frac{\partial y}{\partial u} + \frac{\partial \phi_3}{\partial u}\frac{\partial z}{\partial u}\right) + \left(1-\frac{\alpha}{2}\right)\Delta F \quad (40)$$

An identical procedure to that used above can be used to show

$$\sigma_u = -\frac{\partial F}{\partial \eta_v^2} + \frac{2\alpha}{h_v^2}\left(\frac{\partial \phi_1}{\partial v}\frac{\partial x}{\partial v} + \frac{\partial \phi_2}{\partial v}\frac{\partial y}{\partial v} + \frac{\partial \phi_3}{\partial v}\frac{\partial z}{\partial v}\right) + \left(1-\frac{\alpha}{2}\right)\Delta F \quad (41)$$

$$\sigma_w = -\frac{\partial F}{\partial \eta_w^2} + \frac{2\alpha}{h_w^2}\left(\frac{\partial \phi_1}{\partial w}\frac{\partial x}{\partial w} + \frac{\partial \phi_2}{\partial w}\frac{\partial y}{\partial w} + \frac{\partial \phi_3}{\partial w}\frac{\partial z}{\partial w}\right) + \left(1-\frac{\alpha}{2}\right)\Delta F \quad (42)$$

and

$$\tau_{uv} = -\frac{\partial^2 F}{\partial \eta_u \partial \eta_v} + \frac{\alpha}{h_u h_v}\left(\frac{\partial \phi_1}{\partial u}\frac{\partial x}{\partial v} + \frac{\partial \phi_1}{\partial v}\frac{\partial x}{\partial u} + \frac{\partial \phi_2}{\partial u}\frac{\partial y}{\partial v} + \frac{\partial \phi_2}{\partial v}\frac{\partial y}{\partial u} + \frac{\partial \phi_3}{\partial u}\frac{\partial z}{\partial v} + \frac{\partial \phi_3}{\partial v}\frac{\partial z}{\partial u}\right) \quad (43)$$

$$\tau_{vw} = -\frac{\partial^2 F}{\partial \eta_v \partial \eta_w} + \frac{\alpha}{h_v h_w}\left(\frac{\partial \phi_1}{\partial v}\frac{\partial x}{\partial w} + \frac{\partial \phi_1}{\partial w}\frac{\partial x}{\partial v} + \frac{\partial \phi_2}{\partial v}\frac{\partial y}{\partial w} + \frac{\partial \phi_2}{\partial w}\frac{\partial y}{\partial v} + \frac{\partial \phi_2}{\partial v}\frac{\partial z}{\partial w} + \frac{\partial \phi_3}{\partial w}\frac{\partial z}{\partial v}\right) \quad (44)$$

$$\tau_{wu} = -\frac{\partial^2 F}{\partial \eta_w \partial \eta_u} + \frac{\alpha}{h_w h_u}\left(\frac{\partial \phi_1}{\partial w}\frac{\partial x}{\partial u} + \frac{\partial \phi_1}{\partial u}\frac{\partial x}{\partial w} + \frac{\partial \phi_2}{\partial w}\frac{\partial y}{\partial u} + \frac{\partial \phi_2}{\partial u}\frac{\partial y}{\partial w} + \frac{\partial \phi_3}{\partial w}\frac{\partial z}{\partial u} + \frac{\partial \phi_3}{\partial u}\frac{\partial z}{\partial w}\right) \quad (45)$$

where

$$\frac{\partial^2}{\partial \eta_u \partial \eta_v} = \frac{\partial^2}{\partial \eta_v \partial \eta_u} = \frac{1}{h_u}\frac{\partial}{\partial u}\left(\frac{1}{h_v}\frac{\partial}{\partial v}\right) - \frac{1}{h_u^2 h_v}\frac{\partial h_u}{\partial v}\frac{\partial}{\partial u}$$

$$= \frac{1}{h_v}\frac{\partial}{\partial v}\left(\frac{1}{h_u}\frac{\partial}{\partial u}\right) - \frac{1}{h_u h_v^2}\frac{\partial h_v}{\partial u}\frac{\partial}{\partial v}$$

$$= \frac{h_v}{2h_u}\frac{\partial}{\partial u}\left(\frac{1}{h_v^2}\frac{\partial}{\partial v}\right) + \frac{h_u}{2h_v}\frac{\partial}{\partial v}\left(\frac{1}{h_u^2}\frac{\partial}{\partial u}\right) \qquad (46)$$

with cyclic permutations in u, v, and w.

To determine the form of the operator Δ use equations (30), (32) and (34) to obtain

$$2Ge = -\left(\frac{\partial^2 F}{\partial \eta_u^2} + \frac{\partial^2 F}{\partial \eta_v^2} + \frac{\partial^2 F}{\partial \eta_w^2}\right) + \frac{2\alpha}{h_u^2}\left(\frac{\partial \phi_1}{\partial u}\frac{\partial x}{\partial u} + \frac{\partial \phi_2}{\partial u}\frac{\partial y}{\partial u} + \frac{\partial \phi_3}{\partial u}\frac{\partial z}{\partial u}\right)$$
$$+ \frac{2\alpha}{h_v^2}\left(\frac{\partial \phi_1}{\partial v}\frac{\partial x}{\partial v} + \frac{\partial \phi_2}{\partial v}\frac{\partial y}{\partial v} + \frac{\partial \phi_3}{\partial v}\frac{\partial y}{\partial v}\right) + \frac{2\alpha}{h_w^2}\left(\frac{\partial \phi_1}{\partial w}\frac{\partial x}{\partial w} + \frac{\partial \phi_2}{\partial w}\frac{\partial y}{\partial w}\right.$$
$$\left. + \frac{\partial \phi_3}{\partial w}\frac{\partial z}{\partial w}\right) \qquad (47)$$

From equation (9) it can be shown that

$$2Ge = -\Delta F + 2\alpha\left(\frac{\partial \phi_1}{\partial x} + \frac{\partial \phi_2}{\partial y} + \frac{\partial \phi_3}{\partial z}\right) \qquad (48)$$

By equating terms that do not contain α one obtains

$$\Delta F = \frac{\partial^2 F}{\partial \eta_u^2} + \frac{\partial^2 F}{\partial \eta_v^2} + \frac{\partial^2 F}{\partial \eta_w^2}$$

$$\Delta = \frac{\partial^2}{\partial \eta_u^2} + \frac{\partial^2}{\partial \eta_v^2} + \frac{\partial^2}{\partial \eta_w^2} \qquad (49)$$

This may be written

$$\Delta = \frac{1}{h_u h_v h_w}\left\{\frac{\partial}{\partial u}\left(\frac{h_v h_w}{h_u}\frac{\partial}{\partial u}\right) + \frac{\partial}{\partial v}\left(\frac{h_w h_u}{h_v}\frac{\partial}{\partial v}\right) + \frac{\partial}{\partial w}\left(\frac{h_u h_v}{h_w}\frac{\partial}{\partial w}\right)\right\} \qquad (50)$$

By equating terms that do contain α in equations (47) and (48) we obtain

$$\Delta F = 2\left(\frac{\partial \phi_1}{\partial x} + \frac{\partial \phi_2}{\partial y} + \frac{\partial \phi_3}{\partial z}\right)$$

$$= \frac{2}{h_u^2}\left(\frac{\partial \phi_1}{\partial u}\frac{\partial x}{\partial u} + \frac{\partial \phi_2}{\partial u}\frac{\partial y}{\partial u} + \frac{\partial \phi_3}{\partial u}\frac{\partial z}{\partial u}\right) + \frac{2}{h_v^2}\left(\frac{\partial \phi_1}{\partial v}\frac{\partial x}{\partial v} + \frac{\partial \phi_2}{\partial v}\frac{\partial y}{\partial v} + \frac{\partial \phi_3}{\partial v}\frac{\partial z}{\partial v}\right) + \frac{2}{h_w^2}\left(\frac{\partial \phi_1}{\partial w}\frac{\partial x}{\partial w} + \frac{\partial \phi_2}{\partial w}\frac{\partial y}{\partial w} + \frac{\partial \phi_3}{\partial w}\frac{\partial z}{\partial w}\right) \quad (51)$$

TWO DIMENSIONAL STRESS PROBLEM IN CURVILINEAR CO-ORDINATES

In the plane strain and plane stress analysis in Cartesian co-ordinates, the plane stresses were given by the equations

$$\sigma_x = \frac{\partial^2 F}{\partial y^2}, \quad \sigma_y = \frac{\partial^2 F}{\partial x^2}, \quad \tau_{xy} = \frac{\partial^2 F}{\partial y \partial x}$$

Note that Poisson's ratio is not involved in any of these relations; hence, an arbitrary value may be selected. Choose Poisson's ratio so that $\alpha = 0$. This simplifies the calculations considerably. When $\alpha = 0$ there is no difference between the state of plane strain, or plane stress, and the three dimensional stress condition. Under this condition z is independent. It is then possible to use the expressions for the three dimensional stress condition and the equations previously derived for the curvilinear co-ordinates except that the stress function F may be a function of only two independent variables

$$F = F(u, v) \quad (52)$$

The equation for the transformation from rectilinear co-ordinates to curvilinear co-ordinates are

$$\begin{aligned} x &= x(u, v) \\ y &= y(u, v) \\ z &= w \end{aligned} \quad (53)$$

Then

$$h_u^2 = \left(\frac{\partial x}{\partial u}\right)^2 + \left(\frac{\partial y}{\partial u}\right)^2$$

$$h_v^2 = \left(\frac{\partial x}{\partial v}\right)^2 + \left(\frac{\partial y}{\partial v}\right)^2$$

$$h_w = 1 \quad (54)$$

And the stresses are given by

$$\sigma_u = -\frac{\partial^2 F}{\partial \eta_u^2} + \Delta F = \frac{\partial^2 F}{\partial \eta_v^2}$$

$$\sigma_v = \frac{\partial^2 F}{\partial \eta_v^2} + \Delta F = \frac{\partial^2 F}{\partial \eta_u^2} \qquad (55)$$

$$\tau_{uv} = -\frac{\partial^2 F}{\partial \eta_u \partial \eta_v}$$

Or written out these become

$$\sigma_u = \frac{1}{h_v}\frac{\partial}{\partial v}\left(\frac{1}{h_v}\frac{\partial F}{\partial v}\right) + \frac{1}{h_u^2 h_v}\frac{\partial h_v}{\partial u}\frac{\partial F}{\partial u}$$

$$\sigma_v = \frac{1}{h_u}\frac{\partial}{\partial u}\left(\frac{1}{h_u}\frac{\partial F}{\partial u}\right) + \frac{1}{h_u h_v^2}\frac{\partial h_u}{\partial v}\frac{\partial F}{\partial v} \qquad (56)$$

$$\tau_{uv} = \frac{1}{h_u}\frac{\partial}{\partial u}\left(\frac{1}{h_v}\frac{\partial F}{\partial v}\right) + \frac{1}{h_u^2 h_v}\frac{\partial h_u}{\partial v}\frac{\partial F}{\partial u}$$

If if is assumed that the equations of transformations satisfy the equations

$$\frac{\partial x}{\partial u} = \frac{\partial y}{\partial v} \quad \text{and} \quad \frac{\partial x}{\partial v} = \frac{\partial y}{\partial u} \qquad (57)$$

then

$$h_u^2 = h_v^2 = h^2$$

$$h_w = 1 \qquad (58)$$

The boundary conditions become

$$\frac{\partial F}{\partial x} = \frac{1}{h_u^2}\frac{\partial x}{\partial u}\frac{\partial F}{\partial u} + \frac{1}{h_v^2}\frac{\partial x}{\partial v}\frac{\partial F}{\partial v}$$

$$= \frac{1}{h^2}\left(\frac{\partial x}{\partial u}\frac{\partial F}{\partial u} + \frac{\partial x}{\partial v}\frac{\partial F}{\partial v}\right) \qquad (59)$$

$$\frac{\partial F}{\partial y} = \frac{1}{h_u^2}\frac{\partial y}{\partial u}\frac{\partial F}{\partial u} + \frac{1}{h_v^2}\frac{\partial y}{\partial v}\frac{\partial F}{\partial v}$$

$$= \frac{1}{h^2}\left(\frac{\partial y}{\partial u}\frac{\partial F}{\partial u} + \frac{\partial y}{\partial v}\frac{\partial F}{\partial v}\right)$$

where

$$\frac{\partial F}{\partial x} = \text{constant and } \frac{\partial F}{\partial y} = \text{constant along an unloaded boundary.}$$

The Δ operator takes the form

$$\Delta = \frac{1}{h_u h_v}\left[\frac{\partial}{\partial u}\left(\frac{h_v}{h_u}\frac{\partial}{\partial u}\right) + \frac{\partial}{\partial v}\left(\frac{h_u}{h_v}\frac{\partial}{\partial v}\right)\right]$$

$$= \frac{1}{h^2}\left[\frac{\partial^2}{\partial u^2} + \frac{\partial^2}{\partial v^2}\right] \qquad (60)$$

and the equation

$$\Delta\phi = 0$$

is the equivalent to

$$\frac{\partial^2\phi}{\partial u^2} + \frac{\partial^2\phi}{\partial v^2} = 0 \qquad (61)$$

which simplies the task of finding the harmonic functions.

Shallow Circumferential External Notch

For the mathematical treatment let

$$x = r\cos\theta$$

$$y = r\sin\theta$$

$$z = \omega$$

Then $h^2_r = 1$, $h^2_\theta = r^2$, and $h_w^2 = 1$ and the Δ - operator becomes

$$\Delta = \frac{\partial^2}{\partial r^2} + \frac{1}{r}\frac{\partial}{\partial r} + \frac{1}{r^2}\frac{\partial^2}{\partial\theta^2} + \frac{\partial^2}{\partial\omega^2}$$

Then

$$\Delta F = 2\left(\frac{\partial\theta_1}{\partial r}\cos\theta + \frac{\partial\theta_2}{\partial r}\sin\theta\right) + \frac{2}{r^2}\left[\frac{\partial\phi_1}{\partial\theta}(-r\sin\theta) + \frac{\partial\phi_2}{\partial\theta}(r\cos\theta)\right]$$

$$+ 2\left(\frac{\partial\phi_2}{\partial\omega}\right)$$

$$= 2\left[\frac{\partial\phi_1}{\partial r}\cos\theta + \frac{\partial\phi_2}{\partial r}\sin\theta - \frac{\partial\phi_1}{\partial\theta}\frac{\sin\theta}{r} + \frac{\partial\phi_2}{\partial\theta}\frac{\cos\theta}{r}\right.$$

$$\left. + 2\frac{\partial\phi_2}{\partial\omega}\right]$$

and

$$\frac{\partial^2}{\partial \eta_r^2} = \frac{\partial^2}{\partial r^2}, \frac{\partial^2}{\partial \eta \theta} = \frac{1}{r}\frac{\partial}{\partial r} + \frac{1}{r^2}\frac{\partial^2}{\partial \theta^2}, \frac{\partial^2}{\partial \eta \omega^2} = \frac{\partial^2}{\partial \omega^2}$$

$$\frac{\partial^2}{\partial \eta_r \partial \eta_\theta} = \frac{\partial}{\partial r}\left(\frac{1}{r}\frac{\partial}{\partial \theta}\right), \frac{\partial^2}{\partial \eta \theta \partial \eta \omega} = \frac{1}{r}\frac{\partial^2}{\partial \theta \partial \omega},$$

$$\frac{\partial^2}{\partial \eta_\omega \partial \eta_r} = \frac{\partial^2}{\partial r \partial \omega}$$

so that the stresses become

$$\sigma_r = -\frac{\partial^2 F}{\partial r^2} + 2\alpha\left(\frac{\partial \phi_1}{\partial r}\cos\theta + \frac{\partial \phi}{\partial r}\sin\theta\right) + \left(1 - \frac{\alpha}{2}\right)\Delta F$$

$$\sigma_\theta = -\frac{1}{r^2}\frac{\partial^2 F}{\partial \theta^2} - \frac{1}{r}\frac{\partial F}{\partial r} + \frac{2\alpha}{r^2}\left(-\frac{\partial \phi}{\partial \theta} r \sin\theta + \frac{\partial \phi_2}{\partial \theta} r\cos\theta\right)$$
$$+ \left(1 - \frac{\alpha}{2}\right)\Delta F$$

$$\sigma_\omega = -\frac{\partial^2 F}{\partial \omega^2} + 2\alpha\frac{\partial \phi_3}{\partial \omega}\left(1 - \frac{\alpha}{2}\right)\Delta F$$

$$\tau_{r\theta} = -\frac{\partial}{\partial r}\left(\frac{1}{r}\frac{\partial F}{\partial \theta}\right) + \frac{\alpha}{r}\left(-\frac{\partial \phi_1}{\partial r} r\sin\theta + \frac{\partial \phi_1}{\partial \theta}\cos\theta + \frac{\partial \phi_2}{\partial r} r\cos\theta\right.$$
$$\left. + \frac{\partial \phi_2}{\partial \theta}\cos\theta\right)$$

$$\tau_{\theta\omega} = -\frac{1}{r}\frac{\partial^2 F}{\partial \theta \partial \omega} + \frac{\alpha}{r}\left(-\frac{\partial \phi_1}{\partial \omega} r\sin\theta + \frac{\partial \phi_2}{\partial \omega} r\cos\theta + \frac{\partial \phi_3}{\partial \theta}\right)$$

$$\tau_{\omega r} = -\frac{\partial^2 F}{\partial r \partial \omega} + \alpha\left(\frac{\partial \phi_1}{\partial \omega}\cos\theta + \frac{\partial \phi_2}{\partial \omega}\sin\theta + \frac{\partial \phi_3}{\partial r}\right)$$

Consider now a pure tensile load.

$$F = \phi_0 + x\,\phi_1 + y\,\phi_2 + z\,\phi_3$$

where

$$\phi_i = \phi_i(x, y, z) \quad i = 0, 1, 2, 3$$

Arbitrarily set $\phi_1 = 0$ since only three harmonic functions are needed. Then $\phi_2 = 0$ because of rotational symmetry.

$$F = \phi_0 + z\,\phi_3$$

Now let

$$\phi_s = \frac{\partial \phi_s'}{\partial \omega} \quad \text{and} \quad \phi_0 = \phi_0' + \alpha \phi_s'$$

$$F = \phi_0' + \alpha \phi_s' + \omega \frac{\partial \phi_s'}{\partial z} = F' + \alpha \phi_s'$$

where $\phi_0' = \phi_0(r, \omega)$, $\phi_s' = \phi_s'(r, \omega)$

Because the notch is shallow, the dimensions in the r and ω directions in the vicinity of the notch are small when compared to r itself. Then relatively speaking $\frac{1}{r}\frac{1}{r}$ and $\frac{1}{r^3}\frac{1}{r^2}$ are small when compared to the other magnitudes. Assuming $\frac{1}{r}\frac{1}{r}$ and $\frac{1}{r^3}\frac{1}{r^2}$ are small, the Δ - operator becomes

$$\Delta = \frac{\partial^2}{\partial r^2} + \frac{\partial^2}{\partial \omega^2}$$

Then

$$\Delta F = \Delta F' + \alpha \Delta \phi_s' = \Delta F'$$

and

$$\Delta F' = \Delta \phi_0' + \Delta \left(\omega \frac{\partial \phi_s'}{\partial \omega}\right) = 2 \frac{\partial^2 \phi_s'}{\partial \omega^2} = -2 \frac{\partial^2 \phi_s'}{\partial r^2}$$

or

$$\Delta F = \Delta F' = 2 \frac{\partial^2 \phi_s'}{\partial \omega^2} = -2 \frac{\partial^2 \phi_s'}{\partial r^2}$$

The stresses then become

$$\sigma_r = \frac{\partial^2 F'}{\partial \omega^2}, \quad \sigma_\omega = \frac{\partial^2 F'}{\partial r^2}, \quad \sigma_\theta = \frac{1}{m} \Delta F = \frac{1}{m} (\sigma_r, \sigma_\omega)$$

$$\tau_{r\theta} = 0, \quad \tau_{\theta\omega} = 0, \quad \tau_{\omega r} = -\frac{\partial^2 F'}{\partial r \partial \omega}$$

These are the same equations derived for the two dimensional plane strain condition, and hence the case of a shallow circumferential external notch reduces to a two dimensional problem.

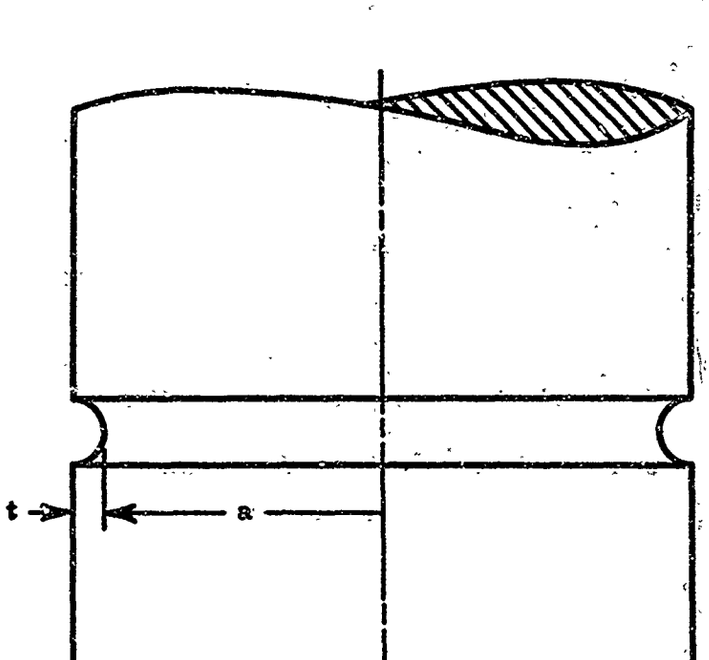

Shallow Circumferential External Notch

APPENDIX B

THE FLOATED SLEEVE TENSILE TEST

A new testing technique has been developed here in which a test sleeve of either uniform or varying wall thickness is fitted with tapered end plugs that do not actually contact the cylindrical specimen thus permitting internal gas-pressure loading without axial or any other restraint such as that imposed by a bladder. The pressurizing gas is permitted to leak out the ends through a clearance gap of about 0.0005 inch so that a "gas-bearing" principle is used but is now more properly called a "gas-floated sleeve." During a run, the clearance gap is maintained fairly uniform and constant as the cylinder expands by a gap-positioner that maintains a programmed torque on the stud connecting the tapered end plugs. See Figure 1 for a schematic of the apparatus. It seems reasonable that this apparatus could be modified for use to 4500°F by preheating the gas (it will take 80 kw) and installing the entire system in a furnace. For biaxial stress studies, axial loading undoubtedly can be applied to the ends through a gas film. This would require flats on the ends of the plugs to match the ends of the specimens.

Several experimental runs have been made on ATJ graphite (for with grain hoop stresses) at 70°F with results as shown in Table 1. The average burst strengths for sleeves with a 40 mil wall thickness were 3490 psi and 3657 psi for specimen lengths of $\frac{1}{2}$ inch and 1 inch, respectively. The average burst strengths for larger sleeves with 80 mil wall thickness were 3315 psi and 3225 psi for specimen lengths of $\frac{1}{2}$ inch and 3 inch, respectively. These strengths are about 8 to 10 percent less than obtained on our gas-bearing system where compared at equal volumes. More work is necessary to explore other ratios of dimensions for the specimens and particularly to see if the corners that exist on these specimens might explain the somewhat lower values.

For a preliminary look at the corner effect on the sleeves two cylinders were made with 80 mil wall thickness over the center one inch of length and then an increasing wall thickness to 93 mils at the ends. This geometry would reduce the stress at the ends by about 16 percent as compared to the middle. Surprisingly at first, the bursting stress was only 3115 psi or slightly less than the value of 3225 psi obtained for the 3 inch sleeve with the same length and a uniform 80 mil wall thickness. The thickness of the wall at the ends was increased even more to 110 mils so that the stress at the ends was about 37 percent less than at the center and, again, the bursting stress was 3150 psi or slightly lower than for a uniform wall thickness.

Note that both tapered end specimens provided quite similar values of 3115 psi and 3150 psi. Thus at least two conclusions seem apparent. The thicker walls would not compensate for a lower bursting strength if it was initiating at the corners; and secondly, thicker walls at the ends can be used if needed for some reason without seriously influencing the bursting strength either up or down. Perhaps the taper would enhance the strength more for a shorter specimen. Recall that these were 3 inches long.

Another few runs were made to explore the difference in circumferential strains around the specimen on the center and at one end. A specimen with 80 mil walls and 3 inches long was used. Observe in Figure 2 that the edge had somewhat more strain; however, this may be no more than differences in strain gage readings as the gages are quite difficult to attach to graphite and obtain precise agreement. The prior evidence on the tapered sleeves suggests that the edge strain is not really so much higher.

In conclusion the floated-sleeve tensile apparatus works quite well and provides values that are a little lower than obtained on the gas-bearing for equal volumes. At this time, the lower value is assumed a result of the sharp corners at the ends.

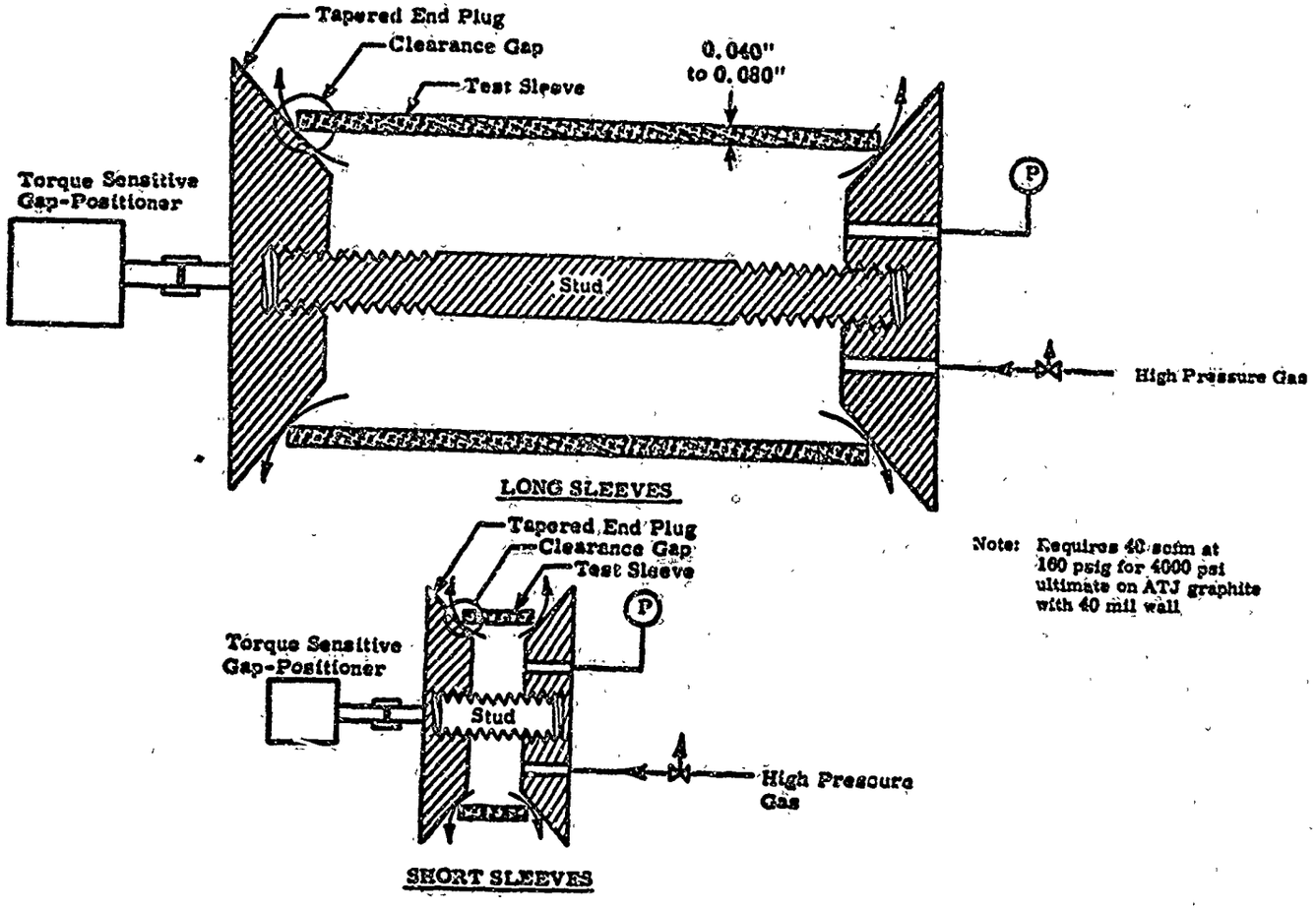

Figure 1. Schematic of Gas-Floated Sleeves Tensile Test Rig

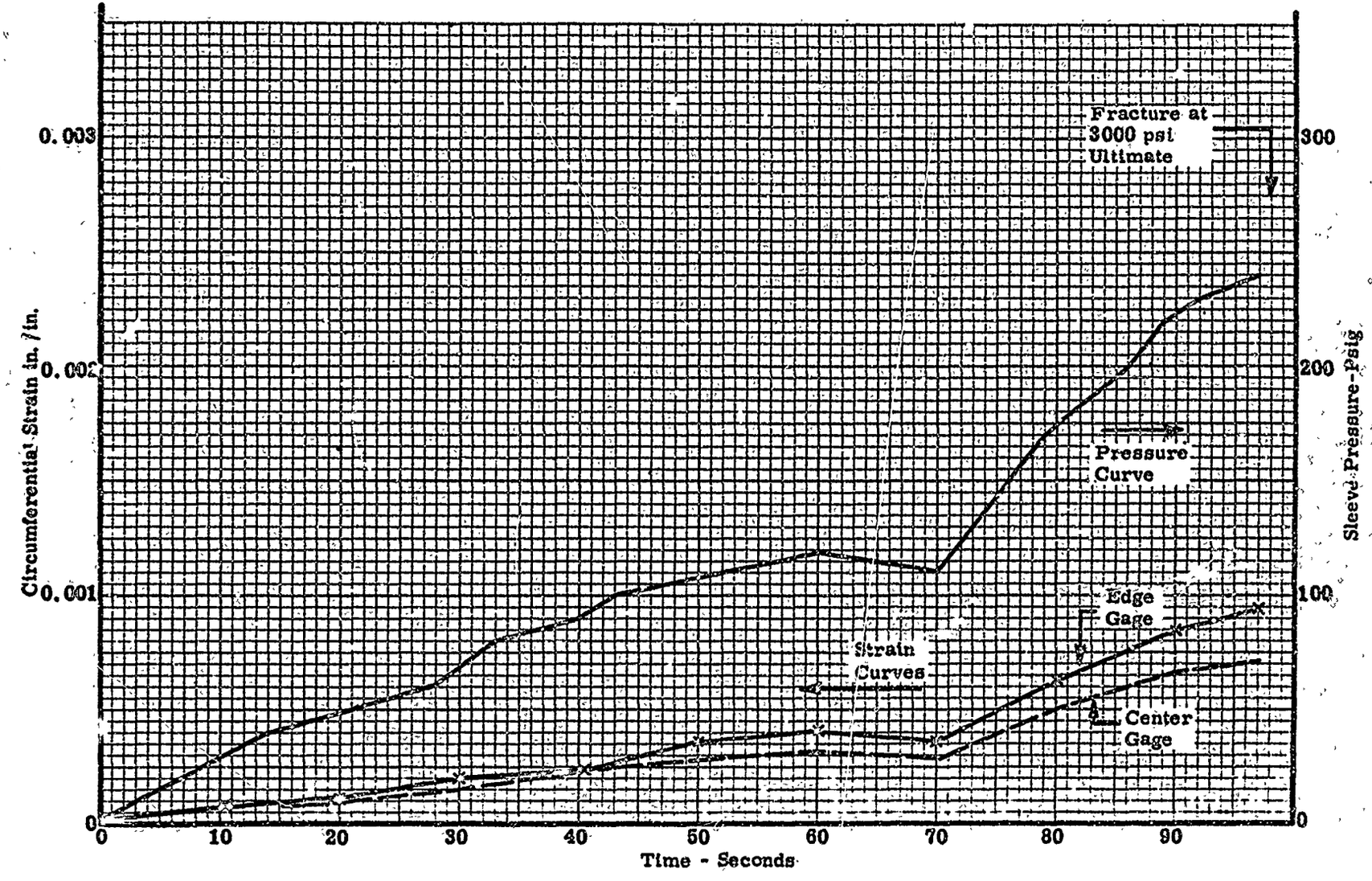

Figure 2. Strain-Time Curve of 3" Long x 2" ID x 0.080" Wall Sleeve

Table 1

Burst Data on ATJ Graphite Sleeves
(All Sleeves Had ID of 2 Inches)

Wall Thickness Inches	Length Inches	Burst Pressure psi	Ultimate Tensile Strength - psi	Specimen Vol. $in.^3$	Remarks
0.040	1	140	3640		$\sigma = 2.6P^5$
0.040	1	120	3120		
0.040	1	145	3770		
0.040	1	132	3430		
		Average	3490	0.125	
0.040	1	134	3480		1
0.040	1	108	2810		1
		Average	3145	0.125	
0.040	1	144	3740		
0.040	1	140	3640		
0.040	1	138	3590		
		Average	3657	0.25	
0.080	1	285	3740		$\sigma = 1.31P^5$
0.080	1	220	2890		
		Average	3315	0.25	
0.080	3	250	3290		
0.080	3	240	3160		
		Average	3225	1.38	2
0.080	3	235	3090		3
0.080	3	245	3220		
		Average	3115		
0.080	3	210	2750		4
0.080	3	270	3550		
		Average	3150		

[1]Inner face sealed with plastic tape.
[2]Strain gages attached at center and $\frac{1}{4}$ inch from end to measure circumferential strains.
[3]One inch of ends tapered up to 0.093 inch wall thickness.
[4]One inch of ends tapered up to 0.110 inch wall thickness.
[5]Burst pressure in psi.

APPENDIX C

FLEXURAL ANALYSIS

Referring to Figure 26, in the main body of the report, it can be seen that the average MOR of the flexural specimens appeared to be 15-20 percent higher than the corresponding tensile values. One reason for this could have been the volume used for the flexural specimen; however, only the smallest tensile specimen (0.0013 $in.^3$) had a strength comparable to the flexural specimen's MOR value.

More probably the differences between the MOR and tensile strengths are due to the method of calculating the MOR. The usual equation,

$$\sigma = \frac{Mc}{I}$$

which assumes the material is perfectly elastic in tension and compression and the elastic moduli in tension and compression are the same, was used. It is well known that for graphite these assumptions are not satisfied. The tensile stress-strain curve for most graphites at 70°F has an initial linear portion, then a slight break, and a final portion that usually can be considered linear. The compressive stress-strain curve is usually linear for the range of stresses encountered in a flexural specimen; however, the tensile modulus is usually greater than the compressive modulus at 70°F.

Figure 1 is a schematic of the cross-section of the flexural specimen whose MOR values are shown on Figure 26 of the report. The specimen dimensions were 0.250 in. by 1.000 in. by 6 in. long and the span lengths were 4 in. by 2 in. The solid line on Figure 1 shows the classical stress distribution. As already mentioned, the stress-strain curves for tension and the difference in tensile and compressive moduli would cause the stress distribution to change from this classical representation. First, let us consider the effect of the two influences separately.

The nonlinearity of the tensile stress-strain curve would cause a shift in the neutral axis away from the centroidal axis. If the initial elastic moduli in tension and compression were equal, the shift would be toward the compressive side of the beam in order to satisfy the relation

$$\int_A \sigma_y \, dA = 0 \qquad (1)$$

Now if the tensile stress-strain curve was linear, but the tensile and compressive moduli were different, then the neutral axis shift would be toward the side with the greater modulus. For this graphite, the shift would be toward the tensile side.

Thus, for a combination of the two, the neutral axis would shift only slightly or possibly not at all. Strain gage measurements, by this laboratory and other laboratories on the tensile and compressive faces of graphite and graphite-like materials, have shown that the strains recorded on the opposite faces were essentially the same. This is as would be expected with no neutral axis shift and with a linear strain distribution.

Now returning to Figure 1, the dashed line represents a stress distribution based on the tensile stress-strain curve for ATJ graphite. It was assumed that the neutral axis did not shift. Using the relation of equation (1) and assuming the compressive stress-strain curve was linear, the compressive distribution was calculated. Note that the ratio of the initial slopes for tension and compression sides is about 1.35 which agrees with experimental measurements of tensile and compressive moduli. The applied moment calculated for this distribution from the equation

$$\int_A y\sigma_y \, dA = M \qquad (2)$$

had a value of 45in.-lbs. The required moment to produce the classical MOR value used in prior Figure 26 was 48 in.-lbs. This is good agreement. Thus the maximum outer fiber stress can be 11 percent lower than the value calculated from the classical equations.

The above discussion points up some of the probable causes for disagreement between MOR and tensile strength values and the fallacy of using a flexural test for tensile strength. At elevated temperature (above 4000°F for most graphites), the problem becomes more acute.

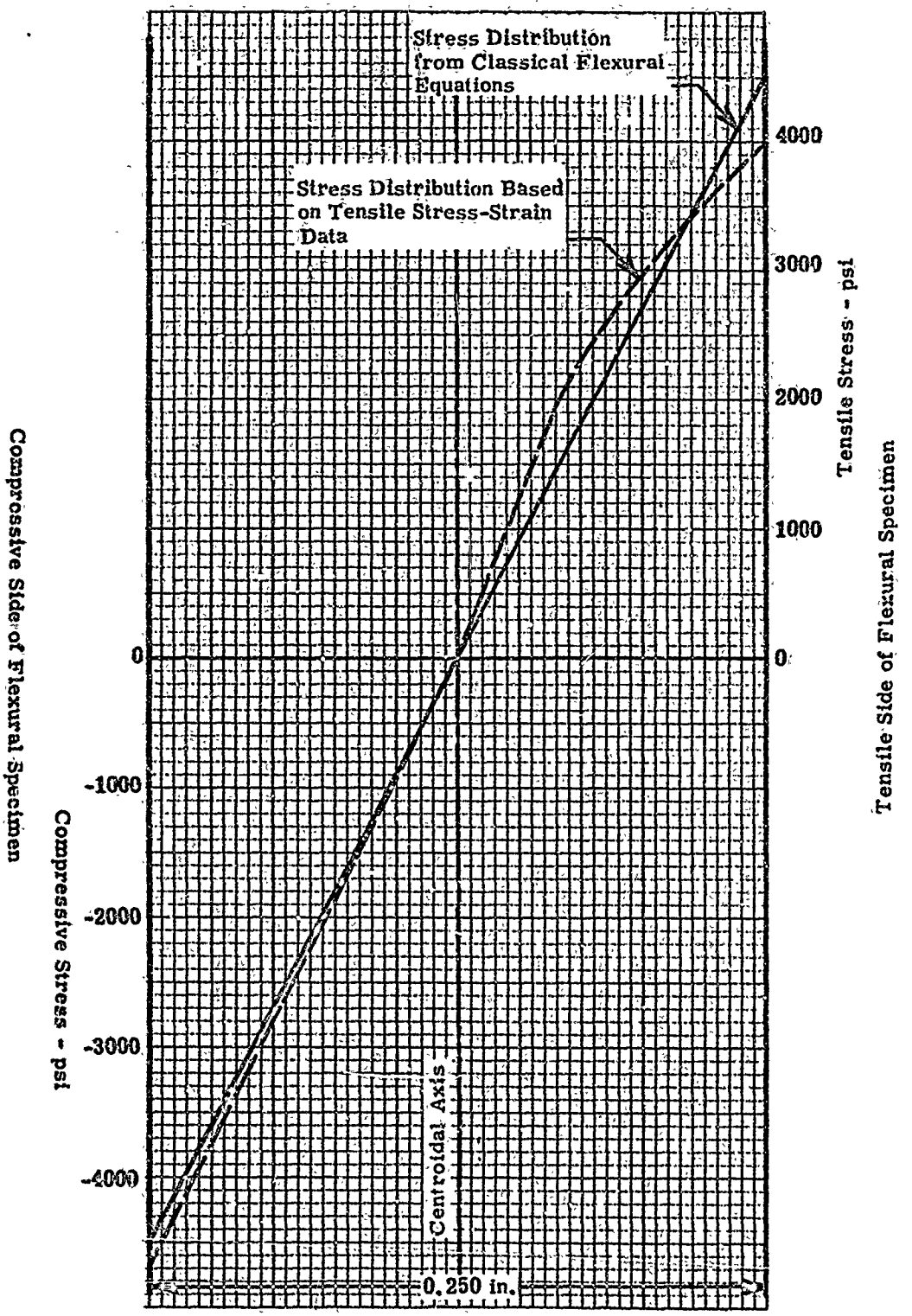

Figure 1. Comparison of Classical Stress Distribution with a Stress Distribution Based on the Known Tensile Stress-Strain Response of ATJ Graphite

UNCLASSIFIED

Security Classification

DOCUMENT CONTROL DATA - R & D

(Security classification of title, body of abstract and indexing annotation must be entered when the overall report is classified)

1. ORIGINATING ACTIVITY (Corporate author) Southerr Research Institute 2000 Ninth Avenue, South Birmingham, Alabama 35205	2a. REPORT SECURITY CLASSIFICATION UNCLASSIFIED 2b. GROUP

3. REPORT TITLE

A STUDY OF NOTCHES IN BRITTLE MATERIALS BY RELATING STRESS INTENSIFICATION AND VOLUME

4. DESCRIPTIVE NOTES (Type of report and inclusive dates)

Final Report - January 1966 to 31 December 1966

5. AUTHOR(S) (First name, middle initial, last name)

Starrett, H. Stuart, and Pears, C. D.

6. REPORT DATE	7a. TOTAL NO. OF PAGES	7b. NO. OF REFS
May 1968	111	5

8a. CONTRACT OR GRANT NO. AF 33(615)-1690 b. PROJECT NO. 7350 c. TASK NO. 735003 d.	9a. ORIGINATOR'S REPORT NUMBER(S) AFML-TR-67-254 9b. OTHER REPORT NO(S) (Any other numbers that may be assigned this report)

10. DISTRIBUTION STATEMENT This document is subject to special export controls and each transmittal to foreign governments or foreign nationals may be made only with prior approval of the Metals and Ceramics Division (MAM), Air Force Materials Laboratory, Wright-Patterson Air Force Base, Ohio 45433.

11. SUPPLEMENTARY NOTES	12. SPONSORING MILITARY ACTIVITY
	Metals and Ceramics Division Air Force Materials Laboratory Wright-Patterson AFB, Ohio

13. ABSTRACT

The effects of notches on the tensile strength of brittle materials were determined experimentally, and the Weibull volume theory was used in conjunction with Neuber sttess distributions to examine the results. The experimental portion was performed on a gas-bearing tensile facility. The primary material used was hot pressed alumina made by Avco. The effects of notches on graphite was also investigated to a lesser degree.

The results showed that notches affected the nominal strength of alumina considerably and that for severe notches the effect was greater for larger specimens. The failure stresses predicted by the Neuber analysis were in fair agreement with the strengths predicted by the Weibull volume analysis when the volume was defined as that encapsulating the material subjected to 50 percent of the peak stress. It is postulated that irreversible damage occurs at above 50 percent of ultimate for these types of materials. This event may permit local stress relief. At the roots of the notches, theoretical strengths of over 80,000 psi were obtained. Nominal tensile and flexural strengths on regular specimens were of the order of 42,000 psi and 36,000 psi, respectively, for the minimum volumes tested. Evidence was obtained that the fracture source may move internally on this material at surface finishes finer than 25 rms.

Notches also reduced considerably the strength of graphite at 70°F and 4000°F, but not at 5000°F where the effect of the stress concentration was negated by the "ductile like" behavior of the material.

This abstract is subject to special export controls and each transmittal to foreign governments or foreign nationals may be made only with prior approval of the Metals and Ceramics Division (MAM), Air Force Materials Laboratory, Wright-Patterson Air Force Base, Ohio 45433.

DD FORM 1 NOV 65 1473

UNCLASSIFIED

Security Classification

UNCLASSIFIED
Security Classification

14. KEY WORDS	LINK A		LINK B		LINK C	
	ROLE	WT	ROLE	WT	ROLE	WT
Brittle Materials Alumina Weibull Stress Concentrations Tensile Strength Design						

UNCLASSIFIED
Security Classification